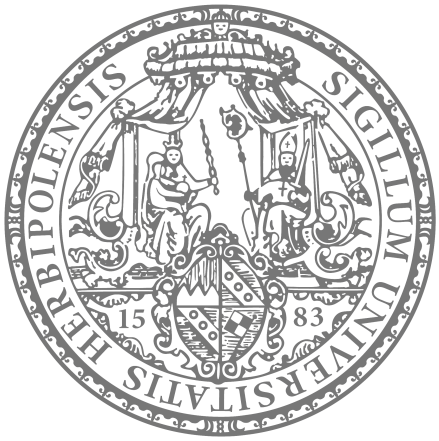

The role of microRNA-378 in cardiac hypertrophy

Untersuchungen zur Rolle der MikroRNA-378 bei kardialer Hypertrophie

Doctoral thesis for a doctoral degree at the Graduate School of Life Sciences,
Julius-Maximilians-Universität Würzburg,
Section - Experimental Biomedicine

Submitted by

Jayavarshni Ganesan

from

Madurai, India

Würzburg 2014

Submitted on: ……..……..

Office stamp

Members of the *Promotionskomitee*:

Chairperson: Prof. Dr. Manfred Gessler

Primary Supervisor: Prof. Dr. Dr. Stefan Engelhardt

Supervisor (Second): Prof. Dr. Utz Fischer

Supervisor (Third): Prof. Dr. Hermann Schindelin

Supervisor (Fourth): …….
(If applicable)

Date of Public Defence: ……..……

Date of Receipt of Certificates: …….

Affidavit

I hereby confirm that my thesis entitled “The role of microRNA-378 in cardiac hypertrophy” is the result of my own work. I did not receive any help or support from commercial consultants. All sources and / or materials applied are listed and specified in the thesis.

Furthermore, I confirm that this thesis has not yet been submitted as part of another examination process neither in identical nor in similar form.

Munich, 14th March 2014

Place, Date Signature

Eidesstattliche Erklärung

Hiermit erkläre ich an Eides statt, die Dissertation “Untersuchungen zur Rolle der MikroRNA-378 bei kardialer Hypertrophie” eigenständig, d.h. insbesondere selbständig und ohne Hilfe eines kommerziellen Promotionsberaters, angefertigt und keine anderen als die von mir angegebenen Quellen und Hilfsmittel verwendet zu haben.

Ich erkläre außerdem, dass die Dissertation weder in gleicher noch in ähnlicher Form bereits in einem anderen Prüfungsverfahren vorgelegen hat.

Munich, 14th March 2014

Ort, Datum Unterschrift

1 INTRODUCTION

1.1 Heart failure

According to the World Health Organization(WHO), cardiovascular diseases(CVDs) are the number one cause of death globally[1]. About 17.3 million people died from CVDs in 2008, representing 30% of all global deaths[1]. The number is expected to reach 23.3 million by the year 2030 and is projected to remain the single leading cause of death[2]. In industrial countries, CVDs account for 45% of all deaths caused by non communicable diseases[3]. They are mainly caused by disorders of the heart and blood vessels and include coronary heart disease, cerebrovascular disease, hypertension, peripheral artery disease, rheumatic heart disease, congenital heart disease and heart failure.

Heart failure can be described as a deficiency in the function of the heart, preventing its ability to fulfill systemic demands leading to premature fatigue, dyspnoea and/or oedema[4]. It can be induced by a number of stimuli, including hypertension, myocardial infarction, coronary artery disease, valvular insufficiency and stenosis, myocarditis, congenital malformations, familial hypertrophic and dilated cardiomyopathies and diabetic cardiomyopathy[5,6]. End stage heart failure is characterized by the following (Fig 1): (1) a genetic reprogramming of the heart akin to the expression profile of a fetal heart accompanied by differing degrees of cardiomyocyte hypertrophy; (2) necrotic or programmed cell death and excess extracellular matrix formation; (3) a reduction of capillarization and presence of regional ischemia, systemic and myocardial (neuro)humoral stimulation, (supra)ventricular dysrrhythmias and hemodynamic dysfunction at the systolic and/or diastolic level[6].

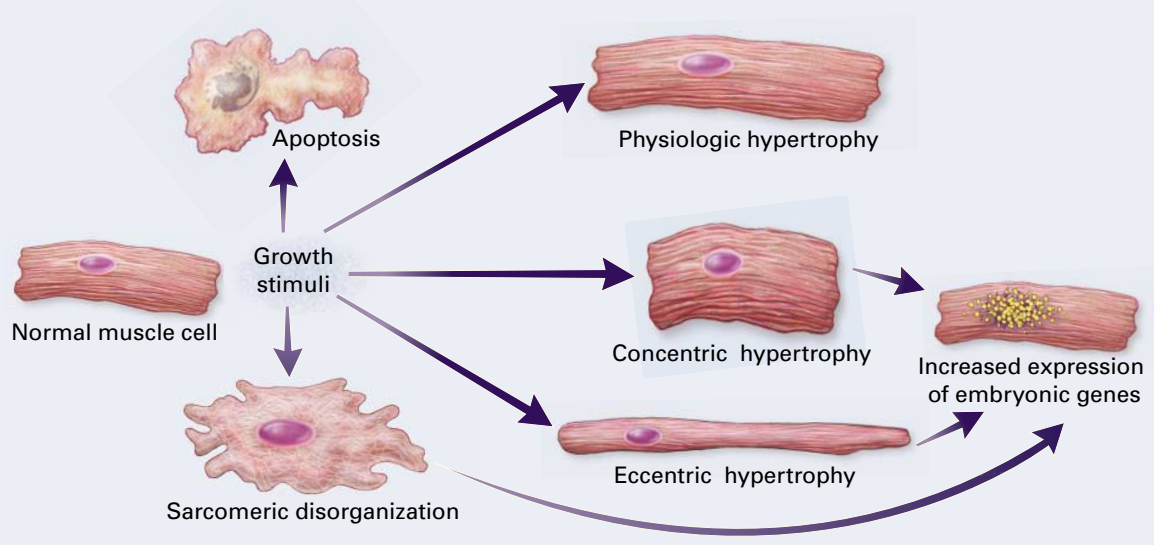

Fig 1. Morphology of cardiac muscle cell during hypertrophy (Illustration from Epstein *et al.* 1999)

1.1.1 Myocardial hypertrophy

Myocardial hypertrophy is an early milestone during the clinical course of heart failure and is an important risk factor for subsequent cardiac morbidity and mortality[7]. Myocardial hypertrophy occurs in response to a variety of physiological, mechanical, hemodynamic, hormonal, and pathologic stimuli. This forces the heart to augment output in the face of increased demands through the initiation of a hypertrophic response characterized by an increase in the contractile protein content of the individual cardiomyocytes without a concomitant proliferative response[6,8].

Hypertrophy can be classified as the following[4]: (1) physiological, which is associated with exercise or pregnancy; (2) pathological, which is associated with disease-inducing stimuli, and (3) developmental, which is associated with the normal growth of the heart after birth until adulthood.

Developmental and physiological hypertrophy are characterized by eccentric hypertrophy with uniform growth of the ventricular wall and septum that is matched with an increase in chamber dimension. The increase in cardiomyocyte size occurs due to the addition of sarcomeres in series and in parallel to both lengthen the cell as well as increase the width of the cell.

Pathological cardiac hypertrophy is characterized by concentric hypertrophy in which the ventricular wall and septum thicken with a net decrease in ventricular chamber dimensions (Fig 2). This remodeling is associated with a greater increase in cardiac myocyte width than length (Fig 1 and 2). However, pathological cardiac hypertrophy can also produce a phenotype of eccentric and dilatory cardiac growth where sarcomeres are predominantly added in series to individual myocytes (Fig 1 and 2). Apart from structural remodeling, pathological hypertrophy is also characterized by metabolic and functional remodeling of the heart. These changes can lead to a shift toward glycolytic metabolism, alterations in calcium handling and contractility, loss of myocytes with fibrotic replacement, systolic or diastolic dysfunction, electrical remodeling, and arrhythmogenesis[9].

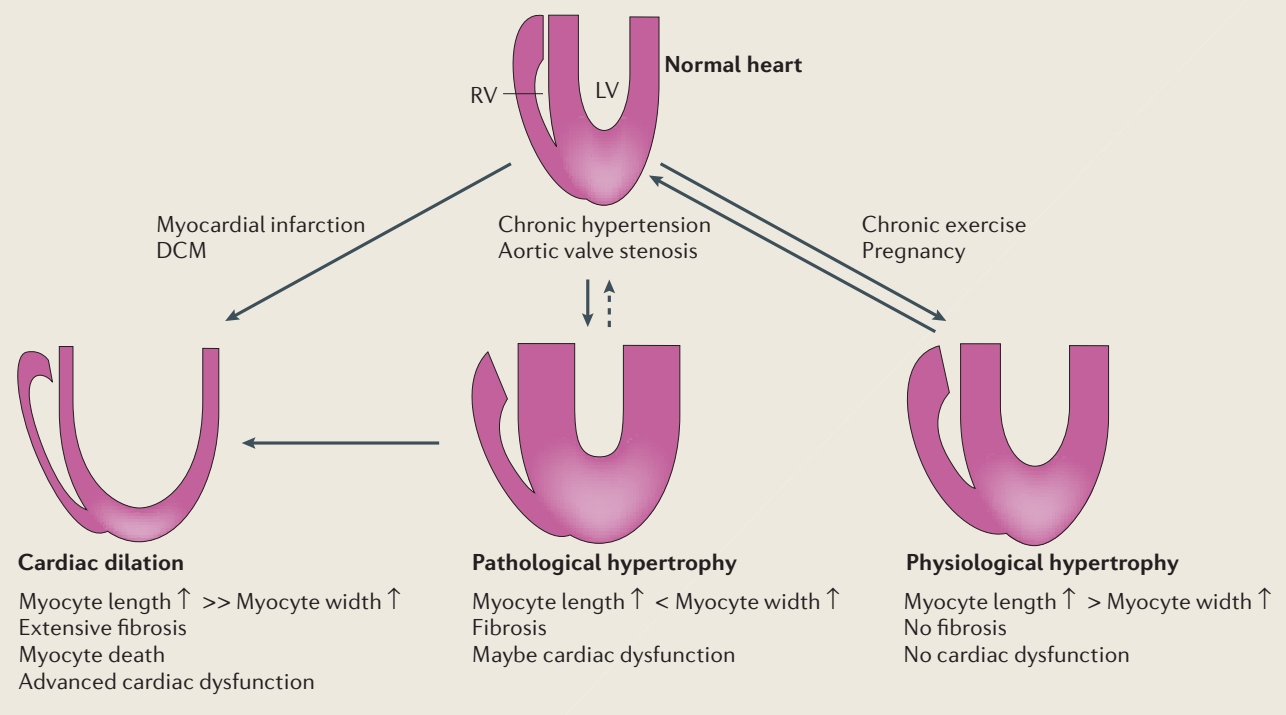

Fig 2: Types of cardiac hypertrophy (Illustration from Heineke *et al.* 2006)

1.1.1.1 Hypertrophic signaling cascades

The stimuli for cardiac hypertrophy can be categorized into the following[4]: (1) biomechanical stretch sensitive mechanisms or (2) neurohumoral mechanisms associated with the release of hormones, cytokines, chemokines and peptide growth factors. Ligands are sensed by cardiac myocytes through an array of membrane-bound G protein-coupled receptors (GPCRs), receptors that have intracellular tyrosine kinase domains or that have intracellular serine/threonine kinase domains, and gp130-linked receptors. Biomechanical signals are thought to be mediated through internal stress sensitive receptors that converge on to a set of intracellular signal transduction circuits leading to the hypertrophic growth response. This response can alter the gene expression profile in the nucleus by increasing the rate of protein translation and slowing down the rate of protein degradation in the cytoplasm. During cardiac hypertrophy, there is an increase in expression fetal genes, including the genes for natriuretic peptides and fetal contractile proteins e.g. *Nppa* and *Myh7,* respectively. The induction of natriuretic peptide genes is considered to be a prognostic indicator of clinical severity[7,8].

The signal transduction pathways involved in the hypertrophic response are inherently complex and abundant. These include the mitogen-activated protein kinase (MAPK), calcineurin/nuclear factor of activated T cells (NFAT) and insulin like growth factor 1 (IGF1)-phosphatidylinositol 3-kinase (PI3K)–AKT/protein kinase B (PKB)–mammalian target of rapamycin (mTOR), regulation of

transcription by the cyclin-dependent kinase-7 (CDK7) and CDK9, and kinase-regulated shuttling of class II histone deacetylases (HDACs)[4].

1.1.1.2 MAPK signaling in cardiac hypertrophy

The MAPK signaling cascade is initiated in cardiac myocytes by GPCRs, receptor tyrosine kinases (IGFI, and fibroblast growth factor receptors), receptor serine/threonine kinases (transforming growth factor-β (TGFβ)), cardiotrophin-1 (gp130 receptor), and by stress stimuli such as stretch. The MAPK signaling pathways link external stimuli and the nucleus by phosphorylating and thereby regulating multiple transcription factors. Based of sequence homology MAPKs can be divided into three subfamilies namely, extracellularly responsive kinases (ERKs), c-Jun N-terminal kinases (JNKs) and p38 MAPKs. JNKs and p38 MAPKs are also called stress responsive MAPKs because they are activated by stress stimuli like ischemia and hyperosmotic shock[10]. Activated p38, JNKs and ERKs each phosphorylate multiple intracellular targets, including numerous transcription factors that induce the reprogramming of cardiac gene expression[4]. ERK1 (also called MAPK3) and ERK2 (also called MAPK1) are part of MAPK cascade consisting of 3 sequentially functioning kinases namely RAF, MAP2K and MAPK1/3[11]. Once activated they reprogram gene expression by phosphorylating a variety of intracellular proteins and transcription factors involved in various functions like growth, proliferation, differentiation, etc.

The upstream activators of MAPK1/3 are two MAPK kinases (MAP2K), MEK1 and MEK2, that phosphorylate a dual site (Thr-Glu-Tyr) in the activation loop of MAPK1/3. p38 kinases are directly activated by the MKK6 and MKK3 and JNKs are directly activated by MKK4 and MKK7. ERK5, also known as big MAPK1, is directly activated by MEK5[12]. Upstream of the MAP2Ks, several MAP2K kinases form a complex network of kinases that either directly sense stress stimulation or are regulated by either MAPKKK kinases or the low molecular mass G proteins of the RHO family, RAS, RAC, RHO and CDC42[4]. The primary MAPKKKs that activate MAPK1/3 are the RAF isoforms, A-RAF, B-RAF and C-RAF or RAF1. RAF is activated by the binding of small G proteins of RAS family to its N-terminus. RAF1 was initially identified as the MAP2K kinase in the MAPK1/3 pathway by its ability to activate MEK1[13]. RAS is a low-molecular-weight GTPase that is activated by GDP to GTP exchange initiated by the membrane bound receptors. It functions like a relay switch positioned downstream of cell surface receptor tyrosine kinases and upstream of a cytoplasmic cascade of kinases. Ras activation can lead to activation of RAF1, PI3K, small GTPase RAL proteins leading to RHO activation[14]. RAS can activate all three MAPK signaling cascades i.e MAPK1/3, JNK and p38 though RAF1 activation is associated only with activation of MAPK1/3.

1.2 MicroRNAs

1.2.1 Discovery

MicroRNAs (miRNAs, miRs) are endogenous ≈22 nt RNAs that can play important regulatory roles in animals and plants by targeting mRNAs for cleavage or translational repression[15]. Post-transcriptional regulation by a tiny regulatory RNA was first described in *Caenorhabditis elegans,* where it was reported that the gene *lin-4* did not encode for a protein but instead produced a pair of small RNAs of approximately 22 and 61 nt long[16]. The longer 61 nt RNA was predicted to fold into a stem loop proposed to be the precursor of the shorter 22 nt RNA. These *lin-4* RNAs had antisense complementarity to multiple sites in the 3' UTR of the *lin-14* gene[16,17]. These discoveries suggested a model of post transcriptional regulation where the *lin-4* RNAs paired to the 3' UTR of *lin-14* mRNA and repressed the translation of the *lin-14* message as part of a regulatory mechanism in the *C. elegans* larval development[16,17]. The shorter *lin-4* RNA is the founding member of an abundant class of tiny regulatory RNA called microRNAs[18-20].

1.2.2 Biogenesis

MicroRNAs are encoded in the genome either in the intergenic regions or within introns of other protein coding genes (Fig 3). MicroRNAs are transcribed by either RNA polymerase II or RNA polymerase III to form long precursor transcripts called primary microRNAs (pri-miRNAs) that can be several kilobases long[21,22]. Transcription by both polymerases follow different regulatory processes and recognize specific promoter elements[23]. A single pri-miRNA transcript can encode several mature microRNAs.

The pri-miRNA is endonucleolytically processed by the nuclear microprocessor complex formed by the RNase III enzyme Drosha and the DGCR8 (DiGeorge critical region 8) protein (also known as Pasha (Partner of Drosha) in *D. melanogaster* and *C. elegans*)[24-28] leading to the excision of a 60-70 nt stem-loop hairpin structure called precursor microRNA (pre-miRNA). DGCR8 functions as a molecular ruler to determine the precise cleavage site enabling Drosha to cleave 11 base pairs away from the single-stranded RNA/double-stranded RNA junction at the base of the stem loop[27,29].

The pre-miRNA is then exported into the cytoplasm by Exportin-5 (XPO5) and Ran-GTP[30]. The binding of Exportin-5 to pre-miRNAs is independent of their sequence or stem-loop structure. However, a defined length of the double stranded stem and 3' overhang are important for a successful binding to Exportin-5 to ensure the export of only correctly processed pre-miRNAs[31-33].

The pre-miRNAs then undergo cytoplasmic miRNA processing through RISC assembly. RISC (RNA induced silencing complex) is a cytoplasmic multiprotein complex composed of the RNase III Dicer, the double-stranded RNA-binding domain proteins TRBP (Tar RNA binding protein) and PACT (protein activator of PKR), and the core component Argonaute-2 (Ago2)[34-37]. MicroRNAs with a high degree of complementarity along the hairpin stem undergo an additional endonucleolytic cleavage step mediated by Ago-2 leading to the generation of a nicked hairpin producing the Ago2-cleaved precursor miRNA or ac-pre-miRNA[38]. The RNase III Dicer then cleaves the pre-miRNA or the nicked ac-pre-miRNA to generate a roughly 22 nt microRNA duplex with a 2 nt overhang at the 3' end. The deletion of Dicer can abolish or decrease the generation of mature microRNAs suggesting that Dicer-mediated cleavage is essential for microRNA processing[39-42]. Dicer and TRBP/PACT then dissociate from the duplex to allow the separation of the functional guide strand that is complementary to the mRNA target and the passenger strand that is subsequently degraded. In principle the microRNA duplex could lead to two different mature microRNAs but usually only one of them is functional while the other is degraded[43]. This strand bias depends on the thermodynamic stability of the bases at both the ends of the duplex i.e. the strand with less stable base pairs at its 5' end becomes the functional guide strand[44].

1.2.3 Mechanism of action

MicroRNAs can regulate gene expression by inhibiting mRNA translation or stability in the cytoplasm[45,46]. This process requires the presence of the Argonaute (AGO) family of proteins, which are key components of the RISC. Mammals encode for four different AGO proteins, AGO1 to AGO4. Of these four, only AGO2 possesses the ability to cleave mRNA at the center of the miRNA-mRNA duplex due to its RNaseH-like P-element induced wimpy testis (PIWI) domain[47].

MiRNA-mRNA interaction involves a contiguous and perfect pairing between the nucleotides 2-8, the so called seed region of the microRNA with complementary sites usually in the 3' UTR of the target mRNA. GU pairs or mismatches and bulges in the seed region generally affect the strength of repression. The site efficacy might be improved due to the presence of an A residue at position 1 of the microRNA and an A or U across position 9. Mismatches in the seed region might be offset by good base pairing particularly to residues 13-16 of the miRNA[48]. Binding of micro-ribonucleoproteins (miRNPs) along with accessory factors, to the 3′ UTR of the target mRNA can induce deadenylation followed by rapid decay of the mRNA[49]. The AGO1 protein can colocalize with mRNA degradation enzymes within P-bodies containing GW182 protein leading to mRNA decay[50]. Alternatively, the miRNPs can repress translation initiation at cap-recognition[51] or the 60S

ribosomal subunit joining stage[52]. The repression can also occur at post-initiation phases of translation due to slowed elongation[53].

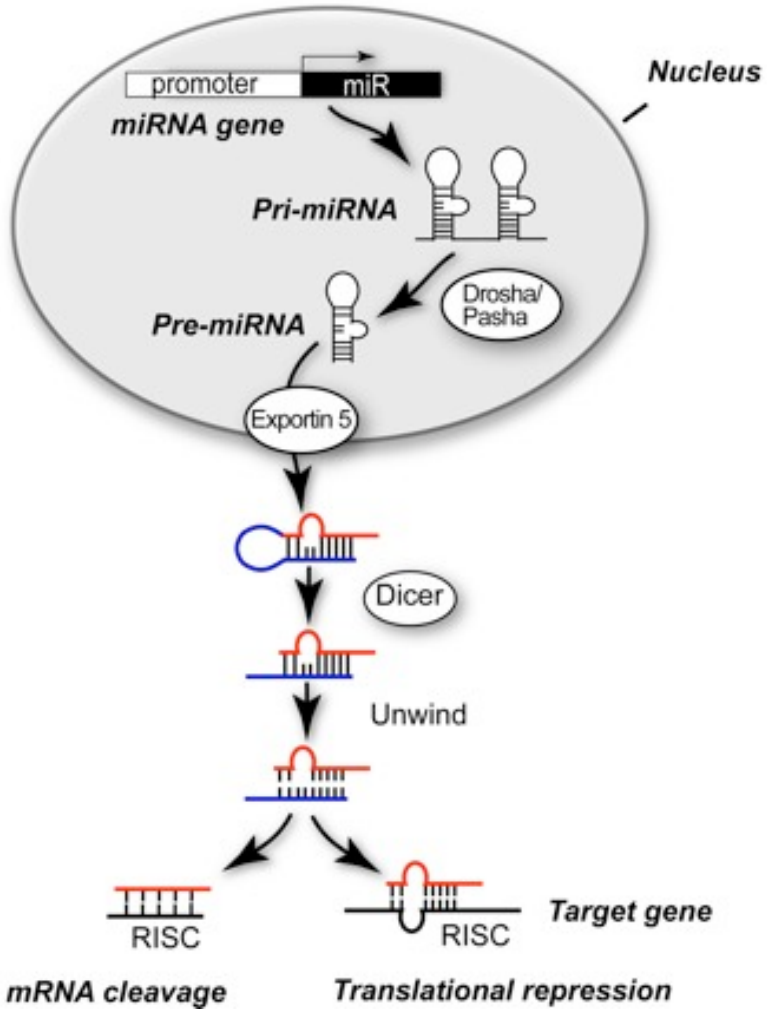

Fig 3 MicroRNA biogenesis

1.2.3 Functional relevance of microRNA action

MicroRNAs preferentially bind to the complementary regions within the 3' UTR of their targets. Approximately 37% of microRNAs are encoded within the introns of other protein coding genes[54]. Among these miRs, a majority of them are cotranscribed and processed with their host genes[55]. This coprocessing of miRs and their protein coding host genes can often regulate important biological phenomena in a synergistic or antagonistic manner by means of complex feedback or feedforward networks (Fig 4a)[56,57]. One well studied example involves the myosin heavy chain genes and a family of intronic miRs encoded by them. The family includes miR-208a (encoded by *Myh6* or α-MHC), miR-208b (encoded by *Myh7* or β-MHC) and miR-499 (encoded by *Myh7b*)[58-60]. These

miRs modulate a number of transcriptional repressors and signaling molecules governing the stress induced response of the heart. The deletion of miR-208a prevented the reactivation of the fetal β-MHC during myocardial hypertrophy preventing the heart from pathological cardiac remodeling. α-MHC is the predominant myosin isoform in the adult heart while β-MHC is predominantly expressed during embryonic development. However, cardiac stress induces the switching of α-MHC to β-MHC affecting cardiac function. It is known that microRNAs target several mRNAs, often at a modest level. This modest regulation can however have significant effects when a microRNA targets multiple factors within a same biological process or signaling cascade (Fig 4b)[56]. This process may add robustness to important gene regulatory networks. Another possibility is the combinatorial action of several microRNAs on one or more targets within a regulatory network (Fig 4c). Such a cooperation of multiple microRNAs could increase redundancy and prevent the reliance on one single miR. Some microRNAs can act as physiological buffers repressing both positive and negative regulators of the same functional regulator (Fig 4d). An example of such a microRNA is the zebrafish miR-430 that represses the expression of TGFβ agonist squint and antagonist lefty[61]. When repression of squint or lefty by miR-430 was inhibited using target protectors, the TGFβ nodal signaling was either enhanced or inhibited. When both squint and lefty were protected or miR-430 was inhibited an imbalance and reduction in the TGFβ signaling was observed suggesting that miR-430 acted like a physiological buffer balancing this signaling process.

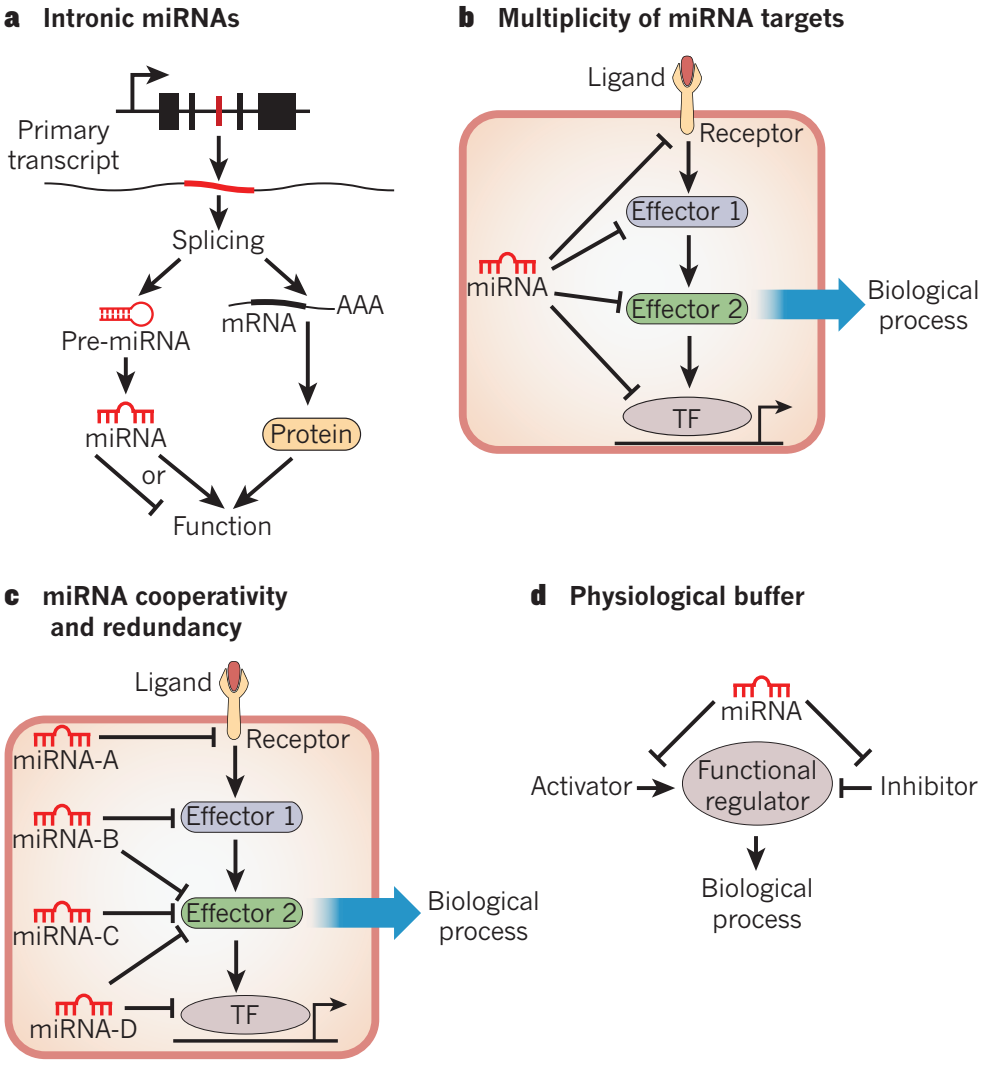

Fig 4: Concepts of microRNA function (Illustration from Small *et al.* 2011)

1.3 Relevance of microRNAs in the heart

The heart is the first organ to form during embryogenesis[62]. Formation of the heart involves a complicated orchestration of a series of events involving a number of genetic pathways regulated by multiple transcription factors and proteins[63]. MicroRNAs have added another dimension to this process by being a part of nearly every stage of this process, from development and function to pathological remodeling. Deletion of Dicer results in a dramatic reduction of mature microRNAs in the heart leading to postnatal death of the mutant mice due to severe heart failure and dilated cardiomyopathy (DCM)[64]. These mice show misexpression of cardiac contractile proteins, profound sarcomere disarray, significantly reduced heart rates and decreased fractional shortening, all of which allude to the critical role played by microRNAs in normal cardiac function and under pathological conditions. Similarly, conditional *Dicer* gene deletion in the myocardium of both juvenile mice results in premature death within a week[65]. In adult mice, the conditional loss of

Dicer induced spontaneous cardiac remodeling along with profound biventricular enlargement, myocyte hypertrophy, myofiber disarray, ventricular fibrosis and strong induction of fetal gene expression. This further demonstrates the importance of microRNAs indicating that modifications in their biogenesis has major cardiovascular implications.

Two highly expressed microRNAs in the heart are miR-1 and miR-133 that are clustered together on the same chromosomal loci[66]. There two miR-1 variants, miR-1-1 and miR-1-2 and 3 miR-133 variants, miR-133a-1, miR-133a-2, miR-133b. Deep sequencing of microRNAs in the heart show that miR-1 is the most highly expressed microRNA accounting for 40% of all microRNAs[67]. MEF2 and SRF cooperatively regulate the two bicistronic microRNA clusters encoding miR-133a-1/ miR-1-2 and miR-133a-2/miR-1-1 in cardiac and skeletal muscle[68,69]. The two miR-1 variants, miR-1-1 and miR-1-2 are cardiac and skeletal-muscle specific and are expressed in a chamber specific manner during cardiogenesis[68]. Both variants are direct targets of muscle differentiation factors SRF, myocardin and MEF2 thus negatively regulating ventricular cardiomyocyte proliferation[70]. MiR-1 directly targets the transcription factor Hand2 that promotes ventricular cardiomyocyte expansion and titrates the level of regulatory proteins to balance differentiation and proliferation during cardiogenesis. The targeted deletion of miR-1-2 in mice leads to a spectrum of abnormalities like ventricular septal defects leading to early lethality or cardiac rhythm disturbances and myocyte hyperplasia[71]. Similarly, the deletion of miR-133a-1 and miR-133a-2 in mice causes lethal ventricular septal defects in half of the mutant embryos and the rest die from DCM and heart failure[72]. The absence of miR-133a expression results in ectopic expression of smooth muscle genes in the heart and aberrant cardiomyocyte proliferation due to elevated expression of miR-133a targets, SRF and cyclin D2.

1.3.1 MicroRNAs in the failing heart

Heart failure is associated with common histological features of myocyte hypertrophy and death, due to compensatory pathological remodeling and minimal functional repair with microRNA involvement. Pathological cardiac remodeling induces a signature pattern of stress responsive microRNAs leading to cardiac hypertrophy and heart failure[73,74]. MiR-1 and miR-133 are both downregulated in cardiac hypertrophy[75,76]. MiR-1 directly targets a number of growth promoting factors like Ras GTPase activating protein (RASA1), cyclin-dependent kinase 9 (CDK9), Ras homolog enriched in brain (RHEB), and fibronectin that are upregulated upon miR-1 downregulation during induction of hypertrophy[75], Overexpression of miR-133 or miR-1 *in vitro*

inhibited cardiac hypertrophy while antagomir based inhibition of miR-133 *in vivo* caused marked and sustained cardiac hypertrophy[76]. MiR-133 also targets several proteins like Ras Homolog Family Member A (RHOA), Cell division control protein 42 homolog (CDC42) and Negative elongation factor A (NELFA).

The loss of a cardiac specific microRNA, miR-208, in mice during pressure overload, protected them against cardiac hypertrophy and upregulation of β-MHC induced hypothyroidism due to the activation of calcineurin signaling[59]. MiR-21 is one of the most significantly upregulated miRNAs in cardiac hypertrophy[73]. AntagomiR-21 based intervention results in antihypertrophic and antifibrotic effects and improved function following hypertrophic stress due to reduced activation of ERK/MAPK cascade[77]. Another microRNA family namely, the miR-199 family of miRNAs are also upregulated in cardiac hypertrophy[78]. MiR-199b is induced by prohypertrophic calcineurin/ NFAT signaling cascade in mouse and human heart failure and targets the nuclear NFAT kinase dual-specificity tyrosine-(Y)-phosphorylation regulated kinase 1a (DYRK1A)[79]. Overexpression of miR-199b in mice show reduced DYRK1A expression with increased sensitivity to pressure overload and calcineurin/NFAT signaling. Antagomir based inhibition of miR-199b *in vivo* reduced NFAT activity and reversed hypertrophy and fibrosis. Hence miR-199b is part of a pathogenic feedforward mechanism involved in pathological cardiac hypertrophy.

1.4 MicroRNA-378

MiR-378 is encoded within the first intron of the gene *Ppargc1b* (Fig 5). The 3' strand of the microRNA was reported to be the predominant one compared to the 5' strand and was initially annotated as miR-422b[80] and was later renamed as miR-378 or miR-378-p and correspondingly the opposite strand was annotated as miR-378* or miR-378-5p. In humans, 11 variants of miR-378 have been annotated so far (called miR-378a-3p/b/c/d/e/f/g/h/i/j and miR-422a). These variants are encoded by different genomic loci but share identical seed sequences. MiR-378 family of miRs are evolutionarily conserved between humans and several other species.

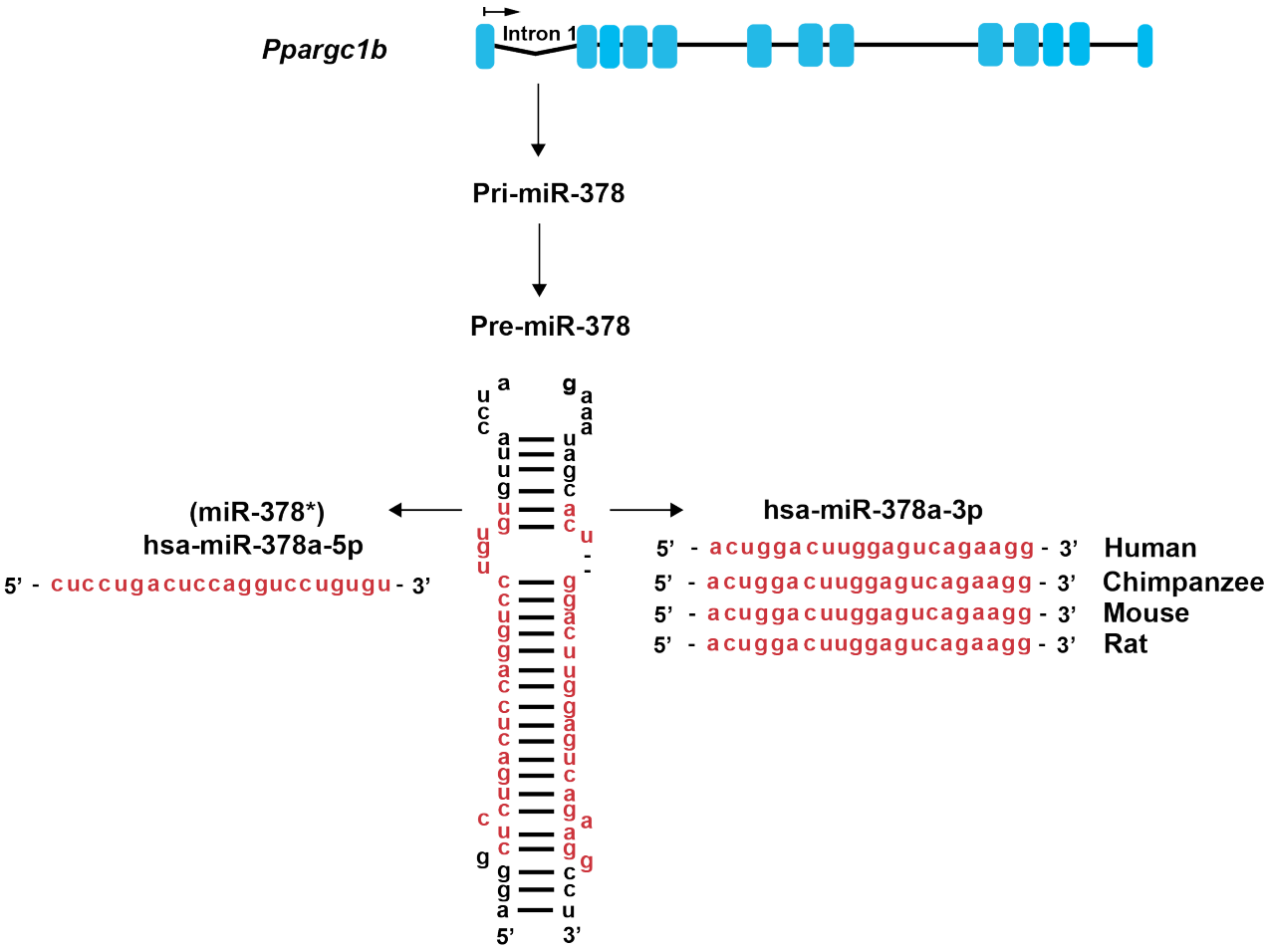

Fig 5: Schematic representation of the *Ppargc1b* locus indicating the location of miR-378 in the first intron and its evolutionary conservation.

Initial studies with miR-378 show that it functions as an oncogene by promoting tumor growth and angiogenesis[81]. Overexpression of miR-378 in grafts of glioblastoma cells enhanced cell survival, reduced caspase-3 activity and repressed two tumor suppressors, suppressor of fused homolog (SUFU) and fused in sarcoma 1 (FUS1) leading to increased growth and vascularization of tumors. Interestingly, in this study the authors studied the 5p strand i.e. miR-378-5p. miR-378 also promotes oncogenic cellular transformation *in vitro* by targeting and repressing the antiproliferative transcription factor TOB2 that represses the proto-oncogene cyclin D1[82]. The transcription factor c-Myc activates a complex cascade of targets including miR-378 ultimately leading to cellular transformation through the functional module of miR-378-TOB2-cyclin D1 that mediates the cross talk between Myc and RAS signaling.

The role of miR-378 in the heart is currently not completely clear. Two *in vitro* studies describe conflicting roles of miR-378 in apoptosis. MiR-378 is significantly downregulated in myocardial infarction in rat[83]. Overexpression of miR-378 in H9C2 cells attenuated ischemia-induced apoptosis by inhibiting caspase-3. The second study focussed on primary neonatal rat cardiomyocytes, where

overexpression of miR-378 increased apoptosis by direct targeting of IGF1R and reduced signaling in the AKT cascade[84]. Also, the inhibition of miR-378 using antimir protected the myocytes against H_2O_2 and hypoxia reoxygenation-induced cell death by promoting IGF1R expression and AKT signaling cascade.

1.5 MicroRNA therapeutics

MicroRNAs have prominent biological functions and form an intrinsic part of cardiovascular function. Manipulation of microRNA expression and function in the body by means of mimics, recombinant viral vectors or antagomirs can have profound therapeutic affect. A promising means of enhancing microRNA expression or replacing downregulated microRNAs is through adeno-associated viruses (AAVs). The availability of a variety of AAV serotypes with varying degrees of tissue enrichment due to their natural tropism towards different tissues and cell types based the presence of specific cellular receptors[85]. AAV type 6 and type 9 have been described to display tropism for skeletal muscle and heart respectively[86].

1.5.1 Adeno-associated viruses

AAVs are human parvoviruses. They are nonpathogenic, non enveloped DNA viruses containing a linear single stranded genome of 4.6 - 4.8 kb and require coinfection with a helper virus for viral replication[87,88]. During infection the AAV DNA gets uncoated and converted to a duplex form that is then integrated into the host cellular DNA in a site specific manner[89]. The AAV genome contains two open reading frames encoding alternatively spliced capsid (Cap) proteins and multifunctional replication (Rep) proteins and are flanked by 145 base pair inverted terminal repeats (ITRs)[90,91]. Recombinant AAVs for targeted gene transfer can be generated through a plasmid vector containing the therapeutic gene cassette flanked by the ITRs with the total size of less than 5 kb for efficient packaging. The recombinant AAVs have been shown to persist for extended durations in the form of episomes after transduction[92]. The absence of viral coding sequences renders AAV vectors highly suitable gene targeting vehicles due to limited toxicity or inflammatory responses except for the generation of neutralizing antibodies that may limit re-administration[90].

1.6 Aim of the study

The aim of this study was to characterize the role of miR-378 in cardiomyocytes and its relevance in the diseased myocardium. To this end, the following points were investigated:

1. Expression profiling: The expression of miR-378 was investigated in human and mouse myocardium in physiological as well as diseased state. MiR-378 expression was also determined in isolated myocardial cells namely, cardiomyocytes and cardiac fibroblasts.
2. Relevance in cardiac hypertrophy: The relevance of miR-378 in cardiomyocyte hypertrophy was investigated by the overexpression of synthetic miR-378 mimics and by the inhibition of endogenous miR-378 in primary cardiomyocytes. An *in vivo* mouse model of pressure overload hypertrophy was used to investigate the role of miR-378 in mouse hearts.
3. Determination of miR-378 targets: Targets of miR-378 were determined using expression profiling and confirmed by studying the regulation of their mRNA and protein levels. Direct interaction of these targets with miR-378 was determined through 3' UTR reporter assays with native and mutated miR-378 binding sites. The functional relevance of the targets of miR-378 in cardiac hypertrophy was determined using shRNA and siRNA-based interference in primary cardiomyocytes.
4. *In vivo* relevance of miR-378: The physiological role miR-378 was investigated in a pressure overload mouse model of hypertrophy by cardiotropic overexpression of miR-378 using adeno-associated virus 9. The resulting effect on cardiac hypertrophy and cardiac function as well as on the targets of miR-378 was investigated.

2 MATERIALS

2.1 Antibodies

Epitope	Host	Reference
Anti-KSR1	Mouse	#611576, BD Biosciences
Anti-MAPK1/3	Rabbit	#9102, Cell Signaling
Anti-PhosphoMAPK1/3	Rabbit	#9101, Cell Signaling
Anti-IGF1R	Rabbit	#3027, Cell Signaling
Anti-GRB2	Rabbit	#3972s, Cell Signaling
Anti-HSP90	Mouse	sc-13119, Santa-Cruz
Anti-α-Actinin	Mouse	A7811, Sigma-Aldrich
HRP-anti-mouse IgG (Secondary antibody)	Goat	115-035-003, Jackson Immunoresearch Laboratories
HRP-anti-rabbit IgG (Secondary antibody)	Goat	111-035-144, Jackson Immunoresearch Laboratories
AlexaFluor 488 anti-mouse IgG (Secondary antibody)	Goat	A11029, Life Technologies

2.2 Bacterial strains

Strain	Genotype	Manufacturer
***E. coli* DH10B (Electrocompetent)**	F- mcrA Δ(mrr-hsdRMS-mcrBC) φ80lacZ ΔM15 ΔlacX74 recA1 endA1 araD139 Δ(ara, leu)7697 galU galK λ - rpsL nupG tonA	Life Technologies

2.3 Buffers and media

BSA Blocking buffer:	Tris-HCl pH 7.5	50 mM
	NaCl	150 mM
	BSA	2% (m/v)
	Nonidet P40	0.2% (v/v)
	NaN_3	0.03% (m/v)
BSA Washing buffer:	Tris-HCl pH 7.5	50 mM
	NaCl	150 mM
	BSA	0.5% (m/v)

	Nonidet P40	0.2% (v/v)
CBFHH medium:	NaCl	137 mM
	KCl	5.36 mM
	$MgSO_4.7H_2O$	0.81 mM
	Dextrose	5.55 mM
	KH_2PO_4	0.44 mM
	$Na_2HPO_4.7H_2O$	0.34 mM
	Adjust pH to 7.3	
BrdU stock:	BrdU	230 mg
	ddH_2O	74.8 ml
DNA loading buffer (5x):	Xylene cyanol	10 g
	0.5 M EDTA	1.4 ml
	Glycerol	3.6 ml
	ddH_2O	up to 1 l
Laemmli buffer (2x):	Tris-HCl 1M pH 6.8	12.5 ml
	SDS 10%	40 ml
	Glycerol	30 ml
	β-mercaptoethanol	1 ml
	Bromophenol blue	traces
LB agar:	Peptone	10 g
	Yeast extract	5 g
	NaCl	5 g
	Agar	15 g
	1 M NaOH	1 ml
	ddH_2O	up to 1 l
LB medium:	Peptone	10 g
	Yeast extract	5 g

	NaCl	5 g
	1 M NaOH	1 ml
	ddH2O	up to 1 l
Lower buffer 4x:	Tris	182 g
	SDS 10%	40 ml
	ddH_2O	up to 1 l
	Adjust pH to 8.8 with HCl	
NRCM incomplete medium:	MEM	10.7 g
	$NaHCO_3$	0.35 g
	Vitamin B12 67% (w/v)	1 ml
	ddH_2O	up to 1 l
	Adjust pH to 7.3 and sterile filtered the solution	
NRCM pre-plating medium:	NRCM incomplete medium	94 ml
	Penicillin/Streptomycin	1 ml
	FCS	5 ml
NRCM culturing medium:	NRCM incomplete medium	93 ml
	Penicillin/Streptomycin	1 ml
	FCS	5 ml
	BrdU stock	1 ml
P1 buffer:	Tris	50 nM
	EDTA	10 nM
	pH 8.0	
	Rnase I (after autoclaving)	100 mg
P2 buffer:	NaOH	200 mM
	SDS	1%

P3 buffer:	Potassium acetate	3M
	pH 5.5	
PBS (10x):	NaCl	80 g
	KCl	2 g
	$Na_2HPO_4.7H_2O$	11.5 g
	KH_2PO_4	2 g
	ddH_2O	up to 1 l
Running buffer (10x):	Tris-HCl	30 g
	Glycine	144 g
	SDS	15 g
	ddH_2O	up to 1 l
SDS lysis buffer:	Tris (1M pH 6.7)	50 mM
	SDS	2 %
	Na_3VO_4	1 mM
	Complete mini	1 tablet per 10 ml
	PhosStop	1 tablet per 10 ml
Sirius Red solution(0.01%):	Direct Red 80	50 mg
	ddH_2O	15 ml
	Sterile filteration	
	Piric acid-solution 1.3%	485 ml
TAE buffer (50x)	Tris	242 g
	Acetic acid	57.1 ml
	Na2EDTA.2H2O	37.2 g
	ddH_2O	up to 1 l
Transfer buffer	Tris (1M pH 8.3)	25 ml
	Glycine	11.26 g
	Methanol	100 ml

	ddH_2O	up to 1 l
Upper buffer (4x):	Tris	61 g
	SDS 10%	40 ml
	ddH_2O	up to 1 l
	Adjust pH to 6.7 with HCl	

2.3 Chemicals

The chemicals used in this study were obtained from AppliChem, Carl Roth, Merck and Sigma-Aldrich unless otherwise mentioned.

2.4 Enzymes

Kit	Manufacturer
Accuprime Pfx DNA Polymersase	Life Technologies
Benzonase	Merck
Collagenase II	Worthington
Difco Trypsin 250	BD Biosciences
DNase	Sigma-Aldrich
Gateway BP Clonase II Enzyme mix	Life Technologies
Gateway LR Clonase II Enzyme mix	Life Technologies
Platinum Taq DNA Polymerase	Life Technologies
Proteinase K	Fermentas
Restriction Endonucleases	New England Biolabs
Superscript II Reverse Transcriptase	Life Technologies
T4 DNA Ligase	New England Biolabs
Trypsin	Gibco
Trypsin 1:250	PAN

2.5 Kits

Kit	Manufacturer
Adeno-X purification kit	Clontech
Adeno-X Rapid titer kit	Clontech
BCA Protein assay kit	Thermo Scientific
BLOCK-iT U6 RNAi Entry vector kit	Life Technologies
ECL plus	Thermo Scientific
Plasmid Maxi/Endofree Maxi kit	Qiagen
Promega Dual Luciferase assay kit	Promega
TaqMan MicroRNA assay (hsa-miR-378a-3p)	Life Technologies
TaqMan MicroRNA assay (hsa-miR-1)	Life Technologies
TaqMan MicroRNA assay (hsa-miR-133a)	Life Technologies
TaqMan MicroRNA assay (U6 snRNA)	Life Technologies
TaqMan MicroRNA Reverse Transcription kit	Life Technologies
TaqMan Universal PCR Master Mix, No AmpErase UNG	Life Technologies
SYBR Green qPCR Master mix	Roche
QIAquick Gel Extraction kit	Qiagen
***In situ* Cell Death Detection kit, Fluorescein**	Roche
QuikChange II Site directed Mutagenesis kit	Stratagene

2.6 Plasmids*

Vector	Insert	Reference
pENTR/U6		Life Technologies
pAd/CMV/V5-DEST30		Life Technologies
pAD-BlockIT-Dest		Life Technologies
pAD-BlockIT-Dest	shRNA-*Mapk1*	pAd-adeno-sh*Mapk1*
pAd/CMV/V5-DEST30	shRNA-control	pAd-adeno-shctrl
pmiR-RL-TK2		Gunter Meister (University of Regensburg)
pmiR-RL-TK2	*Mapk1* 3' UTR (Rat)	pmiR-RL-Mapk1
pmiR-RL-TK2	*Igf1r* 3' UTR (Human)	pmiR-RL-Igf1r
pmiR-RL-TK2	*Ksr1* 3' UTR (Human)	pmiR-RL-Ksr1
pmiR-RL-TK2	*Grb2* 3' UTR (Human)	pmiR-RL-Grb2

2.6 Primers†

The following oligonucleotide primers were obtained from MWG Eurofins and diluted with nuclease free water to a stock concentration of 1 mM.

Gene	Sequence (5' - 3')
Nppa	CTCCCAGGCCATATTGGAĠ (forward)
	TCCAGGTGGTCTAGCAGGTT (reverse)
Nppb	TGGGAAGTCCTAGCCAGTCTC (forward)
	TCTGAGCCATTTCCTCTGAĆ (reverse)
Myh7	GGATGACGTTACCTCCAACA (forward)
	GTGTCTCCTCAGCCTTGCTC (reverse)
Actb	CTCTGAACCCTAAGGCCAAC (forward)
	ACCAGAGGCATACAGGGACA (reverse)
Mapk1	TCTCCCGCACAAAAATAAGG (forward)
	GCCAGAGCCTGTTCAACTTC (reverse)
Igf1r	AGCCATGGTGAGAAGACC (forward)

* These plasmids were published in Ganesan *et al.* Circulation 2013 (169)

† These primers were published in Ganesan *et al.* Circulation 2013 (169)

Gene	Sequence (5' - 3')
	CGCACACGCCTTTGTAGTAG (reverse)
Grb2	GGGGATTTCTCCCTGTCAGT (forward)
	CTGTTCTATGTCCCGGAGGA (reverse)
Ksr1	CCAAGGCCCTAACCAAGAAG (forward)
	GGAAGTTGAACCTGCTGTCC (reverse)
Med13	TTTACCACCTCAACTTCCAAA (forward)
	AAGGCTTCTTACACTGCACCA (reverse)
Crat	AACGCCTACAGAAGGGACTG (forward)
	GGGCTGGAGTAGATGACCAC (reverse)
shRNA-*Mapk1*	CACCGTATTATGACCCAAGTGATGAGCGAACTCATCA CTTGGGTCATAATA (top strand)
	AAAATATTATGACCCAAGTGATGAGTTCGCTCATCACT TGGGTCATAATAC (bottom strand)
***Mapk1* 3' UTR (native)**	AAAAAAACTAGTTTCTTGACCCTGGTCCTGT (forward)
	TTTTTTGAGCTCCCACTGCATCTTTCAAAC (reverse)
***Mapk1* 3' UTR (Mutated)**	CTTTCACGGAATTCTTCAACGTCGAGAGTTCTCCTGC ACCAGGCCCTG (forward)
	CAGGGCCTGGTGCAGGAGAACTCTCGACGTTGAAGA ATTCCGTGAAAG (reverse)
***Igf1r* 3' UTR (native)**	TCACTCATTTTTATGTCCCAC (forward)
	TTTTTTGAGCTCACAAACATTTTATAA (reverse)
***Igf1r* 3' UTR (Mutated)**	CACTCATTAGCGTTTTCAATAGGGCTCTTAAACGTCGT AGATTACGGGTAGTCAGTTGACGAAGATCTGG (forward)
	CCAGATCTTCGTCAACTGACTACCCGTAATCTACGAC GTTTAAGAGCCCTATTGAAAACGCTAATGAGTG (reverse)
***Ksr1* 3' UTR (native)**	AAAAAAACTAGTATTCTTGTTTTTG (forward)
	TTTTTTGAGCTCATGGCCAAC (reverse)
***Ksr1* 3' UTR (Mutated)**	GGTTTGGCTTGGGCGTCCTGGAACGTAGTAATCCAAA GATGTAGCCAGCC (forward)
	GGCTGGCTACATCTTTGGATTACTACGTTCCAGGACG CCCAAGCCAAACC (reverse)
***Grb2* 3' UTR (native)**	AAAAAAACTAGTCTGCCTCCCTTCAGTGTCTC (forward)
	AAAAAAGAGCTCCTGCCAGCTCCTTTCTCTGT (reverse)

Gene	Sequence (5' - 3')
***Grb2* 3' UTR (Mutated)**	GAGTGGTGTCTTTACCTTTTTTATTTTTTTAAATAAGTT AAAGATAACGTCGAGCTTTTCAGTTGATTAGTCTCCT ATCCTATGTACATATTTTCCTCTCAGGGCAGGAGAAAG AGG (forward)
	CCTCTTTCTCCTGCCCTGAGAGGAAAATATGTACATAG GATAGGAGACTAATCAACTGAAAAGCTCGACGTTATC TTTAACTTATTTAAAAAAATAAAAAAGGTAAAGACAC CACTC (reverse)

2.6 Small interfering RNAs (siRNAs)‡

The following cocktail of ON-TARGETplus SMARTpool siRNAs were ordered from Thermo Scientific:

Gene	Name	Target Sequence
***Mapk1* (Rat)**	*si-Mapk1*	ACACUAAUCUCUCGUACAU AAAAUAAGGUGCCGUGGAA UAUACCAAGUCCAUUGAUA UCGAGUUGCUAUCAAGAAA
***Ksr1* (Rat)**	*si-Ksr1*	GAGUUAGGCACUACGCAAA CCACUAAUAGGGACCGUUA GGGAAGGAGUAAAGCGUGU GUGAUGAACUACCGGCAGA
***Igf1r* (Rat)**	*si-Igf1r*	GGGCCAAACUUAACCGUCU CCGGAUAACUGCCCCGAUA GGGAAAAUGUACUUCGCUU CAACAGGACACUCGAGAAU
***Grb2* (Rat)**	*si-Grb2*	ACUCCAAUGACUUCGUAAA CAGUGAACCGGAACGUCUA GCCUCUAACUUCUGCGAAU GGACUAGAGGAGCCGGAUU

2.6 Viruses

Vector	Insert	Virus	Final construct	Reference
pAD-BlockIT-Dest	shRNA-*Mapk1*	Adenovirus	Adeno-sh*Mapk1*	
pAd/CMV/V5-DEST30	shRNA-control	Adenovirus	Adeno-shctrl	D. Ramanujam

‡ These siRNAs were published in Ganesan *et al.* Circulation 2013 (169)

Vector	Insert	Virus	Final construct	Reference
pAAV-MCS-Adapted	hsa-miR-378a	Adeno associated virus 9 (AAV9)	AAV9-CMV-miR-378	L. Zentilin (ICGEB, Trieste, Italy)
pAAV-MCS-Adapted	GFP	Adeno associated virus 9 (AAV9)	AAV9-CMV-GFP	

3 METHODS§

3.1 Cell culture

3.1.1 Isolation of neonatal rat cardiomyocytes *

Neonatal rat cardiomyocytes (NRCM) were isolated from 1 – 2 day old Sprague Dawley rat pups using Collagenase II and Pancreatin enzymes. The isolation procedure was performed under sterile conditions. Briefly, the hearts from the pups were explanted and placed on ice in a tube containing 15 ml of ice cold CBFHH. After trimming away the vessels and atria, the hearts were minced using micro scissors by cutting each heart 7 – 12 times. The minced hearts were then transferred to a 50 ml beaker with 15 ml enzyme solution (0.6 mg/ml Pancreatin and 0.4 mg/ml Collagenase II), covered and placed in a shaker set at 37°C with constant shaking at 220 rpm for 5 minutes. After 5 minutes the enzyme solution was discarded since it mostly contained erythrocytes. Serial digestions were then performed first for 20 minutes, second and third for 25 minutes, fourth for 15 minutes and finally the fifth digestion for 10 minutes. After each digestion the cell suspension was immediately mixed with 2 ml FCS and centrifuged at 1200 rpm for 5 minutes. The resulting pellet was suspended in 4 ml FCS and incubated at 37°C/1% CO_2. After performing all the serial digestions, the FCS suspension containing all the cells were centrifuged again at 1200 rpm for 5 minutes. The resulting pellet was resuspended in 10 ml *pre-plating* medium and filtered (40 µM pore size, BD). The filtrate was then mixed in 40 ml *pre-plating* medium (pre warmed to 37°C). Approximately 15 ml of the medium containing cells was plated onto a 10 cm dish and incubated for 90 minutes at 37°C/1% CO_2 to enable the separation of cardiomyocytes and cardiac fibroblasts. During pre plating the cardiac fibroblasts adhere to the cell culture dish while the cardiomyocytes stay in the supernatant. After 90 minutes the supernatant containing cardiomyocytes is collected in a 50 ml tube and the cardiomyocyte number is quantified by mixing 50 µl cell suspension with 50 µl Tryphan blue. 10 µl of this mixture is used to quantify the cell number (Countess cell counter, Life

§ Parts of this section were published with some modifications in Ganesan *et al.*Circulation 2013 (169)

* Protocol modified from Abcam

Technologies). The cells are then mixed in 5% NRCM medium and plated as required and incubated at 37°C/1% CO_2.

3.1.2 MicroRNA transfection

MicroRNA transfection was performed one day after isolation of primary neonatal rat cardiomyocytes. Prior to the transfection procedure, the medium was exchanged to 5% FCS containing NRCM medium without antibiotics. 50 nM of miR-378 mimic or antimiR-378 along with their respective controls was transfected into NRCM using Lipofectamine 2000. The medium was exchanged to 0.1% FCS containing NRCM medium after 6 hours.

3.2 RNA Analysis

3.2.1 Isolation of RNA

RNA was isolated from NRCM and myocardium using TriFast (Peqlab) according to the manufacturer's instruction. The resulting RNA pellet was suspended in nuclease free water and the concentration was determined using Nanodrop spectrophotometer ND1000 (Peqlab).

3.2.2 Reverse transcription

The Reverse transcription-PCR (RT-PCR) is the preferred technique used to detect and quantify mRNA. The first part of the reaction, reverse transcription, synthesizes cDNA from RNA. The second step amplifies the synthesized cDNA to easily detectable levels. To reverse transcribe the poly(A)-containing mRNAs, Oligo (dT) primers (MWG) were used to prime reverse transcription reactions for cDNA synthesis. A control reaction (RT control) with RNA pooled from all the samples, excluding Reverse transcriptase was also included. The resulting cDNA was then used for quantitative real time PCR analysis. The following procedure was used for the cDNA synthesis:

Reagent	Volume
RNA	1 µg
Oligo(dT) primer (10mM)	2 µl
Nuclease free water	upto 11.9 µl
Incubation for 10 minutes at 70°C	
5x First strand buffer	4 µl
0.1M DTT	2 µl
10mM dNTPs	1 µl
RNase Inhibitor	0.1 µl
Reverse transcriptase	1 µl
Incubation for 1 hour at 42°C	
Incubation for 10 minutes at 70°C	
Nuclease free water	upto 100 µl (10 ng/µl concentration)

3.2.3 Quantitative real time PCR

Quantitative real time PCR follows the general principle of polymerase chain reaction; its key feature is that the amplified DNA is quantified as it accumulates in the reaction in real time after each amplification cycle. Two commons methods of quantification are the use of fluorescent dyes (*SYBR* Green) that intercalate with double-stranded DNA and modified DNA oligonucleotide probes (*TaqMan* probes) that fluoresce when hybridized with a complementary DNA.

3.2.3.1 *SYBR* Green-based real time PCR

To detect mRNA regulation, quantitative real time PCR was performed with *SYBR* Green as the detected fluorophore and *ROX* as the passive reference dye. In the PCR reaction, the unbound *SYBR* Green exhibits little fluorescence. The fluorescence is substantially enhanced when the dye is bound to double stranded DNA. The threshold cycle (C_t) reflects the cycle number at which the fluorescence generated within a reaction crosses the threshold. The comparative C_t method was used to quantify the results of the PCR. An average C_t value was first calculated from triplicate reactions, which was then normalized (to adjust for differences in the amount of cDNA in each reaction) to average C_t values of a control gene. The comparative C_t method is also known as the $2^{-\Delta\Delta C_t}$ method, where $\Delta\Delta C_t = \Delta C_{t,sample} - \Delta C_{t,reference}$. The reactions were stored on ice during the preparation of the PCR plate. Each reaction was performed in triplicate. Along with the samples, two additional control reactions were also included during every PCR. First, was a no transcript control i.e a reaction with water instead of cDNA and second, a reverse transcription control (RT

control) i.e control reaction from reverse transcription PCR without reverse transcriptase enzyme. The RT control reaction was included to check for genomic DNA contamination.

Each reaction consisted of the following:

Reagent	Volume
FastStart Universal SYBR Green master mix	6.25 µl
5' (forward) Primer (20 pmol/µl)	0.25 µl
3' (reverse) Primer (20 pmol/µl)	0.25 µl
cDNA	5 ng
Nuclease free water	Upto 12.5 µl

The following thermal cycling program was used (StepOnePlus, Applied Biosystems):

Stage	Step	Temperature	Time	Cycles
Stage 1	**Taq activation**	94°C	2 min	1x
Stage 2	**Denaturation**	94°C	20 sec	40x
	Annealing	56°C	20 sec	
	Extension	65°C	40 sec	
Stage 3		65°C	1 min	1x
Stage 4		95°C	15 sec	1x
		60°C	15 sec	
		95°C	15 sec	
Stage 5		20°C	2 min	1x

3.2.3.2 *TaqMan probe* based real time PCR for microRNA detection

The *TaqMan MicroRNA Assay* (Applied Biosystems, New Jersey, USA) was used to quantify microRNA expression. *TaqMan* probes depend on the 5'-nuclease activity of the DNA polymerase used for PCR to hydrolyze an oligonucleotide that is hybridized to the target amplicon. The assay uses looped-primer for reverse transcription PCR to specifically detect mature microRNAs. It involves two steps:

I. Reverse transcription step: In this step, cDNA is reverse transcribed from the total RNA using microRNA specific looped-primers.

II. Quantitative real time PCR step: In this step, PCR products are amplified from the cDNA using a *TaqMan MGB* probe. The *TaqMan MGB* probe contains a reporter dye (*FAM™*) linked to the 5' end, a minor groove binder (MGB) at the 3' end and a non fluorescent quencher at the 3' end of the probe. During the PCR reaction, the DNA polymerase cleaves the probes that are bound to the target resulting in the separation of the reporter dye from the quencher leading to an increase in fluorescence which is quantified using the comparative $\Delta\Delta C_t$ method.

The two steps were performed according to manufacturer's instructions.

Reverse transcription:

Reagent	Volume
RT Buffer	1.5 µl
100mM dNTPs	0.15 µl
RNase Inhibitor	0.19 µl
Reverse transcriptase	1 µl
5x RT primer	3 µl
RNA (2ng/µl)	5 µl
Nuclease free water	4.16 µl
Incubation for 30 minutes at 16°C	
Incubation for 30 minutes at 42°C	
Incubation for 5 minutes at 85°C	

Quantitative real time PCR:

Reagent	Volume
2x TaqMan Universal PCR master mix II, no UNG	10 µl
20x TaqMan probe	1 µl
cDNA	1.33 µl
Nuclease free water	7.67 µl

The following thermal cycling program was used (StepOnePlus, Applied Biosystems):

Stage	Step	Temperature	Time	Cycles
Stage 1	Taq activation	95°C	10 min	1x
Stage 2	Denaturation	95°C	15 sec	40x
	Annealing/ Extension	60°C	60 sec	
	Extension	65°C	40 sec	

3.3 DNA analysis

3.3.1 Gel electrophoresis

Agarose gel electrophoresis was used to separate DNA fragments according to their lengths. Electrophoresis enables the separation of the negatively charged nucleic acid molecules through an agarose matrix according to their sizes. Ethidium bromide was used to visualize the separated DNA fragments under UV light (312 nm). 1.5% agarose gel was prepared by dissolving 1.5 g of agarose in 100 ml of 1x TAE buffer by boiling for 2 minutes. The solution was allowed to cool down to 40°C before adding 10 µl of Ethidium bromide (1 mg/ml) to it. The solution was then poured into trays (Peqlab) and allowed to set. The tray was then placed into the electrophoresis chamber filled with 1x TAE. The DNA samples were mixed with 2 - 5 µl of loading buffer and allowed to run for 45 minutes at 120 V. To distinguish the length of the DNA fragments, 1 kb and 100 bp DNA ladders (25 ng/µl, NEB) were run along with the samples. The gel was then visualized under UV lamp. The DNA fragments of the required size were extracted from the agarose gel using *QIAquick Gel Extraction Kit* (Qiagen) according to the manufacturer's instruction.

3.3.2 Transformation of plasmid DNA into *E. coli*

Plasmid DNA was transformed into electrocompetent *E. coli* cells (DH10B). Electrocompetent *E.coli* DH10B cells were thawed on ice and 1 – 2 µl of plasmid DNA was added to 50 µl of the cells. The suspension was mixed, transferred into Gene Pulser 0.1 cm cuvettes (Bio-rad) and a short 1.8 kV electromagnetic pulse was applied using the Bio-rad micropulser. The electroporated cell suspension was mixed with 250 µl of LB medium, transferred into an 1.5 ml microfuge tube and was incubated at 37°C and 350 rpm in a thermomixer (Eppendorf) for 1 hour. 50 – 150 µl of the cell suspension was then plated on LB plates containing the corresponding antibiotic (33 µg/µl Kanamycin or 100 µg/µl Ampicillin). The plates were incubated overnight.

3.3.3 DNA sequence analysis

2 µg of plasmid DNA was diluted to a final volume of 20 µl and the primers at a concentration of 10 pmol/µl in a volume of 10 µl was sent to MWG Eurofins Operon for sequencing. The sequencing results were analyzed using the software eBIOX. *In silico* handling of DNA sequences for the cloning experiments were performed using the softwares - Gene Construction Kit (Textco), MacVector 12.0.6 and Serial Cloner 2.

3.3.4 Mini plasmid DNA purification

Clones were picked from LB agar plates after transformation and inoculated in 5 ml LB broth with the respective antibiotic. The cultures were incubated at 37°C and 180 rpm until the exponential growth phase (8 - 12 hours). 1.5 ml of the log phase culture was centrifuged at 13000 rpm for 2 minutes to spin down the cells. The cell pellet was resuspended in 250 µl of buffer P1, followed by the addition of 250 µl of buffer P2 and 5 min incubation at RT. To this, 300 µl of neutralization buffer P3 was added and centrifuged at 13000 rpm and 4°C for 10 minutes. The supernatant was collected and plasmid DNA was precipitated by the addition of 750 µl of isopropanol and 10 minute centrifugation at 13000 rpm and 4°C. The pellet was washed twice with 70% ethanol, air dried and suspended in 20 µl of nuclease free water.

For maxi cultures, 100 µl of mini culture was inoculated in 100 - 200 ml LB medium with the corresponding antibiotic and incubated overnight at 37°C accompanied by rigorous shaking. Plasmid DNA was purified from these cultures using the Maxi DNA purification kit/Endofree Maxi DNA purification kit (Qiagen).

3.4 Protein analysis

3.4.1 Preparation of protein lysates

Tissues (50-100 mg) were homogenized in 800 µl of protein lysis buffer protease and phosphatase inhibitors (Roche). In the case of adherent cells such as NRCM and NRCF, the stimulated cells were washed with PBS and 250 µl of cold protein lysis buffer was added to the plates. The cells were scraped using a cell scraper and the lysates were transferred into a 1.5 ml tube. The cell lysates were then sonicated. The lysates were then incubated with 1/10th volume of 5% (v/v) Benzonase at RT for 10 min. Benzonase is a genetically engineered endonuclease which degrades all forms of nucleic acids (DNA, RNA). The tubes were then placed in an ultrasonic bath at 4°C for 5 min. The samples were then centrifuged at 12000 rpm for 20 min at 4°C to clear the lysates and were stored at -80°C until use.

3.4.2 Quantification of protein concentration

The concentration of the protein lysates was determined by the bicinchoninic acid colorimetric assay using the BCA protein assay kit (Thermo Scientific). The peptide bonds in the protein reduce the divalent copper ions to monovalent ions, which then chelates with the bicinchoninic acid to form a purple coloured complex with absorption maximum at 562 nm. The absorbance of the samples at 562 nm was measured using an Infinite 200 spectrophotometer (Tecan). The protein concentration was then evaluated with reference to serial dilutions of the internal calibration standard bovine serum albumin.

3.4.3 Western blot

8-12% polyacrylamide gels were used for the separation of proteins of different sizes.

Reagent	**Stacking gel**	**Separating gel**		
		8%	**10%**	**12%**
Acrylamide/ Bisacrylamide 30%/ 0.8% (v/v)	0.5 ml	4 ml	4.5 ml	5 ml
Lower buffer (4X)	-	3.8 ml	3.8 ml	3.8 ml
Upper buffer (4X)	1.25 ml	-	-	-
H_2O	3.2 ml	4.7 ml	4.2 ml	3.7 ml
Glycerol (80%)	-	2.5 ml	2.5 ml	2.5 ml
TEMED	6 µl	12 µl	12 µl	12 µl
APS(10%)	48 µl	72 µl	72 µl	72 µl

The gels were cast using the Mini-PROTEAN casting stand (Biorad). The samples were denatured by boiling at 95°C for 5 min. The gel electrophoresis chamber was filled with 1X running buffer, samples were loaded into the wells and 30 mA current per gel was applied at maximum voltage. The separated proteins on the gel were then transferred onto a PVDF membrane (Millipore) using wet transfer (Mini-PROTEAN transfer system, Biorad). The PVDF membrane was cut to the size of the mini-gel and was activated by immersing in methanol for 2 minutes. The membrane was then placed on the cassette facing the anode and the gel was placed facing the cathode side. The membrane and the gel were sandwiched between 1-2 layers of filter paper. The transfer was carried out at 385 mA current at maximum voltage for 90 min.

After the transfer process, the membrane was blocked with 5% BSA blocking buffer for 1-2 hours at RT on a horizontal shaker and then incubated with the following primary antibody overnight at

4°C: anti-KSR1 (#611576, BD Biosciences), anti-MAPK1/3 (#9102, Cell Signaling), anti-PhosphoMAPK1/3 (#9101, Cell Signaling), anti-IGF1R (#3027, Cell Signaling), anti-GRB2 (#3972s, Cell Signaling). A monoclonal anti-heat shock protein 90 (HSP90, sc-13119, Santa-Cruz) was used as a loading control. For detection of phosphoMAPK1/3, cells were stimulated for 10 min with 10 μM PE before lysis. After incubation, the membrane was washed three times with BSA washing buffer for 10 min at RT. The membranes were then incubated with the appropriate peroxidase-conjugated secondary antibodies (1:10000) at RT for 90 min. The membranes were again washed with the BSA washing buffer.

The proteins were detected by chemiluminescence. ECL Plus (GE Healthcare) was applied to the membrane according to the manufacturer's instructions. The signal was visualized using a Fujifilm LASmini4000 instrument (Fujifilm). The blots were then analyzed using the Multigauge software (Fujifilm).

3.5 Luciferase reporter assay

This assay is used to demonstrate a direct interaction of a microRNA with the 3' UTR of its target. Briefly, the 3' UTR of a target gene is cloned into the MCS located within the 3' UTR of Firefly Luciferase in the reporter construct, pmiR-RL-TK2 (a gift from Prof. Gunter Meister). A direct interaction between the microRNA and the binding site would result in decreased Firefly Luciferase activity. The vector also contains a second luciferase gene (Renilla) under the control of a different promoter for normalization purposes.

3.5.1 Cloning of 3' UTR

3.5.1.1 PCR amplification of 3' UTR

Primers were designed to amplify a 200 bp region from the 3' UTR of the target gene with the miR binding site in the middle. Restriction sites for *SpeI* and *SacI* were added to the forward and reverse primer respectively. To enable proper digestion a stretch of 4-8 bases was added to the 5' end of the primers before the restriction sites. The inserts were amplified from human uterus genomic DNA for human 3' UTR and rat cDNA for cloning the rat 3' UTR. Accuprime *Pfx* polymerase was used for the amplification of the inserts.

Reagent	Volume
10X Accuprime Pfx buffer	5 µl
Forward primer	20 pmol
Reverse primer	20 pmol
Template DNA	100 - 200 ng
Accuprime Pfx polymerase	2.5 units
Nuclease free water	upto 50 µl

The following thermal cycling program was used for amplification:

Stage	Step	Temperature	Time	Cycles
Stage 1	Polymerase activation	95°C	2 min	
Stage 2	Denaturation	95°C	15 sec	35 cycles
	Annealing/ Extension	55 - 65°C	20 sec	
	Extension	68°C	60 sec	
Stage 3	Final extension	68°C	5 min	

After the PCR, the PCR amplified products were run on a 1.5 % agarose gel for 45 minutes and visualized under UV light. The region of gel containing the amplicon was excised using a sterile scalpel in a microfuge tube.

3.5.1.2 Gel extraction of the insert

The amplified insert within the gel was extracted using the QIAquick gel extraction kit (Qiagen, Hilden). 3X volume of buffer QG was added to 1 volume of the gel and incubated at 50°C for 10 minutes. Next, 1X volume of isopropanol was added to the sample and mixed thoroughly. The samples were then added to the QIAquick spin columns and centrifuged for 1 minutes. The run through was discarded and the spin column was washed with PE buffer followed by an additional dry spin to ensure the complete removal all the flow through. The inserts were then eluted by the addition of nuclease free water to the spin column followed by a 1 minute centrifuge.

3.5.1.3 Restriction digestion

The insert and the vector were then digested using with the enzymes *SpeI* and *SacI* (New England Biolabs), followed by incubation at 37°C for minimum 2 hours.

Reagent	Volume
Purified insert/vector	30 µl/1 µg
SpeI	1 µl
SacI	2 µl
NEB Buffer 4	5 µl
BSA(100X)	0.5 µl
Nuclease free water	upto 50 µl

The restriction digestion products were then run on an agarose gel and the digested products were extracted using the QIAquick gel extraction kit. 1µl of the eluted product was again run on an agarose gel to estimate the relative concentration of the insert and the vector.

3.5.1.4 Ligation of the insert and vector

Overnight ligation at 16°C was performed using T4 DNA ligase (New England Biolabs).

Reagent	Volume
10X ligase buffer	1 µl
Vector DNA fragment	10 - 50 ng
Insert DNA fragment	5 - 250 ng
T4 DNA ligase	1 µl
Nuclease free water	upto 10 µl

After overnight ligation, the ligation reaction was deactivated by heating for 10 minutes at 65°C.

3.5.1.5 Transformation of the ligation product

3µl of the ligation reaction was transformed into electrocompetent *E. coli* cells (DH10B) and plated on LB agar plates with Ampicillin. The plates were incubated at 37°C overnight and the resulting colonies were amplified in LB broth with ampicillin followed by plasmid isolation. The clones were screened by restriction digestion with *SpeI* and *SacI* enzymes. The inserts were sequenced to ascertain proper cloning and the vector containing the insert was amplified using the Endofree Maxi kit (Qiagen).

3.5.2 Site directed mutagenesis

The miR binding site in the insert within the reporter construct were mutated using the Quikchange II site directed mutagenesis kit (Stratagene). The QuikChange II site-directed mutagenesis method is performed using PfuUltra^{TM} high-fidelity (HF) DNA polymerase for mutagenic primer-directed

replication of both plasmid strands. The basic procedure utilizes a supercoiled double-stranded DNA (dsDNA) vector with an insert of interest and two synthetic oligonucleotide primers, both containing the desired mutation. The oligonucleotide primers, each complementary to opposite strands of the vector, are extended during temperature cycling by PfuUltra HF DNA polymerase, without primer displacement. Extension of the oligonucleotide primers generates a mutated plasmid containing staggered nicks. Following temperature cycling, the product is treated with Dpn I. The Dpn I endonuclease is specific for methylated and hemimethylated DNA and is used to digest the parental DNA template and to select for mutation-containing synthesized DNA.

3.5.2.1 Mutagenic primer design

Forward and reverse primers containing the mutated miR binding sites in the middle (25-45 bp long) with a melting temperature (T_m) ≥ 78°C were designed for the mutagenesis reaction. The PCR reaction for the generation of the mutant strand was set up according to the following table:

Reagent	Volume
10X reaction buffer	5 µl
dsDNA template	5-50 ng
Oligonucleotide primer 1	125 ng
Oligonucleotide primer 2	125 ng
dNTP mix	1 µl
PfuUltra HF DNA polymerase	1 µl

The PCR was performed according to the following parameters:

Stage	Step	Temperature	Time	Cycles
Stage 1	Polymerase activation	95°C	30 sec	
Stage 2	Denaturation	95°C	30 sec	18 cycles
	Annealing/ Extension	55°C	1 min	
	Extension	68°C	60 sec/kb of plasmid length	
Stage 3	Final extension	68°C	5 min	

3.5.2.2 DpnI digestion and transformation

The PCR products were digested with 1 µl of DpnI restriction enzyme (10 U/µl) for 1 hour at 37°C. This reaction ensures the digestion of the parental i.e. non mutated supercoiled dsDNA. The digested product is then transformed into electrocompetent *E. coli* cells (DH10B) and plated on LB agar plates with Ampicillin. The plates were incubated at 37°C for minimum 16 hours and the resulting colonies were screened for the presence of mutated 3' UTR by sequencing.

3.5.3 Measuring luciferase activity

The luciferase reporter assay is performed on NRCMs transfected with the reporter constructs containing the native and mutated 3' UTR sites along with miR mimics/antimirs.

3.5.3.1 Transfection

0.1-0.12 million NRCMs per well were seeded onto a 96 well plate for the assay. After 24 hours, the NRCMs were transfected simultaneously with 150 ng of native/mutated reporter construct and miR mimic/antimiR (12.5 - 25 nM). Luciferase activity was then measured after 24 hours using the Dual luciferase reporter assay kit (Promega).

3.5.3.2 Luciferase assay

The cells were washed with 1X PBS followed by the addition of 20 µl 1X passive lysis buffer. The plate was gently rocked on a shaker at RT for 15 - 30 minutes to ensure cell lysis. Homogenous cell lysates were obtained by manually scraping the wells. 50µl of LARII reagent (luciferase substrate) was added to each well and the firefly luminescence was measured immediately in Infinite 200 spectrophotometer (Tecan). To measure renilla luciferase activity, the luminescence reaction was stopped by the addition of 50 µl Stop and Glo reagent, followed by the measurement of luminescence. The firefly luciferase activity was normalized to the renilla luciferase activity.

3.6 Generation of adenoviral shRNA constructs

3.6.1 Cloning of shRNA entry vector

An shRNA entry vector for the overexpression of shRNA of interest was generated using the BLOCK-iT RNAi kit (Life Technologies). The kit facilitates the generation of a vector to express short hairpin RNA (shRNA) for use in RNA interference (RNAi) analysis of a target gene in mammalian cells. The double stranded oligo encoding the shRNA of interest was cloned in the pENTR/U6 vector as shown in **Fig 6**. The presence of human U6 promoter, which is recognized by Polymerase III, helps in highly sustained expression of the shRNA molecules. The shRNA molecule that is expressed from the U6 RNAi cassette leads to the formation of an intramolecular stem-loop

structure similar to the structure of a miRNA. This hairpin is then processed by the endogenous Dicer enzyme into a 21-23 nt siRNA duplex.

Two single-stranded DNA oligonucleotides; one encoding the target shRNA ("top strand" oligo) and the other its complement ("bottom strand" oligo) were designed using the Life Technologies' RNAi Designer, an online tool. The top and bottom strand oligos were then annealed to generate a double stranded oligo suitable for cloning into the pENTR/U6 vector. A sequence of 4 nucleotides CACC was added to the 5' end of the top strand to enable directional cloning and similarly AAAA was added to the 5' end of the bottom strand oligo. As per the instructions of the kit, the shRNA sequence was initiated with a G residue since the transcription if the native U6 snRNA initiated at G. If G was part of the target sequence then a complementary C was added to the 3' end of the top strand oligo. The top and bottom strands were synthesized by MWG Eurofins. The two oligos were annealed according to the following table:

Reagent	**Volume**
Top strand oligo (200µM)	5 µl
Bottom strand oligo (200µM)	5 µl
10X annealing buffer	2 µl
Oligonucleotide primer 2	125 ng
Nuclease free water	8 µl

The reaction was incubated at 95°C for 4 minutes and then left to cool down at RT for 10 minutes.

After the annealing reaction the final concentration of the double stranded oligo was 50 µM. This was then serially diluted. First dilution: 1µl of 50 µM ds oligo was diluted with 99 µl of nuclease free water. Second dilution: 1 µl of the first dilution was mixed in 89µl of nuclease free water along with 10 µl of 10X annealing buffer. The dilutions were stored at -20°C until further use.

The double stranded oligos was then ligated to the pENTR/U6 vector using T4 DNA ligase with a 10:1 molar ratio of ds oligo insert:vector for ligation as previously described. The ligated vector was then transformed into electrocompetent *E. coli* cells (DH10B) and plated on LB agar plates with Kanamycin.

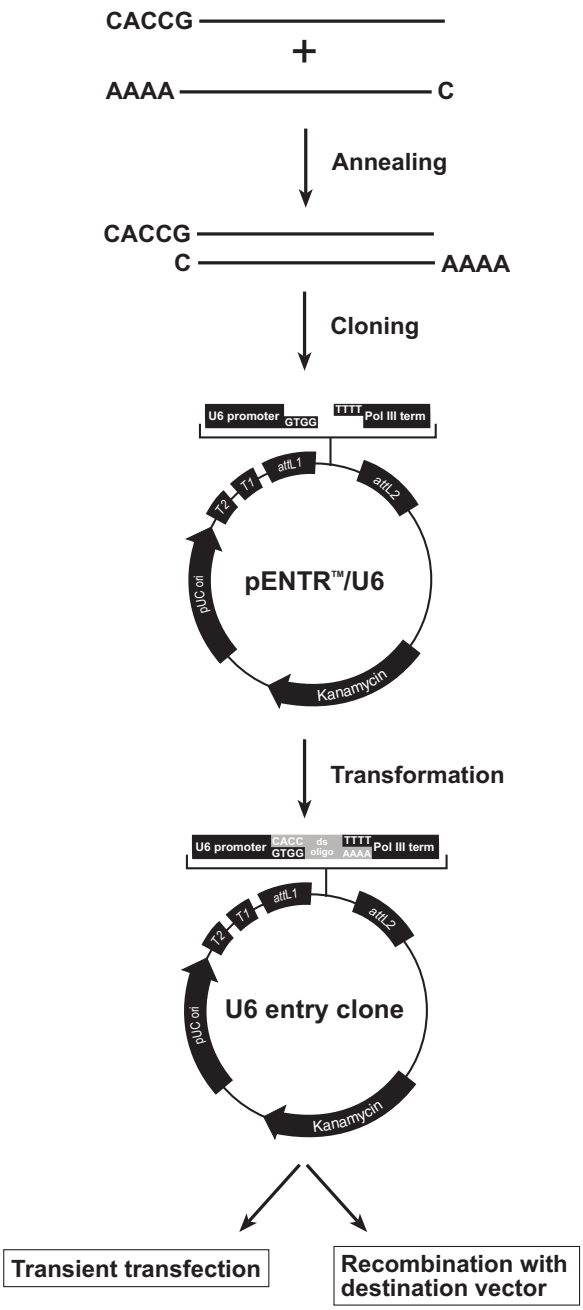

Fig 6: Flowchart depicting the generation of the shRNA entry clone (Illustration from the BLOCK-iT RNAi manual - Invitrogen)

3.6.2 Generation of the shRNA destination vector

The entry vector was then used to generate the destination vector (pAD/CMV vector) by means of a Gateway LR recombination reaction for the generation of adenovirus overexpressing the shRNA. The pENTR/U6 shRNA entry vector possesses attL sites, which can be recombined with a destination vector containing attR sites. The LR Clonase II (Life technologies) enzyme mix contains bacteriophage lambda recombinant Integrase and Excisionase, and *E.coli*- encoded protein,

Integration Host Factor, facilitating the *in vitro* recombination reaction. The recombination reaction was set up according to the following table:

Reagent	Volume
Entry clone (pENTR/U6 shRNA)	15 - 150 ng
Destination vector (pAD/CMV)	150 ng
LR Clonase II	2 µl
TE buffer pH 8.0	upto 10 µl

The recombination reaction was carried out at 25°C for 5 hours after which it was inactivated by the addition of 1µl Proteinase K followed by a 10 minute incubation at 37°C. After the recombination, 1 µl of the recombined destination vector (pAD/CMV shRNA) was transformed into electrocompetent *E. coli* cells (DH10B) and plated on LB agar plates with Ampicillin. Positive clones were confirmed by sequencing followed by Endofree purification using the Endofree Maxi kit (Qiagen).

3.6.3 Generation of adenoviruses

6 µg of Endofree purified pAd/CMV shRNA destination vector was digested with *PacI* restriction enzyme and incubated for 2 hours at 37°C. The digested plasmid was precipitated with Ethanol and 0.1 volume of 3M sodium acetate followed by 3 volumes of 100% Ethanol and precipitation at -80°C. The DNA was then pelleted by centrifugation at 4°C, which was followed by a washing step with 70% Ethanol. The pellet was finally suspended in nuclease free water. 2 µg of the plasmid DNA was transfected into HEK293 cells using the transfecting agent Effectene (Qiagen). The DNA was mixed with buffer EC to a total volume of 150 µl and the samples were incubated at RT for 5 min with 16 µl of enhancer. The samples were then incubated at RT for 10 min with 25 µl of Effectene reagent to allow complex formation. The transfection complexes were mixed with 1 ml of growth medium and were added onto a 6 cm dish containing 80% confluent HEK cells in 2 ml of medium. The cells were incubated in a humidified 37°C/5% CO_2 incubator until 80% of the cells were cytopathic.

For the first virus amplification, the cell suspension was centrifuged at 850 g at 4°C for 10 min followed by resuspension of the pellet in 1 ml of 10 mM Tris (pH 8). The suspension was subjected to freeze-thaw cycle twice by freezing it in liquid nitrogen and thawing in a water bath at 37°C. This was centrifuged again at 850 g for 10 min at 4°C to get rid of the cell debris following, which the supernatant was stored at -80°C.

For the second amplification, 500 µl of the viral particle from the first amplification was added to a 10 cm dish containing 90% confluent HEK cells. The cells were incubated in a 37°C/5% CO_2 incubator until 80 - 90% of the cells were rounded up and floating. The cells were pelleted as above and the cell pellet was resuspended in 2 ml of 10 mM Tris (pH 8). The freeze-thaw cycles were repeated and the virus was stored at -80°C.

The third amplification process was performed similar to the second amplification process. 15 cm plates with 90% confluent HEK cells were used for this process. The adenovirus containing cells were harvested 2 days post infection. The cells were pelleted as above and the cell pellet was resuspended in 3 ml of 10 mM Tris (pH 8). The freeze-thaw cycles were repeated 3 times and the virus was stored at -80°C.

3.6.4 Adenoviral purification and titration

The adenoviruses produced were purified and concentrated using the Adeno-X purification kit (Clontech, France). HEK293 cells were diluted to a concentration of 1.83 x 10^6 cells/ml in a total volume of 40 ml. The virus was mixed with the cells, seeded onto five 15 mm cell culture dishes and were cultured in 37°C/5%CO_2 incubator until the cytopathic effect was observed (3 – 5 days). The cells were harvested by centrifuging at 1500 rpm for 10 min and the pellet was resuspended in fresh medium. The cell suspension was then subjected to freeze-thaw cycle thrice to lyse the cells. After centrifugation, the supernatant was incubated with 5 µl of Benzonase at 37°C for 30 min. Equal volume of 1X dilution buffer was added to the lysate and was passed through an 0.45 µm syringe pre-filter. The adenovirus loaded into the equilibrated filter assembly was allowed to pass through the filter at a flow rate of 3 ml/min. After the wash buffer was passed through the filter, the virus was collected in a sterile tube by passing 3 ml of elution buffer through it. The purified virus was then stored at -80°C.

The Adeno-X rapid titer kit (Clontech) was used to titer the produced adenoviruses. HEK cells were infected with serial dilutions of the viral particles for 48 hours. Then, the cells were fixed with ice-cold methanol and incubated with an anti-hexon antibody (1:1000 diluted in 1% BSA/1X PBS) followed by incubation with HRP-conjugated anti-rat antibody (1:500 diluted in 1% BSA/1X PBS). Subsequent exposure of the plate to DAB substrate solution (1:10 diluted in 1X stable peroxidase buffer) caused the infected cells to become brown. The infected cells (brown or black cells) were then counted using an inverted microscope with 20X objective in a minimum of 3 fields per dilution. The virus titer was then determined using the below formula:

Virus titer = (Infected cells per field) * (Fields per well) / (Volume if virus) * (Dilution factor)

3.7 Functional assays

3.7.1 Hypertrophy assay

3.7.1.1 Immunostaining

For the hypertrophy assay, 50,000 NRCMs per well were seeded into 96-well IBIDI plates in MEM containing 5% FCS for 24 hours. The next day the cells were transfected with respective mimics/ antimirs and were incubated for a further 24 hours in 5% FCS. The medium was then changed to MEM containing 0.1% FCS and after 24 hours, were stimulated with 50 μM phenylephrine (PE) in MEM containing 0.1% FCS for 48 hours. Unstimulated control cells were incubated in MEM containing 0.1% FCS. The cells were fixed with 100 μl 4% PFA for 5 min at RT. To remove the excess PFA, the cells were washed thrice with 200 μl of PBS and were permeabilised with 100 μl of 0.2% TritonX. The plate was then incubated with 100 μl of mouse α-actinin (1:1000 diluted in PBS) in a humidified chamber at 37°C for 30 min. After washing with PBS, the plate was incubated with Alexa488-conjugated goat anti-mouse IgG (1:200 diluted in PBS) and DAPI (1:100 diluted in PBS) for 30 min. The cells were washed three times with PBS and 150 μl of 50% glycerol was added to the plate. The plate was covered using an aluminium seal cap. The cardiomyocyte area, as visualised by the α-actinin staining, was analysed using automated microscopy.

3.7.1.2 Automated cell-size determination microscopy

The cell size of the cardiomyocytes was determined by automated microscopy and image segmentation. Images were acquired automatically using a 10X objective on an AxioObserver.Z1 (Zeiss), a motorized scanning stage (Märzhäuser), Lumen200 fluorescence illumination system (Prior) and Retiga4000 CCD fluorescence camera (QImaging). Metamorph imaging software (Molecular Devices) was used to drive the microscope automatically and for subsequent analysis of the acquired images. A macro function journal consisting of three subjournals was created. The first subjournal drove the positional scanning of the plate, focusing and image acquisition (4 images per well) in two different fluorescent channels – DAPI and green fluorescence (488 nm). The second journal created separate montage stacks of the images acquired at the two fluorescent intensities and also an overlay montage stack by merging the 2 images together. The third subjournal determined the cell size and number, as indicated by the α-actinin staining for cardiomyocyte area and nuclei staining with DAPI, using the cell scoring plug-in of the software.

3.7.2 TUNEL assay

Cleavage of genomic DNA during apoptosis may yield double stranded, low molecular weight DNA fragments (mono- and oligo-nucleosomes) as well as single strand breaks (“nicks”) in high

molecular weight DNA. Terminal deoxynucleotidyl transferase dUTP nick end labeling (TUNEL) is a method for detecting DNA fragmentation by labeling the terminal end of nucleic acids. This assay was performed using the *In situ* cell death detection kit, Fluorescein (Roche). The assay involved two stages namely, Stage 1: Labeling of DNA strand breaks, by Terminal deoxynucleotidyl transferase (TdT), which catalyzes polymerization of labeled nucleotides to free 3'-OH DNA ends in a template independent manner (TUNEL-reaction). Stage 2: Fluorescein labels incorporated in nucleotide polymers are detected and quantified by fluorescence microscopy. The assay was performed either with transfected NRCM plated on 12 mm coverslips or on paraffin embedded cardiac tissue.

3.7.2.1 Isolated NRCMs

For NRCMs, 12mm coverslips were placed in a 12 well plate and coated with Poly-D-Lysine for 1 hour in dark. The wells and coverslips were then gently washed with 1X PBS. 0.4 million NRCM were seeded onto the 12 well plate containing the coverslips. After 24 hours, the NRCM were transfected with mimics/antimirs as described in the section 3.1.2. After 72 hours of transfection the NRCMs were washed with 1X PBS and fixed with 500µl of 4% PFA for 5 minutes. The cells were washed three times with 1X PBS following which, the TUNEL reactions were performed. The cells were permeablized with 0.2% Triton-X for 2 minutes at room temperature. Then, they were washed thrice with 1X PBS. The TUNEL reaction mix was prepared by mixing 5 µl of vial 1 (Enzyme) and 45 µl of vial 2 (labeling solution). 25 µl of the reaction mix was added to the coverslips with cells and placed on slides. These slides were incubated in for 1 hour at 37°C in dark in a humidified chamber. As a negative control, only the labeling solution without the enzyme was added to the cells. As a positive control, the cells were incubated with DNase I for 10 minutes at RT followed by the addition of the TUNEL reaction mix. After the incubation the cells were gently rinsed three times with 1X PBS and mounted on a slide with Vectashield fluorescence mounting medium containing DAPI. The slides were microscopically analyzed and 20X images were acquired under DAPI and green fluorescence (488 nm) channels using Metamorph imaging software (Molecular Devices). The two images were overlaid and the percentage of apoptotic cells were calculated.

3.7.2.2 Paraffin embedded cardiac tissue

For paraffin embedded tissue sections, the slides containing the sections were first dewaxed and rehydrated by immersing the slides in 100% Toluol (2 times, 10 minutes each), followed by 100% Ethanol (twice, 5 minutes each), 90% Ethanol (5 minutes), 70% Ethanol (5 minutes), 50% Ethanol (5 minutes) and finally 1X PBS (5 minutes). The sections were then permeablized with Proteinase K (20 µg/ml in 10 mM TrisCl, 7.4-8 pH) for 15 minutes at 37°C. This was followed by washing the

sections in 1X PBS (three times, 5 minutes each). The sections were covered with the TUNEL reaction mix containing the enzyme and labeling mixture and incubated for 1 hour at 37°C in a humidified chamber in dark. After incubation, the sections were washed again with 1X PBS (three times, 5 minutes each). The sections were then mounted with Vectashield fluorescence mounting medium containing DAPI, covered with coverslip and sealed using nail polish. The slides were microscopically analyzed and 10X images were acquired under DAPI and green fluorescence (488 nm) channels using Metamorph imaging software (Molecular Devices). The two images were overlaid and the percentage of apoptotic cells was calculated.

3.7.3 RNAi knockdown assay

3.7.3.1 RNAi with shRNA

For shRNA knockdown experiments, hypertrophy assay was performed with adenoviruses encoding shRNA against *Mapk1* and an shRNA control. 50,000 NRCMs per well were first seeded on to optically optimized 96 well plates and cultured for 24 hours in 5% FCS containing MEM medium at 37°C and 1% CO_2. The cells were then infected with Adeno-*shMapk1* and Adeno-shctrl. The medium was changed the next day and transfection with 50 nM Antimirs was performed according to the method described before. After 48 hours, the cells were stimulated with PE to induce hypertrophy. After two days, immunostaining and automated cell size measurements were performed.

3.7.3.2 RNAi with siRNA

For siRNA knockdown experiments, hypertrophy assay was performed with siRNAs targeting the four miR-378 targets, i.e. si-*Mapk1, si-Grb2, si-Ksr1* and *si-Igf1r*. 50,000 NRCMs per well were seeded on to optically optimized 96 well plates and cultured for 24 hours in 5% FCS containing MEM medium at 37°C and 1% CO_2. The next the cells were transfected with 100 nM siRNA and/or 50 nM antimiR along with the respective controls as described before. After 48 hours, the cells were stimulated with PE to induce hypertrophy. After two days, immunostaining and automated cell size measurements were performed.

3.8 Animal experiments

3.8.1 β_1-adrenergic receptor transgenic mice

β_1-transgenic was used as one of the heart failure models in the study. The mice were generated by overexpression of ß$_1$-adrenergic receptor under the control of cardiomyocyte specific α-MHC promoter[93]. The transgenic mouse line TG4 that had 15-fold increase in its receptor numbers than the wild type litter mates was used in the study. These mice had high cardiac contractility at young

age but developed progressive heart failure with myocyte hypertrophy, decreased contractility and reduced cardiac function at 9 months of age.

3.8.2 Pressure overload induced hypertrophy

Pressure overload hypertrophy was induced by thoracic aortic constriction (TAC) performed on 8 weeks old male C57BL/6N mice (Charles River Laboratories). Briefly, animals were anesthetized with isoflurane (2%) and, after opening the chest, the aorta was ligated with a 6-0 nylon fibre around a 27G cannula. In sham surgery, only the chest was opened, but no ligation of the aorta was carried out. Cardiac dimensions and function were analyzed by pulse–wave Doppler echocardiography essentially before TAC/sham surgery and before sacrificing the animals.

3.8.3 Generation of AAV vectors

Recombinant AAV-miR-378 and AAV-GFP vectors used in this study were prepared by the AAV Vector Unit at the International Centre for Genetic Engineering and Biotechnology Trieste[94]. Briefly, infectious recombinant AAV vector particles were generated in HEK293T cells by a cross-packaging approach whereby the vector genome was packaged into AAV capsid serotype-9[95]. Viral stocks were obtained by $CsCl_2$ gradient centrifugation; rAAV titers, determined by measuring the copy number of viral genomes in pooled, dialyzed gradient fractions[96] were in the range of $1x10^{12}$ to $1x10^{13}$ genome copies per milliliter. For the AAV-miR-378 preparation, the genomic pre-miR sequence was sub-cloned into the vector plasmid derived from pAAV-MCS (Agilent Technologies) containing a modification in the multiple cloning site to match the insert ends. In all the vectors used in this study, the transgene is expressed under the transcriptional control of the CMV immediate early promoter. The AAVs were injected into the tail vein of 5 week old male C57BL/6N mice (Charles River Laboratories).

3.8.4 Echocardiographic analysis

Vevo 700 was used for echocardiographic measurements (Visual Sonics). Mice were subjected to anesthesia by inhalation (2% isoflurane/98% O_2) and were fixed on a hot plate maintained at 37°C. Isoflurane concentration was adjusted such that the heartbeat was in the range of 450±50 beats per min. The chest was shaved and ‘Aquasonic’ ultrasound transmission gel (Parker laboratories, New Jersey) was applied. The ultrasonic probe in the long axis (B-mode) was placed on parasternal line and the left ventricle, and the position was determined. The echocardiogram was then recorded in the short axis mode (M-mode) by rotating the transducer by 90°C. Left ventricular internal diameter (LVID), left ventricular posterior wall thickness (LVPW) and intraventricular septal thickness (IVS) was determined under both systolic (s) and diastolic (d) phases. The cardiac function parameters

such as ejection fraction (EF) and fractional shortening (FS) were calculated using the following formulae:

$FS\ \% = (LVID_d - LVID_s)/LVID_d * 100$

$EF\ \% = (LV_d - LV_s)/LV_d * 100$

3.8.5 Histochemical and immunohistochemical analysis

3.8.5.1 Sirius red and fast green staining

For the analysis of collagen deposition, paraffin sections of the myocardium were stained with Sirius red and Fast green. The slides containing the sections were first dewaxed and rehydrated by immersing the slides in 100% Toluol (2 times, 10 minutes each), followed by 100% Ethanol (twice, 5 minutes each), 90% Ethanol (5 minutes), 70% Ethanol (5 minutes), 50% Ethanol (5 minutes) and finally double distilled water (5 minutes). The slides were treated with preheated Bouin's solution at 55°C for 1 hour. The slides were then washed under running water for 10 minutes. This was followed by the addition of 0.1% Fast green for 10 minutes at RT. The slides were then rinsed in 1% acetic acid for 2 minutes and running water for 5 minutes. The sections were stained with the Sirius red solution for 30 minutes followed by a brief 10 second wash with double distilled water. This was followed by dehydration of the sections by immersing the slides in 70% Ethanol for 10 seconds, followed by 100% Ethanol for 1 minute and finally 100% Toluol for 3 minutes. The slides were mounted with DEPEX, a synthetic mounting medium and covered with a coverslip. The slides were analyzed and images under 10X magnification were obtained. Sirius red staining was measured in an automated manner using Metamorph imaging software (Molecular Devices). Collagen content was calculated as the percentage of the area in each section that was stained with Sirius red.

3.8.5.2 WGA staining

For analysis of cardiomyocyte hypertrophy, myocardium tissue sections (6 μm) were stained with SYTOX Green (Life Technologies) - for staining of cell nuclei and ALEXA 647 labelled wheat-germ agglutinin (WGA, Invitrogen) - for determination of myocyte cross sectional areas. The slides containing the sections were first dewaxed and rehydrated by immersing the slides in 100% Toluol (2 times, 10 minutes each), followed by 100% Ethanol (twice, 5 minutes each), 90% Ethanol (5 minutes), 70% Ethanol (5 minutes), 50% Ethanol (5 minutes) and finally 1X PBS (3 times, 5 minutes each). The sections were stained with ALEXA 647 labelled WGA (1:500, diluted with 1X PBS) and nuclear stain SYTOX green (1:500) and incubated for 1 hour at RT. After incubation, the slides were washed 3 times with 1X PBS. The slides were mounted with Vectashield fluorescence

mounting medium and covered with a coverslip. The sections were then analyzed under the microscope and images were acquired. Confocal images were taken at 20x magnification at areas of transversely cut muscle fibers. Individual cells were analyzed in an automated manner. Common morphology filters were used in the MetaMorph software (Molecular Devices) to draw lines separating individual cells based on the WGA staining. Thresholding was applied to exclude regions of background (no cells) or extensive fibrosis. Nuclei were extracted from the green channel. Using morphology filters nuclei that were touching any cell borders were automatically excluded. The remaining nuclei were used to select for cardiomyocytes with centralized nuclei. Cells with a width of less than 7 μm or an area of less than 50 μm were considered non-myocytes and excluded from the analysis. Averages for area and breadth (width of the object perpendicular to the longest chord) of analyzed cells (>20 cells per section) were exported using the MetaMorph integrated morphometry analysis function.

3.9 Statistical analysis

Data are shown as mean±SEM. Statistical analysis was performed with Prism (GraphPad Software). The Student t test or 2-way ANOVA followed by the Bonferroni test was used as appropriate. Data were analyzed for normality using Shapiro-Wilk or Kolmogorov-Smirnov test. Testing for common variance was carried out using F test. If necessary, Box-Cox transformation was used to meet the requirement of normality and equal variances before comparing means.

4 RESULTS**

4.1 Screening of potential microRNAs

To identify candidate microRNAs, two strategies were simultaneously employed. The first was to screen for miRs that could potentially regulate cardiomyocyte hypertrophy and the second was to screen for miRs based on their expression and regulation in the failing heart.

Libraries of multiple synthetic microRNAs were screened to identify hypertrophy regulating microRNAs[97]. The screen employed automated microscopy and an edge detection algorithm to assess cardiomyocyte size. Results of the screen showed several microRNAs with prohypertrophic and antihypertrophic effects on myocyte size. Of these, miR-378 was found to negatively regulate hypertrophy. Interestingly, miR-378 also appeared as one of the candidates in global expression profiling studies performed in the lab[98]. The results of the expression profiling study were analyzed according to the following criteria:

I. Expression strength in the heart

II. Deregulation in the failing mouse heart

III. Enrichment in isolated cardiomyocytes compared to cardiac fibroblasts.

Expression profiling results from early and late stages of heart failure showed several deregulated microRNAs. Of these microRNAs, miR-378 emerged as a potentially interesting microRNA that was highly expressed in the mouse heart and downregulated in the failing heart. Also, expression profiling from isolated adult mouse cardiomyocytes and adult cardiac fibroblasts showed that miR-378 was highly enriched in cardiomyocytes compared to cardiac fibroblasts.

4.2 MiR-378 expression

4.2.1 MiR-378 expression in mice

MiR-378 is a muscle enriched microRNA. qPCR analysis in lung, heart and skeletal muscle showed the highest enrichment in skeletal muscle followed by heart (Fig 7A). An analysis of the microRNA levels from the embryonic stages showed reduced miR-378 levels that increased after birth suggesting that the expression of the microRNA undergoes a boost during mouse ontogenesis (Fig 7B).

** This section (including the figures) was published in Ganesan *et al.*Circulation 2013 (169)

4.2.2 MiR-378 expression in cardiomyocytes

The two major cell types in the myocardium are cardiomyocytes and cardiac fibroblasts. An analysis of miR-378 levels in these two cell types showed a 10fold enrichment of the microRNA levels in cardiomyocytes (Fig 7C).

4.2.3 MiR-378 expression in the failing heart

Failing myocardium shows an activation of the fetal gene program[99]. Two different heart failure models were analyzed to determine the regulation of miR-378: first, a β1-adrenergic receptor-transgenic mouse model, which leads to severe heart failure[93] and second, a transthoracic aortic constriction (TAC) model for chronic pressure overload. Both mice models showed a significant decrease of miR-378 levels by 54% and 42% respectively (Fig 7D).

In line with the mouse models of heart failure, human failing myocardium showed a similar pattern of miR-378 downregulation. Human heart biopsies from dilated cardiomyopathy patients showed a significant decrease in miR-378 expression levels (Fig 7E) suggesting a prominent role for this microRNA in the progression of heart failure.

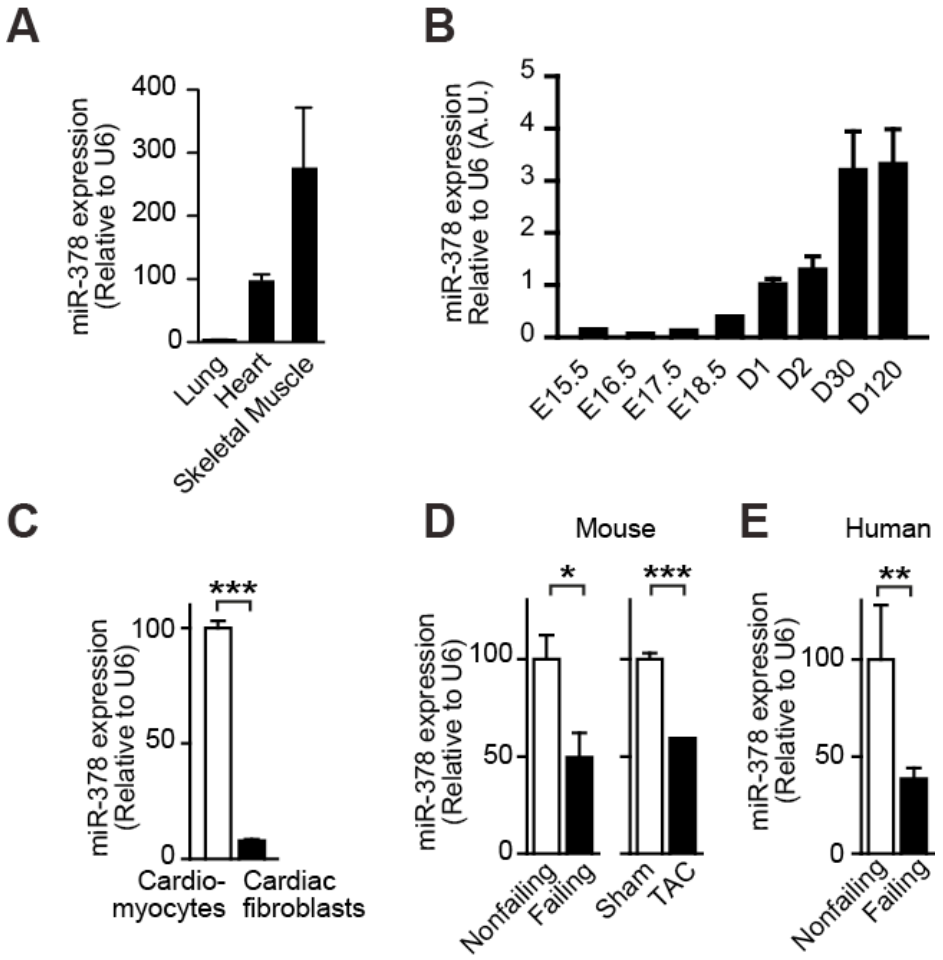

Fig 7: miR-378 expression (**A**) qPCR analysis of miR-378 expression in various tissues (n=4). (**B**) Myocardial expression of miR-378 during development and after birth: Levels of miR-378 were determined by quantitative real-time PCR in RNA prepared from myocardial tissue obtained at the age indicated. (n=1 for E15.5, E16.5, E17.5, E18.5; n=4 for D1, D2, D30, D120) (C) miR-378 expression determined by qPCR in neonatal rat cardiomyocytes compared to cardiac fibroblasts (n=3 independent cell isolations). (**C**) Myocardial miR-378 expression in cardiac disease determined by qPCR. (Left) Quantitation of miR-378 in left ventricular myocardium from a murine heart failure model (β1-adrenergic receptor-transgenic mice or wild-type litter mates) and from transthoracic aortic constriction (TAC) or sham-operated controls (n=5). (**D**) Quantitation of miR-378 in human heart biopsies from patients with dilated cardiomyopathy (n=12) or non failing control biopsies (n=5). (D) Experimental error is shown as SEM, statistical significance is shown as $p < 0.05$ (*), $p < 0.01$ (**), $p < 0.001$ (***) or n.s. (non-significant).

4.3 Manipulation of miR-378 expression in NRCM

4.3.1 miR-378 inhibits cardiomyocyte hypertrophy

Synthetic miR-378 mimic and a miR-control (miR-ctrl) were transfected into NRCM under basal and phenylephrine (PE)-stimulated conditions and the resulting affect on cardiomyocyte size was measured. The transfection of miR-378 had only a marginal affect under basal conditions but largely prevented PE-induced cardiomyocyte hypertrophy (Fig 8A). PE treatment resulted in an increase in the expression of hypertrophic markers like *Nppa* and *Nppb*. miR-378 transfection led to a significant decrease in the levels of both *Nppa* and *Nppb* under PE-stimulated conditions (Fig 8B). A reciprocal affect on the myocyte size was observed when the endogenous miR-378 was knocked

down using an antimiR-378. Transfection of antimiR-378 led to an increase in myocyte size under both basal as well as PE stimulated conditions (Fig 8C).

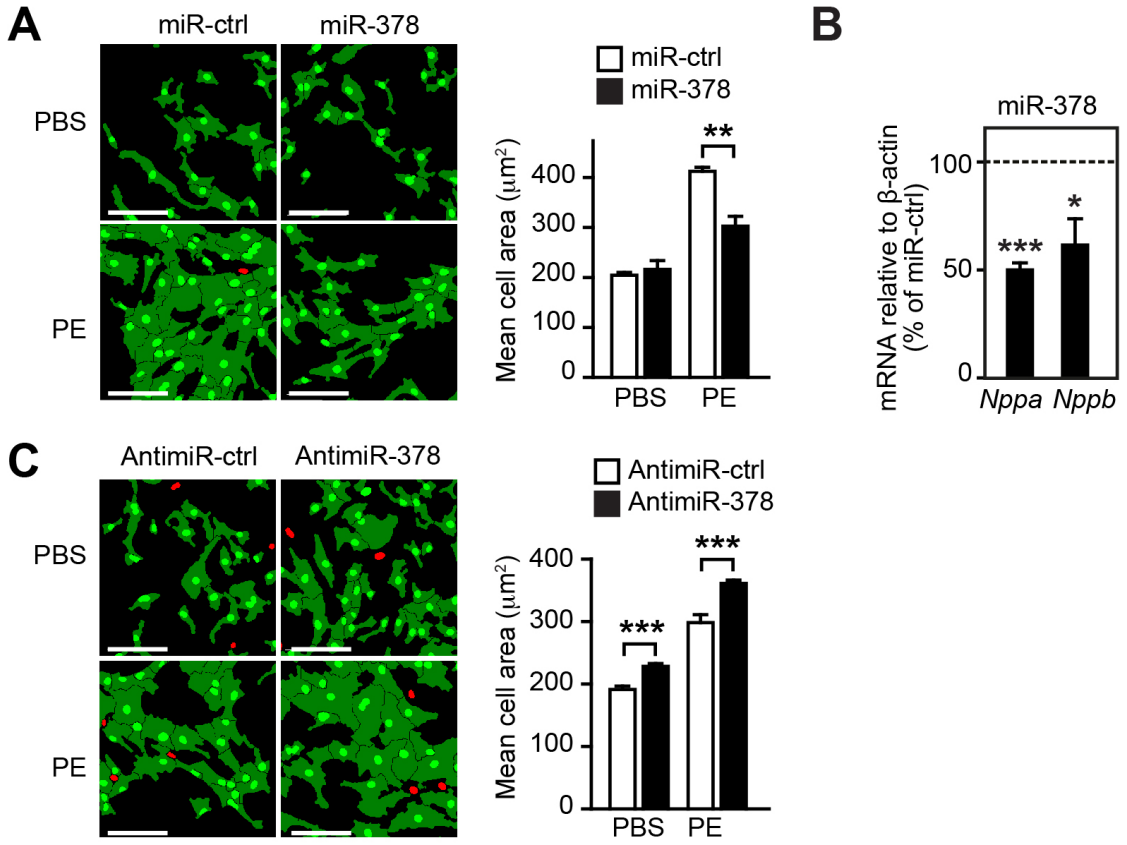

Fig 8 miR-378 inhibits phenylephrine (PE)-induced hypertrophy of NRCM (**A**) NRCM were transfected with miR-378 or a control molecule (miR-ctrl) followed by PE stimulation. (Left) Processed microscopic images of immunofluorescent staining of cardiomyocytes with an antibody against alpha-actinin (green cells). Non-myocyte nuclei are automatically detected and marked in red. Scale bar = 100 µm50. (**B**) qPCR analysis of atrial natriuretic peptide (*Nppa*) and brain natriuretic peptide (*Nppb*) as markers of hypertrophy. Shown are the expression levels upon miR-378 transfection of PE-stimulated NRCM relative to cells transfected with miR-ctrl (dotted line). Graph shows results from 4 independent experiments. (**C**) Transfection of an antagonist against miR-378, antimiR-378. Experimental conditions were analogous to (A). Bar graphs in (A) and (C) show results from five independent experiments performed in triplicate.

4.3.1 MiR-378 increases apoptosis in NRCM

Consistent with a previous report[84], transfection of synthetic miR-378 into NRCM lead to increased apoptosis under both basal and PE stimulated conditions (Fig 9A). In addition, knockdown of endogenous miR-378 using antimiR-378 increased cell densities under both basal as well as PE-stimulated conditions (Fig 9B).

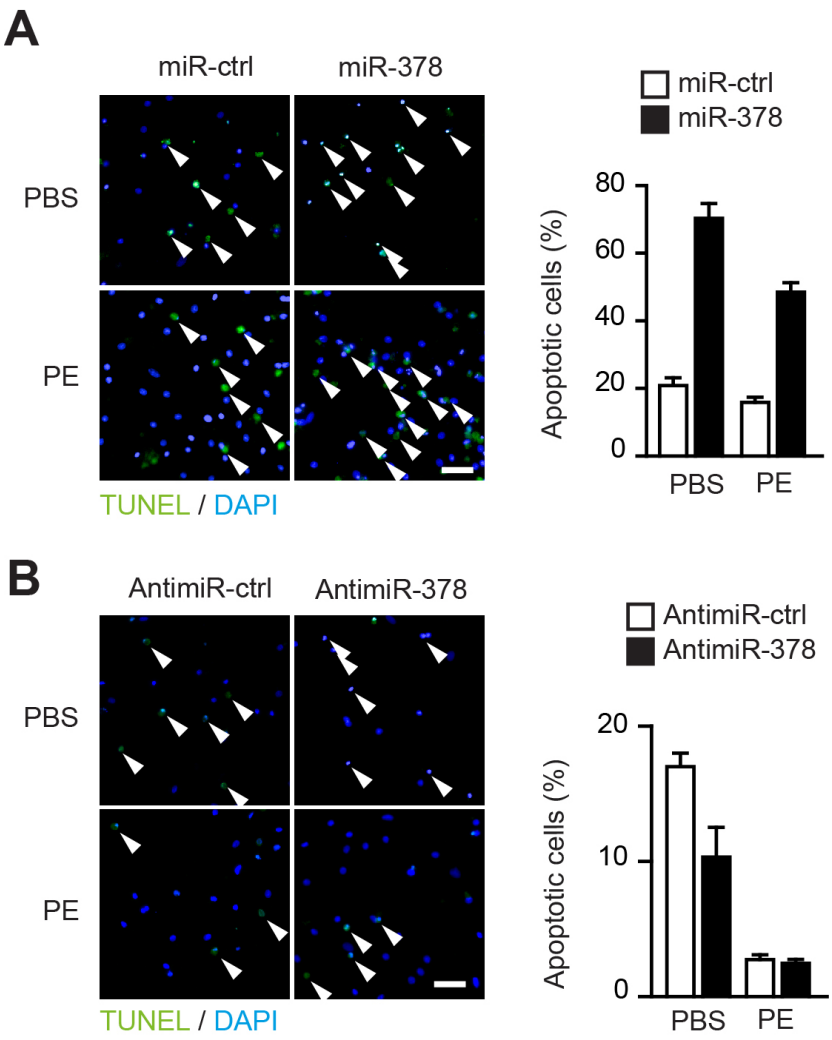

Fig 9 miR-378 increases apoptosis in NRCM (**A**) Apoptosis was analyzed in isolated NRCM by terminal deoxynucleotidyl transferase dUTP nick end labeling (TUNEL). Representative pictures of TUNEL staining, 96 hours after transfection with synthetic miR-378 or a scrambled sequence (miR-ctrl). The quantification shows results from 3 independent experiments performed in duplicate. Arrows indicate apoptotic cell nuclei, scale bar = 50 μm. (**B**) Inhibition of endogenous miR-378 reduces apoptosis in NRCM. Experiments as in (A), except that antimiR-378 or antimiR-ctrl were transfected. Results are from three independent experiments performed in duplicate.

4.4 Screening of potential miR-378 targets

4.4.1 Selection of potential miR-378 targets

Bioinformatic target prediction tools were employed to identify targets with conserved miR-378 binding sites. TargetScanHuman[100] (v6.2) predicted 191 conserved targets of miR-378 with a total of 195 conserved sites and 67 poorly conserved sites. Functional association of miRs with signaling pathways was investigated using a recently developed bioinformatic tool miTALOS[101]. The results showed the highest enrichment of targets within the mitogen-activated kinase (MAPK) signaling pathway. Based on evolutionary conservation and pathway analysis, four targets with miR-378 binding sites were chosen. The four targets, mitogen-activated kinase 1 (MAPK1, also termed

ERK2), kinase suppressor of ras 1 (KSR1), growth factor receptor bound protein 2 (GRB2), and the receptor for insulin-like growth factor 1 (IGF1R) are key components of the MAPK signaling cascade. To screen for potential miR-378 targets, a global mRNA expression profiling study was performed in NRCM transfected with synthetic miR-378 mimic and stimulated with PE. The results (Fig 10A) showed a downregulation of *Grb2* and *Ksr1* mRNA levels upon miR-378 transfection. The mRNA levels of *Igf1r* and *Mapk1* were unaltered.

4.4.2 Regulation of miR-378 targets

To assess the regulation of the targets on the mRNA level quantitative real time PCR (qPCR) was performed on RNA isolated from synthetic miR-378 mimic-transfected NRCM. mRNAs of all four targets were found to be downregulated (Fig 10B). Next, the regulation of these targets on the protein level was assessed using immunoblot detection in NRCM transfected with synthetic miR-378 mimic. The quantification confirmed reduced protein levels of GRB2, IGF1R, KSR1 and MAPK1 (Fig 10C). A reciprocal increase in protein expression was observed in NRCM transfected with antimiR-378. Since all four targets belong to the MAPK signaling cascade, the activation of MAPK1 and MAPK3 was assessed by probing the immunoblots with antibodies against phosphorylated MAPK1 and MAPK3. Significant reduction in MAPK1 and MAPK3 activation with miR-378 and a corresponding increase in the MAPK activation with antimiR-378 transfection was observed.

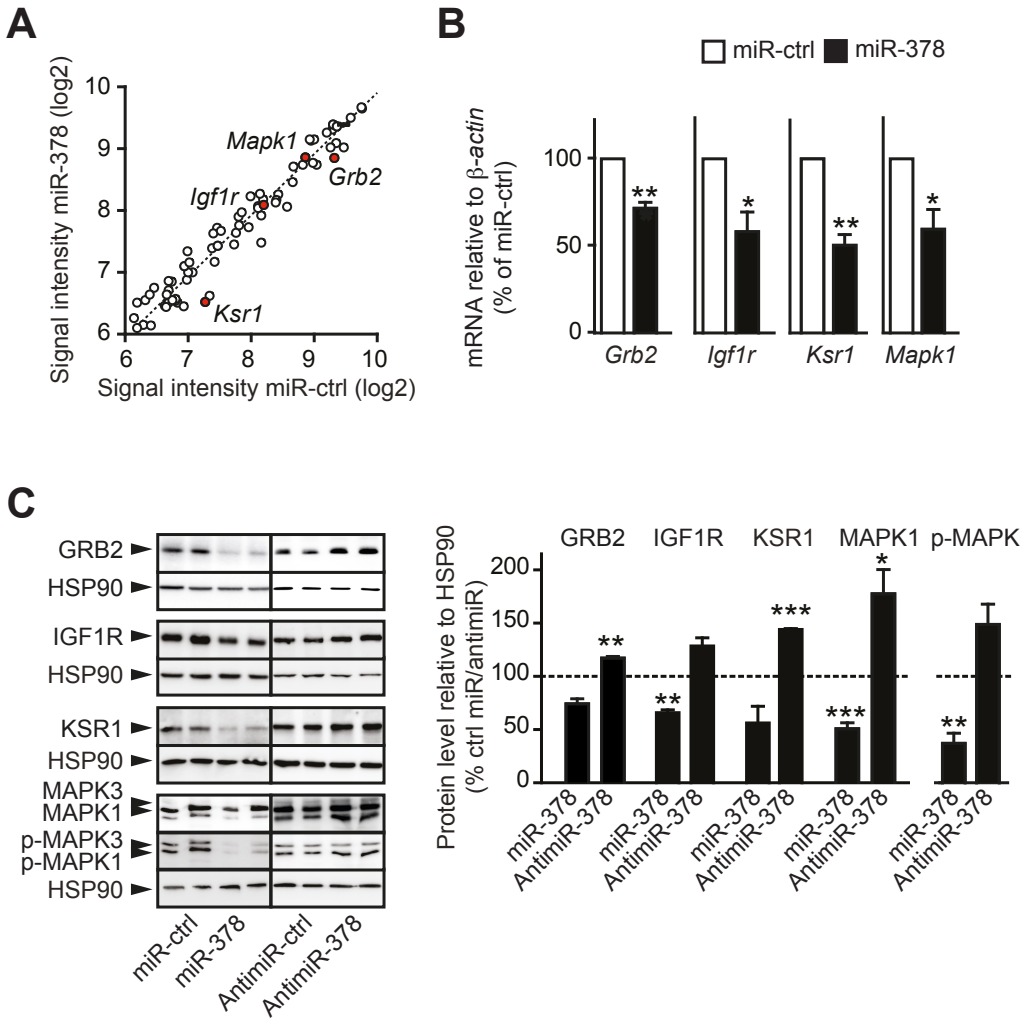

Fig 10 miR-378 targets several key components of the MAPK1 pathway. (**A**) Microarray analysis of the 80 most abundant mRNAs in cardiomyocytes and their alteration after miR-378 transfection. The diagram plots data in log2 scale from NRCM that were transfected with miR-378 or miR-ctrl and subsequently treated with PE. The dotted line marks theoretical values for unaltered expression in the presence or absence of miR-378. Bioinformatic analysis using miTALOS predicted the MAPK signaling pathway as the single most enriched signaling pathway, members of which are marked in red. (**B**) Validation of microarray data by quantitative PCR. NRCM were transfected with miR-378. Data show cycle threshold values for mRNAs of interest relative to β-actin. All data retrieved from 5 independent experiments. (**C**) MiR-transfected NRCM as in (B) were lysed and analyzed on Western blots with antibodies against the proteins of interest, including activated MAPKs (p-MAPK1/3); detection of HSP90 served as a loading control. (Left) Representative Western blots. (Right) Quantitative analysis of Western blot data. A dotted line in the graph denotes the signal intensity obtained in NRCM transfected with miR-ctrl or antimiR-ctrl and to which the other data were normalized. Data are from two to eight independent cell isolations with two to three replicates each. Statistical significance was evaluated with Student's t-test comparing the two treatments to their respective controls.

4.4.3 Direct interaction of miR-378 with the 3' UTR of the four targets

To assess direct binding of miR-378 to the 3' UTR of the four targets, luciferase reporter constructs with native 3' UTR of each of the targets were generated (Fig 11A-D). Reduced firefly luciferase activity was observed in NRCMs transfected simultaneously with the reporter constructs and synthetic miR-378 mimics. NRCMs transfected with antimiR-378 showed an increase in the firefly luciferase activity. To test the specificity of this interaction the miR-378 binding sites in the reporter

constructs were mutated and the luciferase activity was measured again. Simultaneous transfection of the mutated constructs with either the synthetic miR-378 or antimiR-378 did not alter luciferase activity.

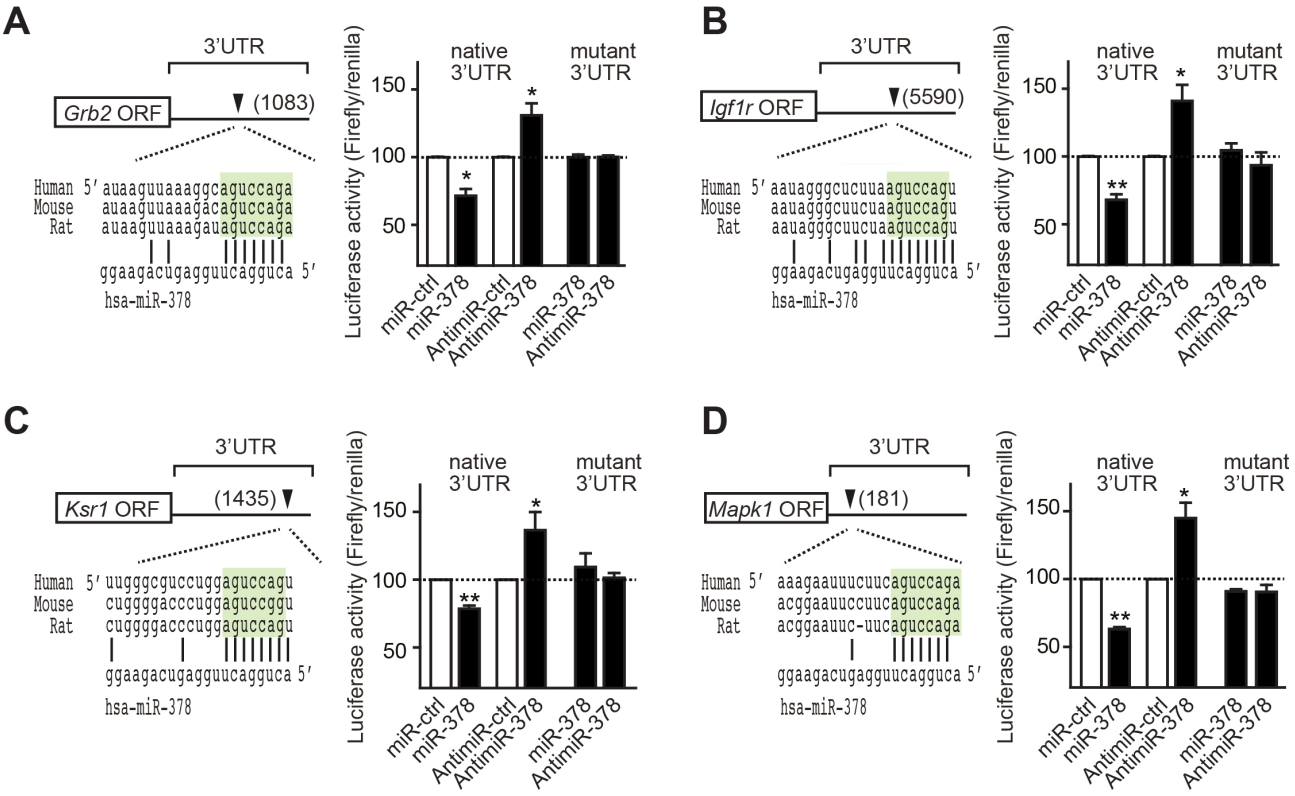

Fig 11 miR-378 interacts directly with the MAPK-pathway factors (**A**)-(**D**) Luciferase activity of reporter constructs carrying luciferase cDNA and parts of the 3'UTR of target mRNAs. (Left panels) Localization of binding sites for human miR-378 (hsa-miR-378) in the 3'UTR of target mRNAs and their evolutionary conservation. miR-378 seed pairing in the target regions is shaded in green. (Right panels) Quantitative analysis of 3'UTR luciferase activities. NRCM were transfected with miR-378 or antimiR-378 (with miR-ctrl and antimiR-ctrl) along with reporter constructs with native 3' UTR or mutated 3' UTR. The dotted line denotes the signal intensity obtained in controls, to which other data were normalized. Data are from three independent experiments performed in triplicate.

4.5 Functional relevance of miR-378 targets

To assess the relevance of target inhibition in the repression of cardiomyocyte hypertrophy by miR-378, a strategy utilizing the opposing phenotypic effects of miR-378 and antimiR-378 on cardiomyocyte cell size was designed (Fig 12A). First, miR-378 induced repression of the target protein(s) resulted in reduced myocyte size. In addition, when endogenous miR-378 was knocked down using an antimiR-378, the resulting derepression of the target protein(s) resulted in increased myocyte size. If the targets are functionally relevant in this scenario then interference with their expression (e.g. by short hairpin RNA or short interfering RNA) should specifically counteract antimiR-378-induced hypertrophy.

4.5.1 Inhibition of MAPK1 derepression using a short hairpin RNA

The strategy given in Fig 12A was first tested for *Mapk1*. An adenovirus was used to deliver a short hairpin RNA against *Mapk1 (*sh-*Mapk1)* in NRCM along with a scrambled control (sh-ctrl). The sh-*Mapk1* efficiently silenced MAPK1 expression while having no effect on MAPK3 (Fig 12C, upper right) and inhibited the antimiR-378 induced hypertrophy under PE stimulation (Fig 12B-C). AntimiR-378 induced an increase in NRCM size with sh-ctrl, which was inhibited by sh-*Mapk1* (Fig 12C, lower right).

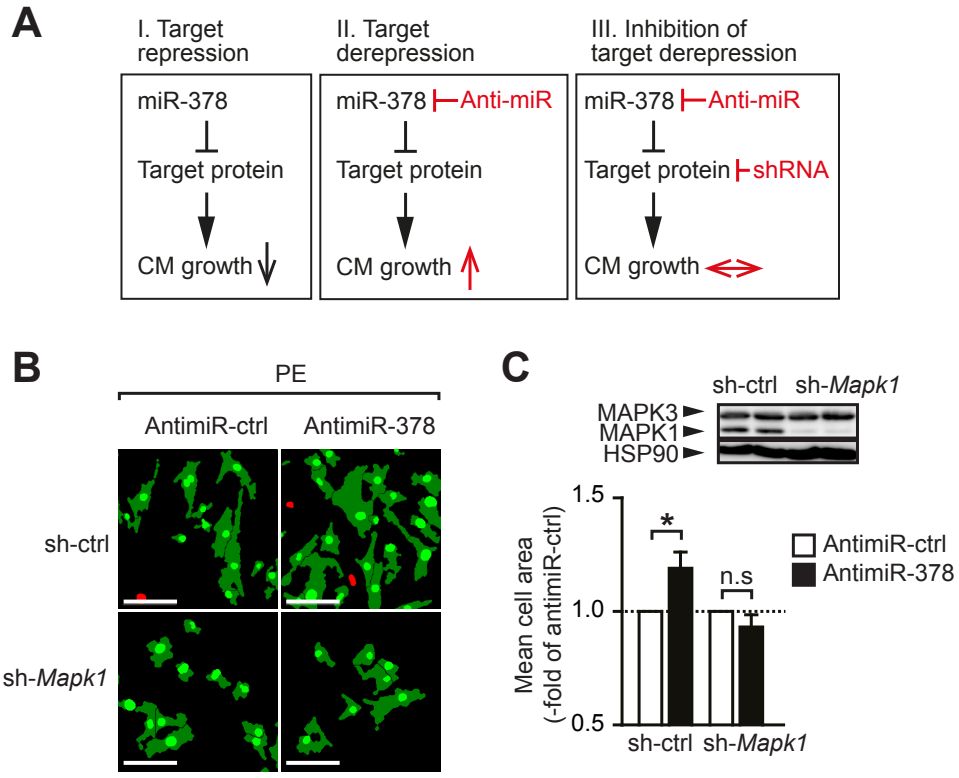

Fig 12 MAPK1 inhibition controls cardiac hypertrophy. (**A**) Schematic illustration of target repression by miR-378 (left panel), target de-repression by antimiR-378 treatment (center panel), and inhibition of the latter by short hairpin-mediated RNA interference on *Mapk1* (right panel). (**B**) Effect of specific inhibition of the miR-378 target MAPK1 on antimiR-378-induced cardiomyocyte hypertrophy. (Left) Processed microscopic images of immunofluorescent staining of cardiomyocytes with an antibody against alpha-actinin (green cells). Scale bar=100 µm. (**C**) (Upper panel) Immunodetection of MAPK1 and MAPK3 on Western blot after knockdown of MAPK1 in NRCM by adenovirus-delivered shRNA. (Lower panel) Quantification of the data in (B) from three independent experiments performed in triplicate.Statistical significance was determined by 2-way ANOVA and Bonferroni test (C). Statistical significance is shown as *P<0.05,**P<0.01, ***P<0.001, or NS.

4.5.2 Inhibition of target derepression using short interfering RNAs

The strategy outlined in Fig 12A was tested for all four miR-378 targets using a short interfering RNA (siRNA) to inhibit the target derepression by antimiR-378 (Fig 13A). The siRNAs against

Grb2, Igf1R, Ksr1 and *Mapk1* were able to efficiently silence their mRNA expression (Fig 13B). Functional relationship of the four targets with miR-378 with respect to hypertrophy was assessed by simultaneously transfecting NRCMs with antimiR-378 and each of the four siRNAs. The siRNAs against all four targets were able to efficiently inhibit the prohypertrophic response of antimiR-378 (Fig 13C) suggesting that the inhibition of the four targets by miR-378 was indeed responsible for the reduction in myocyte growth.

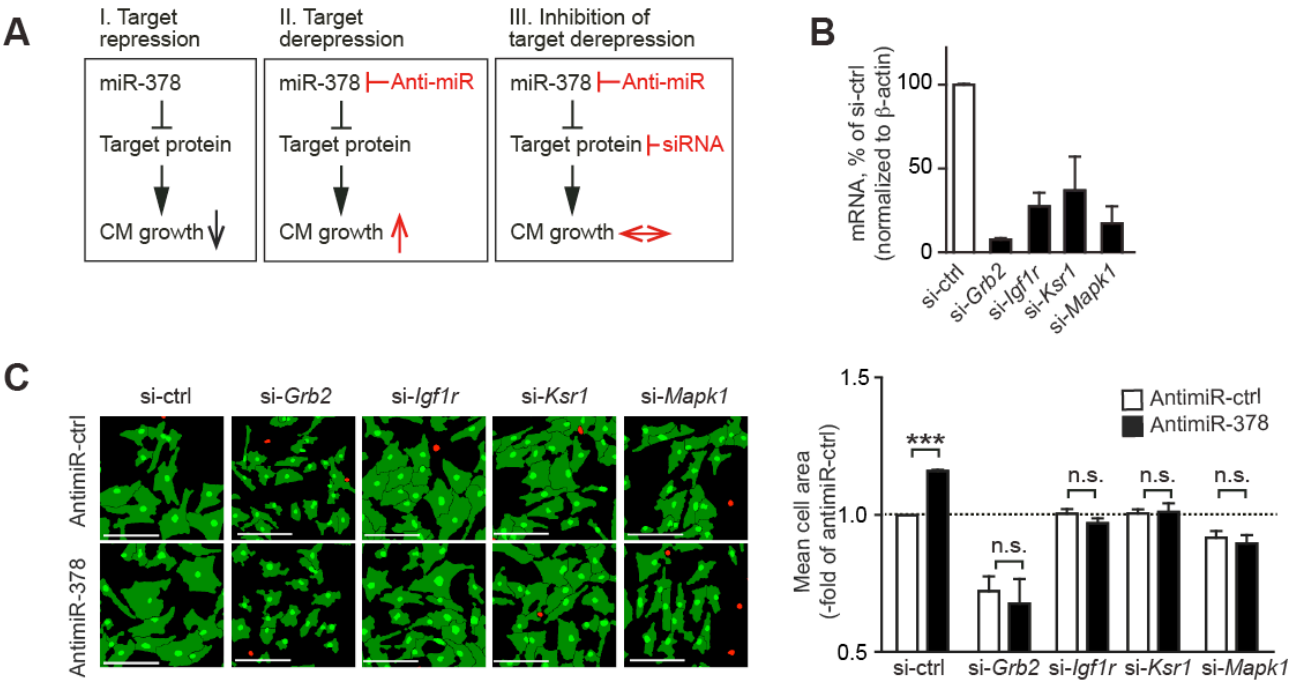

Fig 13 Inhibition of the four factors of MAPK pathway controls cardiomyocyte hypertrophy in NRCM. (**A**) Schematic illustration of target repression by miR-378 (left panel), target de-repression by antimiR-378 treatment (center panel), and inhibition of the latter by short interfering RNA interference on *Grb2, Igf1r, Ksr1 and Mapk1* (right panel). (**B**) Effect of specific inhibition of the four targets using siRNA on their respective mRNA levels. (**C**) Effect of specific inhibition of the four miR-378 targets on antimiR-378-induced cardiomyocyte hypertrophy. (Left) Processed microscopic images of immunofluorescent staining of cardiomyocytes with an antibody against alpha-actinin (green cells). Scale bar=100 µm. (Right) Quantification of data (n=3; 3 replicates each). Statistical significance was determined by 2-way ANOVA and Bonferroni test (C). Statistical significance is shown as *P<0.05,**P<0.01, ***P<0.001, or NS.

4.6 Cardiotropic expression of miR-378 *in vivo*

4.6.1 Exogenous expression of miR-378 using AAV9

Transthoracic aortic constriction-induced pressure overload leads to a decrease in miR-378 expression in mice (Fig 7C). To assess the contribution of miR-378 downregulation on the cardiac phenotype an *in vivo* study was designed using AAV9 to exogenously restore the miR-378 levels in cardiomyocytes. Five week old C57BL/6 N mice were injected with AAV9-miR-378 or PBS via the tail vein followed by aortic banding (TAC) or sham surgery (where only the chest of the animals were opened). Three weeks later, echocardiographic measurements were performed after which the

mice were euthanized and analyzed (Fig 14A). Quantification of miR-378 expression in the mice showed a 2.5 fold increase in miR-378 expression in the sham mice that received AAV9-miR-378 compared to the control (ctrl) group that received PBS (Fig 14B). After TAC, the control mice showed a decrease in miR-378 expression that was effectively compensated by the AAV9-miR-378 intervention (Fig 14B). The exogenous expression of miR-378 had no significant effect on expression of the opposite strand of miR-378 (i.e. miR-378-5p). TAC-induced pressure overload increased the ventricular weight of the control mice which was decreased in mice that received AAV9-miR-378 suggesting partial attenuation of cardiac hypertrophy in these mice (Fig 14C). Pulmonary edema, an indirect parameter of cardiac dysfunction characterized by increased lung weight was decreased in the mice that received AAV9-miR-378 after TAC (Fig 14D). The levels of two other antihypertrophic microRNAs, miR-1 and miR-133a were also quantified in these mice (Fig 14E[††]). qPCR data showed that AAV9-miR-378 intervention did not change the expression levels of the two miRs compared to the sham groups. This excludes the possible involvement of miR-1 and/or miR-133a in the partial attenuation of cardiac hypertrophy.

[††] Performed by Deepak Ramanujam

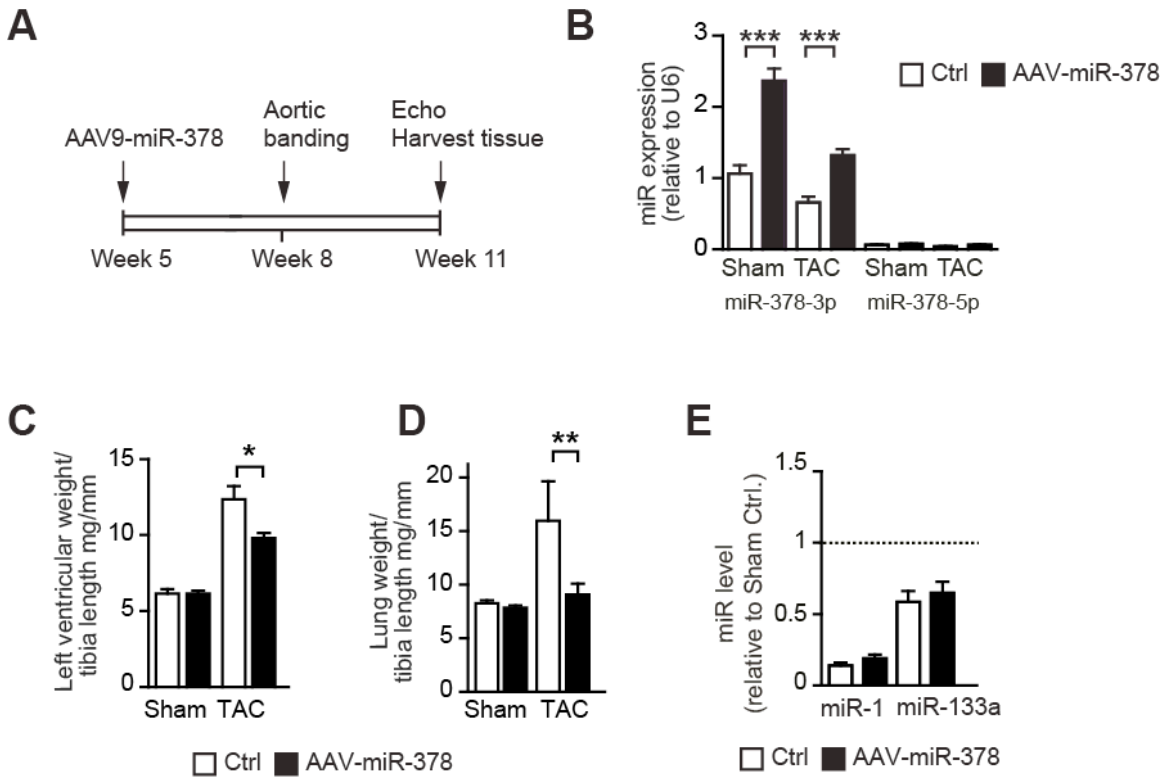

Fig 14. Cardiotropic expression of miR-378 prevents cardiac hypertrophy in vivo. (A) Experimental strategy for exogenous expression of miR-378 using AAV9 in mice. 5-week-old mice were infected with an AAV9 vector that encodes miR-378 and then subjected to thoracic aortic constriction (TAC; causing chronic pressure overload) or control surgery (sham). At week 11, echocardiographic measurements were taken, and animals were euthanized for further analysis. (**B**) Quantification of miR-378 in mouse hearts showed that infection with AAV9–miR-378 effectively compensated for the disease-associated loss of miR-378 (open bars). (**C**) Effect of AAV9–mediated expression of miR-378 on left ventricular (LV) hypertrophy (shown as ratio of ventricular weight to tibia length). (**D**) Effect of AAV9–miR-378 on lung weight as a measure of pulmonary congestion. (**E**) Quantification of miR-1 and miR-133a in mouse hearts. Group sizes for A-D are as follows: 5 or 11 sham-treated mice that received AAV9–miR-378 or control, and 7 or 8 TAC-treated mice that received AAV9–miR-378 or control, respectively. All data were evaluated by 2-way ANOVA/Bonferroni posttest. Statistical significance is shown as *P<0.05,**P<0.01, ***P<0.001, or NS.

4.6.2 Effect of miR-378 restoration on cardiac function

Echocardiographic data were obtained and analyzed to assess cardiac function in the mice after TAC. The data showed increased left ventricular (LV) mass, LV internal diameter and LV volume after TAC in the control group while the mice injected with AAV9-miR-378 showed reduced LV mass, LV internal diameter and LV volume (Fig 15A-C). Consequently, both fractional shortening and ejection fraction, impaired in the control group after TAC were significantly improved with AAV9 intervention (Fig 15D-E). The administration of AAV9-miR-378 significantly prevented cardiac dysfunction induced by chronic pressure overload and partially attenuated cardiac hypertrophy. This was supported by the reduction in the mRNA levels of cardiac hypertrophic markers *Nppa, Nppb and Myh7* in the mice that received AAV9-miR-378 compared to the control group after TAC (Fig 15F).

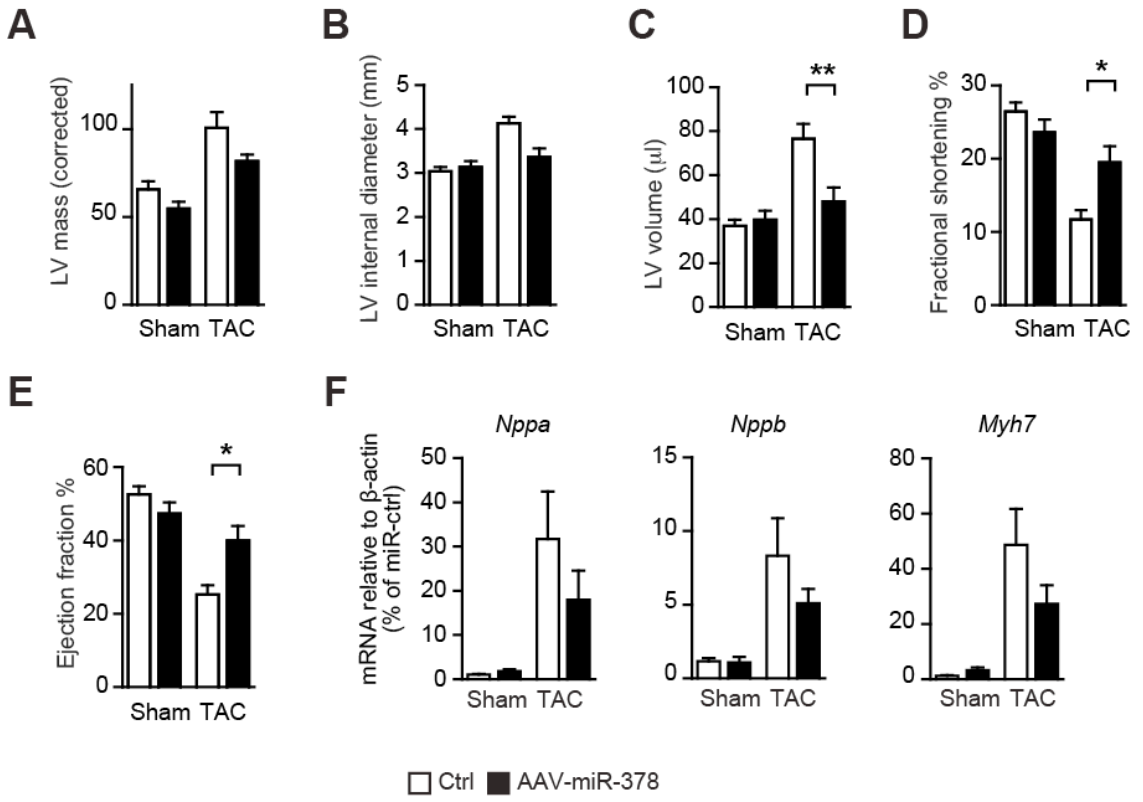

Fig 15. AAV9-miR-378 intervention prevented cardiac dysfunction induced by chronic pressure overload. (**A**)-(**E**) Echocardiographic data on LV mass, LV internal diameter, LV volume, fractional shortening and ejection fraction from mice infected with AAV9–miR-378. (**F**) mRNA levels of the hypertrophy markers *Nppa, Nppb*, and *Myh7* determined by qPCR. Group sizes for A-F are as follows: 5 or 11 sham-treated mice that received AAV9–miR-378 or control, and 7 or 8 TAC-treated mice that received AAV9–miR-378 or control, respectively. All data were evaluated by 2-way ANOVA/Bonferroni posttest. Statistical significance is shown as *P<0.05,**P<0.01, ***P<0.001, or NS.

To exclude a possible effect of AAV9 on cardiac function in these mice, the PBS control group was compared with AAV9-GFP injected mice. Five week old mice were injected with either PBS (ctrl) or AAV9-GFP followed by TAC or sham surgery after 3 weeks (experimental strategy was similar to Fig 14A). Cardiac function was assessed by echocardiographic analysis in both ctrl and AAV9-GFP groups. Both the groups had similar LV weight and similar cardiac function (Fig 16). The control and AAV9-GFP groups had no significant difference in various parameters like LV internal chamber diameter, LV posterior wall thickness, fractional shortening, ejection fraction (Fig 16). Since the TAC induced hypertrophy is almost identical in both the groups, it can be concluded that the antihypertrophic effect of AAV9-miR-378 was not an intrinsic property of AAV9, but a specific response to miR-378 restoration in the mice.

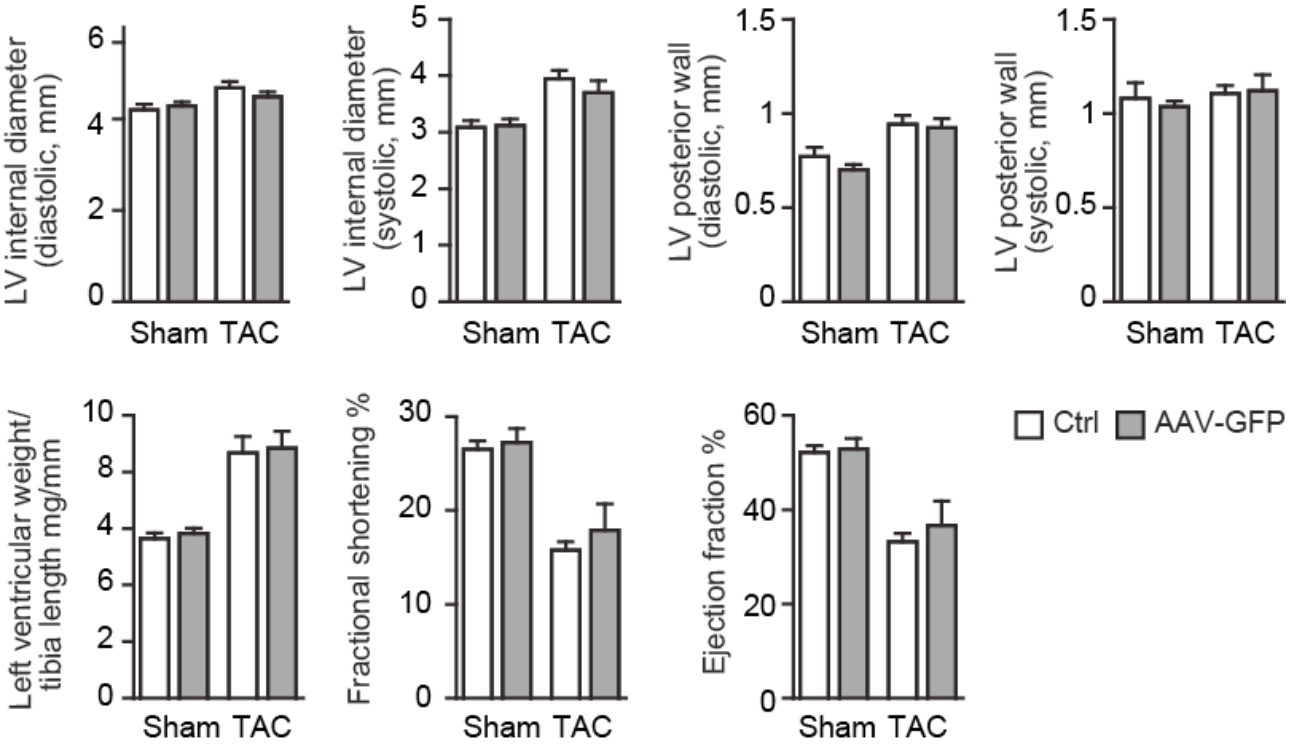

Fig 16. Assessment of parameters for cardiac morphology and function indicates no difference between AAV9-GFP and PBS-control. To test whether an intrinsic property of AAV9 causes the beneficial effects observed with AAV9-miR-378, a control construct for expression of GFP from an AAV9 vector was created (AAV9-GFP) and compared to a PBS control. 5 weeks-old wild type male mice were treated by tail vein injection with either AAV9-GFP (1 x 1012 genome copies/mouse) or PBS. After 3 weeks, thoracic aortic constriction (TAC) was performed. Echocardiographic analysis was performed at 11 weeks of age. Shown here are the LV weight/tibia length data for the two groups along with echocardiography data for fractional shortening, ejection fraction, LV internal diameter (systole and diastole) and LV posterior wall thickness (systole and diastole). Group sizes are: 12 and 4 sham-treated mice that received AAV9-GFP or PBS respectively, and 7 and 6 TAC-treated mice that received AAV9-GFP or PBS, respectively.

4.6.3 Immunohistochemical analysis of cardiac tissue in AAV9 treated mice

Morphometric analyses were performed on subendocardial myocardium to assess the inhibition of cardiac hypertrophy in the AAV9-miR-378 treated mice after TAC. Paraffin-embedded heart sections were stained for wheat germ agglutinin (WGA) to mark the cell borders and SYTOX green to mark the nuclei, followed by automated image processing. Only the cardiomyocytes sectioned in the short axis with a central nucleus were used for quantification of myocyte cross sectional area and myocyte breath. The quantification showed a clear increase in the myocyte hypertrophy after TAC in the control group which was reduced in the AAV9-miR-378 group (Fig 17A-B[‡‡]). Given the proapoptotic effect of miR-378 *in vitro,* the extent of apoptosis in these mice was analyzed using TUNEL staining. AAV9-miR-378 intervention had no effect on apoptosis after TAC (Fig 17C-D). This suggests that the reduction in LV weight and LV mass is due to the antihypertrophic effect of AAV9-based miR-378 restoration and not due to cell death.

The progression of heart failure is accompanied by increased fibroblast proliferation leading to stiffening of cardiac muscle and impaired cardiac function. Although miR-378 is a cardiomyocyte enriched microRNA, indirect paracrine influences on fibroblast proliferation cannot be excluded. This can be assessed by staining for Collagen deposition using Sirius red. Paraffin embedded heart tissue was stained with fast green and Sirius red followed by automated quantification of the sirius red staining. Chronic pressure overload induced by TAC lead to increased interstitial fibrosis as seen by the increased Sirius red staining in the control group (Fig 17E-F). AAV9-miR-378 intervention prevented TAC-induced increase in fibrosis, which is in agreement with reduced cardiac hypertrophy and improved function.

‡‡ Performed by Andrea Ahles

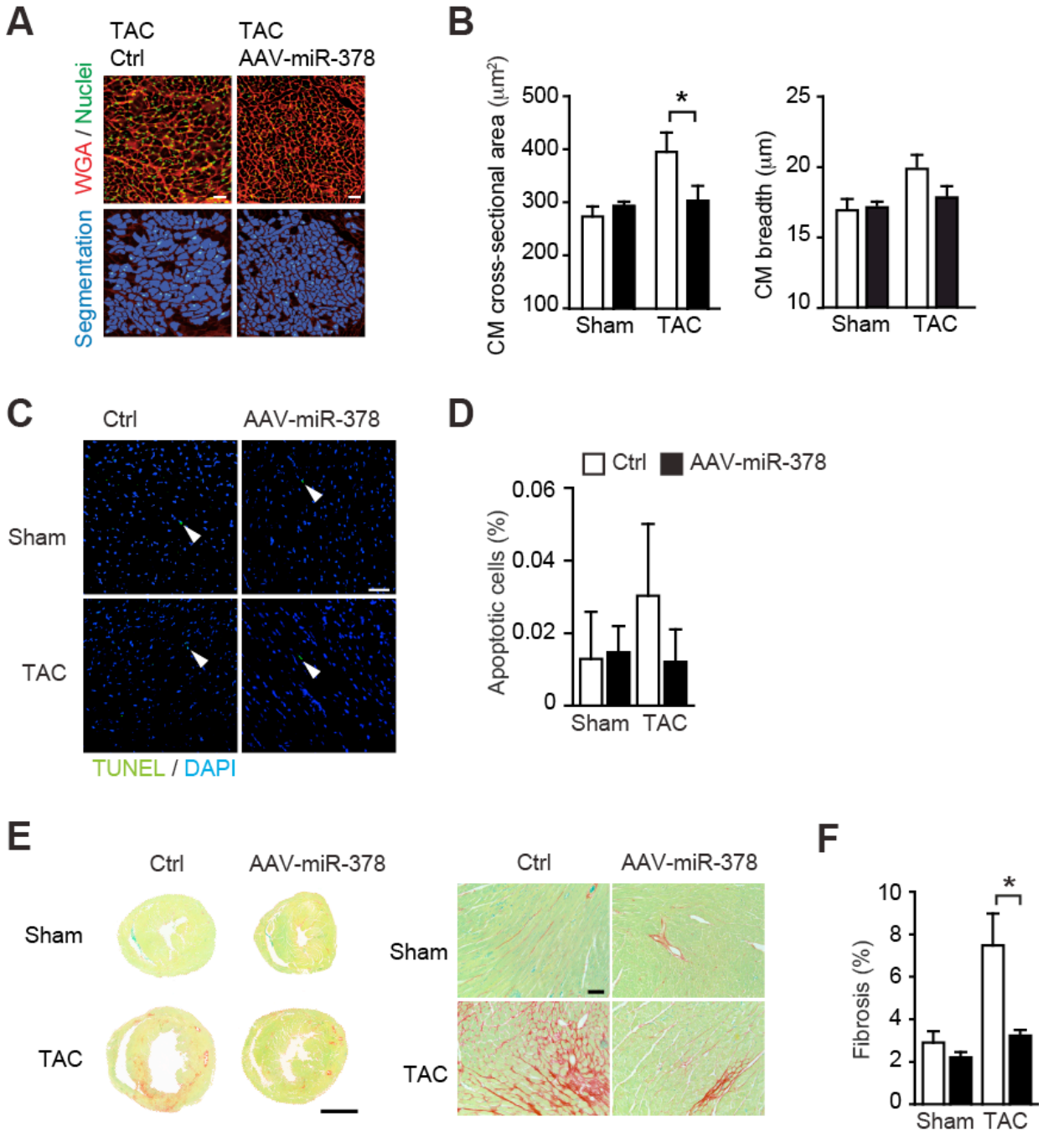

Fig 17. Immunohistochemical analysis. (A) Analysis of cardiomyocyte hypertrophy in cardiac tissue sections stained with WGA and SYTOX green. Individual cells were analyzed in an automated manner by pixel counting on digitized images. Scale bar=50 µm. (**B**) Quantitative analysis of cardiomyocyte (CM) cross-sectional areas and CM breadth (7 control-treated mice and 4–5 AAV9–miR-378–treated mice). (**C**) Exogenous expression of miR-378 does not affect cardiomyocyte apoptosis in vivo. Apoptosis was analyzed in paraffin sections of mouse hearts by TUNEL staining. Representative pictures of TUNEL staining in ctrl and AAV-miR-378-treated mouse hearts. (**D**) Quantification of apoptosis in hearts from mice that had been infected with AAV-miR-378 after TAC (n=7 animals) or sham surgery (n=5). Data from non-infected sham- or TAC-treated control mice are shown in parallel (n=5 each with four fields of view per animal), scale bar = 100 µm. (**E**) Quantification of interstitial fibrosis. Heart tissue sections (left) stained with Sirius red/fast green in the AAV9–miR-378–treated and control group after sham or TAC treatment. (center) Representative images at higher magnification. (**F**) Quantification of left ventricular fibrosis determined from whole-heart sections. Group sizes for E-F are as follows: 5 or 11 sham-treated mice that received AAV9–miR-378 or control, and 7 or 8 TAC-treated mice that received AAV9–miR-378 or control, respectively. All data were evaluated by 2-way ANOVA/Bonferroni posttest. Statistical significance is shown as *P<0.05,**P<0.01, ***P<0.001, or NS.

4.6.4 Effect of miR-378 restoration on MAPK pathway factors

The effect of exogenous expression of miR-378 on the four prohypertrophic targets was analyzed by quantifying their expression levels. Western blot and qPCR analysis of the four targets (*Mapk1*, *Ksr1*, *Igf1r* and *Grb2)* showed a marked upregulation of the four targets upon pressure overload in the control group (Fig 18 A-C). In contrast, the AAV9-miR-378 treated group showed significantly reduced protein levels of KSR1 and MAPK1 (Fig 18 A-B). The mRNA levels of *Igf1r* were also significantly reduced and a trend towards repression of the *Grb2* mRNA levels was observed (Fig 18C). The maintenance of physiological levels of miR-378 upon TAC inhibited the upregulation of the four prohypertrophic targets. The mRNA levels of two other published targets of miR-378 and miR-378* namely *Crat* and *Med13*[102] respectively, were also analyzed by qPCR (Fig 18D[§§]). The restoration miR-378 did not affect the expression of these two targets. Hence a correlation between these two targets and miR-378 is not evident in the heart.

To summarize, the *in vivo* AAV9-miR-378 study clearly demonstrates the antihypertrophic activity of miR-378 in cardiomyocytes together with a functional effect on four targets within the MAPK signaling cascade. miR-378 directly target the activation of MAPK signaling pathway upon pressure overload, at four distinct levels leading to reduced cardiac hypertrophy and improved cardiac function.

[§§] Performed by Deepak Ramanujam

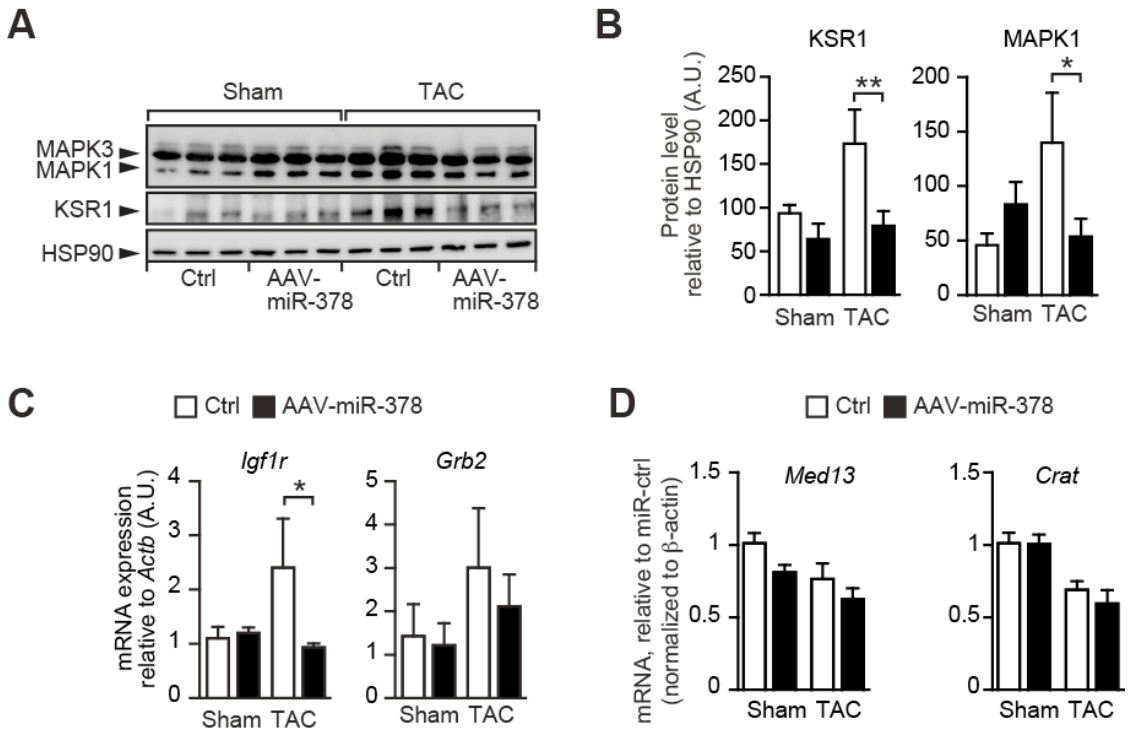

Fig 18. Cardiotropic expression of miR-378 reduced four MAPK factors. (**A**) Western blot analysis of miR-378 target levels in the myocardium of TAC mice treated with AAV9–miR-378. Heat shock protein 90 (HSP90) served as a loading control. (**B**) Quantification of western blot data. (**C**) qPCR analysis of mRNA levels of *Igf1r* and Grb2. (**D**) qPCR analysis of *Med13* and *Crat* in myocardial tissue obtained from AAV9-miR-378 treated mice and control mice after sham or TAC treatment. Group sizes are: 5 sham-treated mice that received AAV9-miR-378 or PBS, and 7 and 5 TAC-treated mice that received AAV9-miR-378 or PBS, respectively. All data were evaluated by 2-way ANOVA/Bonferroni post test. Statistical significance is shown as *P<0.05,**P<0.01, ***P<0.001, or NS.

5 DISCUSSION

MicroRNAs have emerged as key regulators of gene expression during the progression of heart failure. MiR-378 is a muscle-enriched microRNA that is deregulated in the failing heart. In this study we elucidated the role of miR-378 in regulating cardiac hypertrophy, both *in vitro and in vivo.*

5.1 MiR-378 and hypertrophy

The antihypertrophic effect of miR-378 combined with its downregulation in the failing heart suggests a cardioprotective role for this microRNA. Another study in primary cultures of cardiomyocytes also corroborated the antihypertrophic effect of miR-378 under PE stimulation, while identifying *Grb2* as a miR-378 target[103]. The study showed that miR-378 overexpression in primary cultures of cardiomyocytes blocked PE-induced Ras activity preventing the activation of ERK/MAPK and PI3-AKT signaling cascades downstream of Ras as well as blocking PE-induced phosphorylation of S6 ribosomal kinase, pGSK-3β and nuclear accumulation of NFAT. These observations are in line with the results of our current study. Apart from studying the role of miR-378 in primary cardiomyocytes we have also verified our results *in vivo* in a mouse model of chronic pressure overload (TAC). The downregulation of the microRNA under failing conditions in the heart could lead to insufficient control thereby further exacerbating myocardial hypertrophy. Downregulated miR-378 expression in these mice and increased myocyte size demonstrate the exacerbating effect of the insufficient control. When this control is re-exerted via compensation of the microRNA using an adeno-associated virus 9 construct, the progression of the hypertrophy and loss of function is halted leading to significant recovery of the mice.

5.2 MiR-378 and cardiac fibrosis

Extracellular fibrillar collagen functions as scaffolding tissue for the maintenance of cardiac structure[6]. Another important hallmark of the failing heart is the increased collagen deposition along with myocardial hypertrophy. The TAC mice show increased interstitial fibrosis, thus further contributing to ventricular dysfunction. The restoration of miR-378 in these mice via AAV9 showed a near complete attenuation of fibrosis, thus helping in the restoration of cardiac function. Even though miR-378 is enriched within cardiomyocytes, a paracrine effect of the miR cannot be excluded. Thus, a restoration of the lost miR-378 in the TAC mice led to reduced accumulation of myocardial fibrillar collagen.

5.3 MiR-378 and apoptosis

There are contradictory reports on the role of miR-378 in apoptosis, which can be resolved to some extent with the results of this study. A study conducted in H9c2 cells showed attenuation of ischemia-induced apoptosis by caspase-3 inhibition under miR-378 overexpression[83]. Another study in primary cardiomyocyte cultures showed increased apoptosis levels under miR-378 overexpression suggesting a proapoptotic role of the miR in primary cultures[84]. This discrepancy could be attributed to the type of cells used in the studies (H9c2 versus primary cardiomyocyte cultures). Our study confirms a proapoptotic role of miR-378 in primary cardiomyocyte cultures. However, a more definite approach would be to determine the effect of the miR *in vivo*. Our study clearly showed that miR-378 does not promote apoptosis in mice. The restoration of miR-378 levels via AAV9 showed no discernible increase in apoptosis which is in line with the improved cardiac function observed in these mice. Primary cardiomyocyte cultures often show increased sensitivity to apoptotic stimuli, which is not observed *in vivo*[104]. *In vitro* experiments involving transfection of synthetic miR-378 mimics lead to very high cellular levels of microRNA. *In vivo* experiments with the AA9 constructs lead to the restoration of miR-378 to normal physiological levels unlike transfection in an *in vitro* setting.

5.4 Hypertrophy and *Mapk1/3*

A key target of miR-378 is *Mapk1*, which along with *Mapk3* is central signal transduction node. The role *Mapk1/3* in cardiac hypertrophy is under much debate. Experiments conducted in primary neonatal rat cardiomyocytes show *Mapk1/3* activation in response to agonist stimulation or cell stretching[105-107]. The essential role of *Mapk1/3* signaling was further demonstrated using antisense oligonucleotides to prevent PE-induced cardiomyocyte hypertrophy[108]. Endothelin-1 and PE-induced hypertrophy was blocked in studies in NRCM using dominant negative *Map2k1* or *Raf1* cDNA further suggesting a requirement of *Map2k1-Mapk1/3* activation for the initiation or effective progression of hypertrophy in culture[109,110]. *Mapk1/3* activation is also observed in chronic pressure overload stimulation induced by aortic banding in mice[111]. Genetic studies conducted in *Mapk3*$^{-/-}$ and *Mapk1*$^{+/-}$ mice as well as in transgenic mice with inducible expression of an *Mapk1/3*-inactivating phosphatase in the heart (dual-specificity phosphatase 6) induced apoptosis and heart failure in mice but had no effect on hypertrophy[112]. More recently, *in vivo* and *in vitro* studies with mice lacking *Mapk1/3* or overexpressing *Map2k1* showed that *Mapk1/3* regulated the balance between eccentric and concentric cardiac growth[113]. Our present study cannot resolve the open questions but it appears that the control over MAPK1/3 levels exerted by miR-378 reduced cardiac

hypertrophy induced by pressure overload. This leads to further speculation that miR-378 might play an important role in fine tuning the activation of MAPK1/3 cascade during the initiation and progression of hypertrophy and further, a timely intervention by means of an AAV9 miR-378 construct helps regain the control lost due to the downregulation of mir-378 levels in the failing heart.

5.5 *Ksr1*

Apart from *Mapk1*, miR-378 also directly targets *Ksr1*. KSR1 is a scaffold protein that brings together the various components of the ERK/MAPK cascade[114]. KSR proteins contain five conserved domains (Fig 19)[115]: CA1, which is unique to KSR1 and lacking in KSR2; CA2, a proline-rich sequence; CA3, a cysteine-rich domain that mediates interactions with membrane lipids; CA4, a serine/threonine-rich region that binds extracellular signal-regulated kinase/mitogen-activated protein kinase (ERK/MAPK); and CA5, the putative kinase domain. C-TAK1 binds to the N-terminal region and phosphorylates the 14-3-3 docking sites S297 and S392. MAPK and MAP2K (MEK) and RAF bind to the C-terminal region that contains the CA5 domain. RAF kinases share three conserved regions: CR1, a cysteine-rich domain that contains part of the Ras-binding domain and also interacts with membrane lipids; CR2, a serine/threonine rich region that forms part of the MST2 (mammalian sterile-twenty-like-2) binding region; and CR3, the kinase domain, which can bind MAP2K.

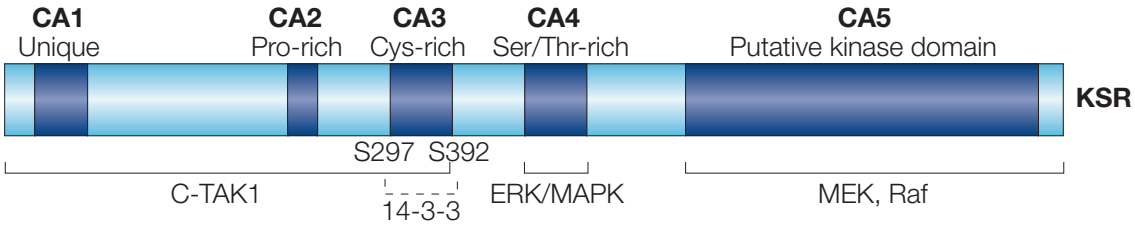

Fig 19. Conserved domains in KSR1 (Illustration from Kolch 2005)

Binding of 14-3-3 proteins to S392 in KSR or S259 in RAF1 sequesters KSR1 and RAF1 in the cytosol (Fig 20). The kinase activity of KSR1 is yet unclear although several studies have conclusively support its kinase-independent function as a molecular scaffold. Studies have shown that cooperation of KSR1 protein with Ras to transform cells required the cysteine-rich CA3 domain in the non-catalytic region, but not the KSR1 kinase domain suggesting a scaffolding role for KSR1[116].

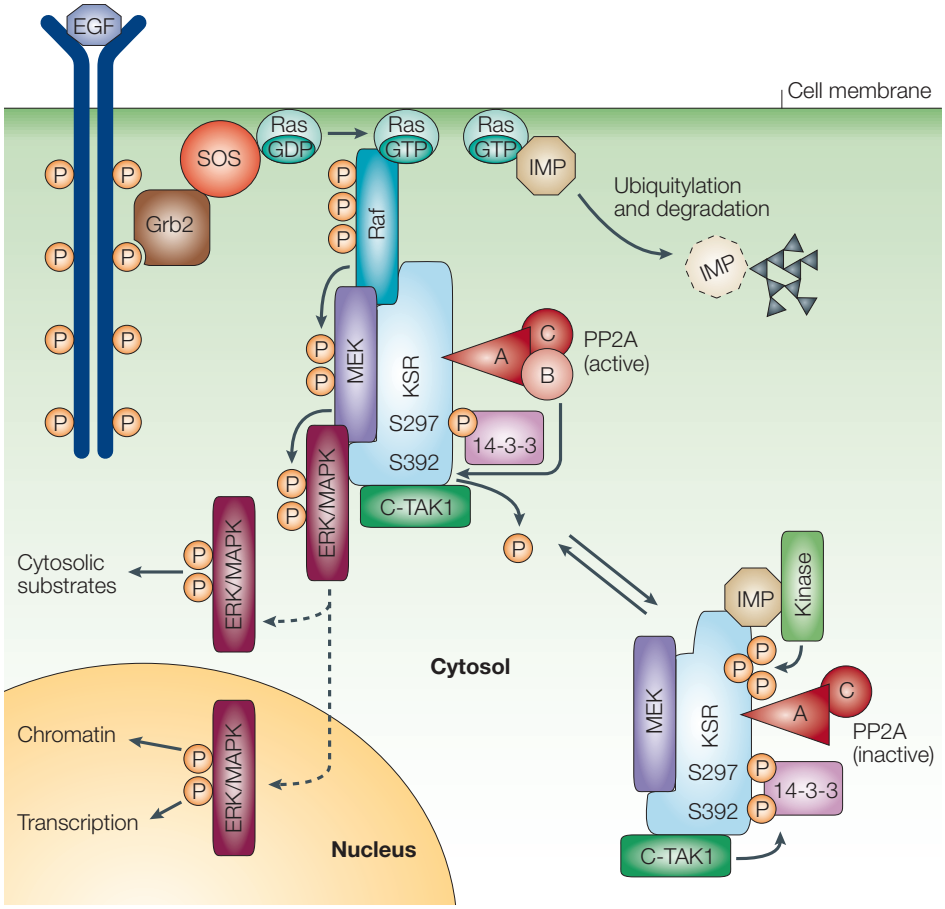

Fig 20. The KSR regulation cycle (Illustration from Kolch 2005)

KSR1 scaffolds the three-tiered RAF–MEK–ERK module (Fig 20). Studies have shown that titrating the levels of KSR1 expression affects ERK/MAPK pathway signaling in a bell-shaped-curve manner. That is, an increase in KSR1 expression enhances the assembly of the module until the concentration of the scaffold exceeds that of its client proteins causing them to bind individually rather than forming a complete signaling module[117].

Studies in KSR deficient mice showed that KSR1 facilitated MAPK activation by enhancing the Ras/MAPK signaling pathway[118]. In response to growth factors, KSR1 is translocated to the cell membrane leading to MEK activation, by facilitating an interaction with activated Raf[119]. In quiescent cells, KSR1 is retained in a Triton insoluble compartment by the protein ‘impedes mitogenic signal propagation’ (IMP)[120] and in the cytoplasm by 14-3-3 proteins that dock to the serine-phosphorylated residues 297 and 392. S392 is phosphorylated by Cdc25C-associated kinase-1 (C-TAK1)[119] and nucleoside diphosphate kinase, mitochondrial-23 (Nm23)[121]. Growth stimulus induces the dephosphorylation of S392 by protein phosphatase-2A (PP2A) and the destruction of IMP that enables the translocation of KSR1 to the cell membrane. In mice, the knockout of Ksr1 causes defects in antigen-triggered T-cell proliferation and disorganized hair

follicles[115]. Importantly, *Ksr1*$^{-/-}$ mice are less susceptible to oncogene-induced tumours than their wild-type counterparts[115], implying that KSR1 supports the proliferative and transforming functions of the ERK/MAPK pathway. This is consistent with the notion that ablation of KSR1 abolishes the sustained activation of ERK/MAPK that is required for mitogenesis. Cardiac specific *Ksr1* deletion has not yet been reported.

5.5.1 Hypertrophy and KSR1

Until now there have been few reports highlighting the role of KSR1 in the regulation of hypertrophy. Experiments involving siRNA against KSR1 in our study clearly showed a correlation between the abolition of the antimiR-378 induced hypertrophy with KSR1 inhibition suggesting in its involvement in the regulation of cardiac hypertrophy. Interestingly, other proteins linked to KSR1 and Ras signaling have been shown to regulate cardiac hypertrophy.

CNK - RASSF1

Connector enhancer of KSR (CNK) was identified in a genetic screen in D. melanogaster as an enhancer of the dominant negative phenotype caused by the isolated KSR kinase domain[122]. Studies show that CNK functions downstream of receptor tyrosine kinases (RTKs) and Ras, but upstream or parallel to RAF[122]. CNK coordinates other signaling pathways by interacting with many proteins that include: RAL (Ras-like protein) and its exchange factors, Ral guanine nucleotide dissociation stimulator (Ral-GDS) and RalGDS-like factor (RLF); Ras-association domain family-1 (RASSF1), and Rho, through which CNK1 selectively enhances Rho stimulated transcription[115,122,123]. Ras is a family of low-molecular-weight guanine nucleotide binding proteins that has long been associated with hypertrophy[124]. RASSF1 is a member of the RASSF family of tumor suppressor proteins that consist of at least 10 different proteins, RASSF1-10. Seven isoforms of RASSF1 have been recognized, RASSF1A through RASSF1G, which are derived from alternative splicing and different promoter usage[125]. RASSF1A has been described as a pivotal protein in regulating cardiac hypertrophy in mouse. Its absence causes increased hypertrophy and remodeling under conditions of sustained mechanical stress by increased activation of the MAPK1/3 signaling pathway.

5.6 Hypertrophy and IGF1R

The insulin signal transduction pathway is an important player in cardiac growth regulating several aspects of cellular physiology and growth. IGFs are secreted polypeptides that act by binding to tyrosine kinase receptors[126]. They usually circulate in the bloodstream and extracellular space

mediating endocrine and/or paracrine effects on numerous signal transduction networks. They are produced throughout the body especially in the liver, skeletal muscle and heart.

The GH - IGF axis

Growth hormone (GH) is a key regulator of growth in animals. GH stimulation leads to activation of IGF-1 secretion in local tissues leading to metabolic and growth promoting effects and stimulation of protein synthesis. IGF-1 mediates many of the effects of growth hormone (GH) on peripheral tissues[127]. Any interference in this signaling axis can have profound cardiac manifestations. A very specific cardiomyopathy has been described in a majority of patients with acromegaly (increased serum GH and IGF-1 levels), characterized by biventricular concentric myocardial hypertrophy with interstitial fibrosis, lympho-mononuclear infiltration and areas of monocyte necrosis[128]. This suggests that IGF-1 may be important in the development of ventricular hypertrophy.

IGFs are characterized by a signal peptide, a B-chain, a C-peptide, and an A-chain. The C-peptide of the propeptide is proteolytically cleaved and two disulfide bonds between the A- and B-chains, and a third disulfide bond within the A-chain are present in the mature peptide. In mammalian IGF-1 and IGF-2, the C-peptide is retained in the mature peptide[129].

The IGF-1 receptor (IGF1R) is assembled in a β–α–α–β structure that is similar to that of the insulin receptor. The difference between the two receptors lies in the extracellular α subunit that controls the ligand binding specificity of the receptor[130]. IGF1R can be activated by the binding of both IGF1 and IGF2.

A number of studies have described a role of IGF1 in the development of cardiac hypertrophy. Studies have shown that mild or short-term overload-induced physiological hypertrophy where the heart enlarges until it establishes a new operational plateau. Severe and/or sustained overload lead to pathological hypertrophy, characterized by increased fibrosis and decreased cardiac output (Fig 9 and Fig 11E-F). Transverse aortic constriction lead to activation of the IGF1-IGF1R autocrine axis accompanied by an increase in the mRNA levels of IGF1[131] and IGF1R (Fig 12C). IGF1 has been implicated to be the primary factor contributing to the development of cardiac hypertrophy under conditions of pressure overload[132]. It has also been described that IGF-I-stimulated collagen production in primary cultures of mechanically loaded cardiac fibroblasts[133]. This is consistent with increased cardiac fibrosis observed in patients with acromegaly and increased IGF1 stimulation. Sustained expression of IGFI in a transgenic mouse model initially induced an analog of physiologic hypertrophy, characterized by increased cardiac mass and improved systolic

performance. However, later this hypertrophy progressed to a pathological condition characterized by decreased systolic performance and increased interstitial fibrosis[134]. IGF1 has been reported to be a direct target of miR-1. Consequently, pressure overload-induced downregulation of miR-1 ia accompanied by IGF1 upregulation[135](Fig 8E).

In our study *Igf1r* has been clearly shown to be a target of miR-378, which is also described by other studies[84]. Transgenic mice overexpressing *Igf1r* in the heart displayed cardiac hypertrophy with increased myocyte size though there was no evidence of histopathology[136]. These mice also displayed enhanced systolic function at 3 months of age maintained until 12–16 months of age. The phosphoinositide 3-kinase (PI3K)-Akt- p70S6K1 pathway was found to be significantly activated in hearts from these transgenic mice. Cardiac hypertrophy induced by overexpression of IGF1R was completely blocked by a dominant negative PI3K mutant, suggesting that IGF1R promoted compensated cardiac hypertrophy in a PI3K dependent manner. Analysis of MAPK1/3 signaling in these mice showed increased phosphorylation as well as increased total MAPK1 levels. The IGF1-PI3K axis has been implicated in physiological hypertrophy, while the Gaq pathway is supposed to regulate pathological hypertrophy[137]. This distinction however, does not seem completely consistent. The activation of MAPK1/3 signaling in IGF1R transgenic mice suggest a possible interaction between the two pathways. Our current study suggests a clear role of IGF1R in pathological cardiac hypertrophy both in vitro as well as in vivo. The regulation of IGF1R by miR-378 contributes to the protective effect of miR-378 compensation under pressure overload-induced pathological hypertrophy. This accompanied by the fact that sustained IGF1 expression lead to pathological cardiac hypertrophy overtime further suggests the involvement of IGF1-IGF1R activation in pathological cardiac hypertrophy. This hypothesis is further supported by studying another miR, namely miR-1 in a similar scenario. miR-1 has been shown to directly target both IGF1 and IGF1R[135] and negatively regulate hypertrophy.

AKT is a serine/threonine protein kinase, primarily regulated by PtdIns(3,4,5)P_3-mediated membrane recruitment and by PDK1 activity. PI3K-dependent PDK1 activation leads to direct AKT phosphorylation at Thr308. There are three genes encoding AKT namely, *Akt1, Akt2* and *Akt3* . Of the three, *Akt1* and *Akt2* are the main cardiac isoforms. *Akt1* null mice showed impaired growth and resistance to exercise induced cardiac hypertrophy[138]. Similarly, overexpression of a dominant negative AKT1 mutant in the heart inhibited physiological hypertrophy. Cardiac overexpression of constitutively active AKT1 mutant initially promoted physiological hypertrophy that eventually progressed to pathological hypertrophy[139,140]. This suggests that the role of AKT in hypertrophy is dependent on the magnitude of AKT1 activation and its cellular location. Also, in

another study, overexpression of AKT led to a decrease in miR-1 expression levels suggesting that the PI3-AKT cascade need not always be protective[135]. Perhaps microRNAs like miR-378 and miR-1, mediate the fine tuning of AKT and MAPK signaling cascades and balance their adaptive and maladaptive features.

5.7 Hypertrophy and *Grb2*

GRB2 is a scaffolding protein composed of two Src-homology type 3 (SH3) domains flanking a single SH2 domain[141,142]. The SH3 domains bind to polyproline peptide motifs on the Ras guanine nucleotide exchange factor SOS. The SH2 domain of Grb2 binds to phosphotyrosine motifs present on activated FAK, Shc, and receptor tyrosine kinases. Grb2 knockout mice are unable to form epiblast and display defective endoderm differentiation, due to which they do not survive embryonic development. However, *Grb2* haploinsufficient mice are able to survive embryogenesis and appear normal at birth[143]. Biomechanical stress during cardiac pressure overload is mediated through integrins that trigger downstream molecules like activation of tyrosine kinase FAK and small GTPase Ras and the subsequent recruitment of adapter protein GRB2, which in turn can activate various MAPK cascades via the Ras guanine nucleotide exchange factor SOS[144]. *Grb2* haploinsufficient mice showed attenuated p38 MAPK and JNK activation, but not ERK activation suggesting a differing dose response thresholds of various MAPK cascades to Ras activation[145]. Raf-1 activation may require a relatively small amount of Ras-GTP loading since the MAPK kinase kinase(MAPKKK) directly binds to Ras unlike other p38 and JNK that do not directly bind to Ras and instead are dependent upon other intermediary proteins. Our study supports this view since our results show that inhibition of GRB2 along with the other factors in ERK/MAPK cascade is able to attenuate ERK activation.

Grb2 haploinsufficient mice did not develop cardiac hypertrophy or fibrosis in response to pressure overload[145]. Also, transgenic mice expressing dominant negative forms of p38 MAPK in the heart developed cardiac hypertrophy but not fibrosis after pressure overload despite markedly reduced p38 MAPK suggesting that cardiac hypertrophy and fibrosis is dependent upon a signal transduction pathway that includes GRB2 but not p38 MAPK. These observations clearly demonstrate the importance of GRB2 in pressure overload mediated cardiac hypertrophy and fibrosis. Our current study supports these results further demonstrating the prohypertrophic role of GRB2 both in culture and in mice. Inhibition of GRB2 using an siRNA protected NRCMs against the prohypertrophic effect of antimiR-378. In mice, the AAV-miR-378 intervention re exerted the

control over pressure overload-induced activation of MAPK cascade by the regulation of GRB2 levels.

5.8 Downregulation of miR-378 in the failing heart

The location of miR-378 within the first intron of the gene *Ppargc1b* and its cotranscription with the transcriptional coactivator PGC1β suggests a possible interconnection between the two. Another interesting observation is the downregulation of PGC1β during heart failure. The downregulation of miR-378 in the failing heart could be attributed to the downregulation of PGC1β. The PGC1 family of coactivators are a class of extensively researched regulators of metabolic pathways. They work as inducible coregulators of nuclear receptors regulating metabolic pathways controlling cellular energy[146]. Coactivators, PGC-1α and PGC1β and the nuclear receptors estrogen-related receptors α and γ (ERRα and γ) form a key signaling node responsible for the regulation of cardiac genes involved in multiple mitochondrial energy transduction and ATP-generating pathways[147]. Members of the nuclear receptor superfamily relay physiologic and nutritional cues to critical gene regulatory responses. The molecular links between external stimuli, cellular signaling events, and nuclear receptor-mediated transcriptional control has multiple implications in the failing heart[146]. Nuclear receptors receive regulatory input through multiple mechanisms including levels of endogenous ligand, availability of heterodimeric nuclear receptor partners, and posttranslational modifications. Activating signals trigger the recruitment of coactivator complexes onto the nuclear receptor platform, leading to enzymatic modification of chromatin, increased access of the RNA polymerase II machinery to RNA, and activation of target gene transcription. Availability of PGC1 family of coactivators serve critical regulatory functions linking physiologic stimuli to nuclear receptor activity.

PGC-1α and PGC-1β are preferentially expressed in tissues with high oxidative capacity, such as heart, slow-twitch skeletal muscle, and BAT, where they serve critical roles in the regulation of mitochondrial functional capacity and cellular energy metabolism. PGC-1 coactivator docking to specific transcription factors provides a platform for the recruitment of regulatory protein complexes that exert powerful effects on gene transcription[148].

Mir-378 and miR-378* are coexpressed and coregulated with PGC-1β[102,149]. MiR-378* has been described as a molecular switch involved in the orchestration of the Warburg effect in breast cancer cells via interference with a well-integrated bioenergetics transcriptional pathway leading to a reduction in tricarboxylic acid cycle gene expression and oxygen consumption as well as an increase in lactate production and in cell proliferation[149].

MiR-378/miR-378* knockout mice showed resistance to high fat diet-induced obesity and exhibited enhanced mitochondrial fatty acid metabolism indicating that they were essential for the control of mitochondrial metabolism and systemic homeostasis[102]. Also, the two miRs were found to directly target carnitine O-acetyltransferase, a mitochondrial enzyme involved in fatty acid metabolism, and MED13, a component of the mediator complex that controls nuclear hormone receptor activity, respectively. Consequently, the two targets were reported to be elevated in the livers of the miR-378/miR-378* knockout mice. Interestingly, the authors did not find any regulation of the two mRNAs in the hearts of the knockout mice. Also, the hearts of the knockout mice did not display increased fat or triglyceride accumulation or any other phenotype. Moreover, an analysis of the two targets in our current study showed no regulation in the hearts of the AAV-miR-378 treated mice (Fig 11D) suggesting that perhaps miR-378 regulates a different pool of targets in the heart.

5.8.1 *Pgc1α* and *Pgc1β*

Fuel and energy metabolic disturbances are a signature of cardiac hypertrophy and heart failure [150]. The development of pathologic cardiac hypertrophy due to pressure overload is associated with a relative increase in glucose utilization and reduction in fatty acid oxidation and a shift towards a fetal metabolic profile[151]. This metabolic shift is related to the downregulation of expression and activity of PGC-1α, ERRα and downstream target genes. Since miR-378 and PGC-1β are coexpressed and coregulated, their downregulation may contribute to the metabolic shift. This metabolic shift may initially be an adaptive function to divert flux away from mitochondrial pathways, over the long-term this response is likely to be maladaptive leading to energy starvation and heart failure[152]. The phenotype of PGC-1 loss-of-function mice demonstrates that reduced PGC-1/ERR activity can lead to cardiac dysfunction[153-155]. Similarly, inhibiting PGC-1 expression via cardiac-specific overexpression of HDAC5 also produces a cardiomyopathy that is associated with mitochondrial abnormalities and myocardial lipid accumulation.

PGC-1α overexpression in cardiac myocytes in vitro and in vivo in transgenic mice is sufficient to trigger mitochondrial proliferation suggesting the importance of PGC-1 coactivators in perinatal mitochondrial biogenesis[156]. Conversely, in mice with combined PGC-1α/β gene disruption, perinatal mitochondrial biogenesis is arrested and the mice die within days after birth from heart failure[153]. Together, these results indicate that the PGC-1 coactivators are necessary and sufficient for postnatal metabolic maturation and cardiac function.

In pressure overload hypertrophy and heart failure, the repression of PGC-1α and its transcriptional partners is responsible for the shift away from fatty acid oxidation toward glucose oxidation and

impaired ATP production[157]. PGC-1α knockout mice show accelerated cardiac dysfunction and heart failure following pressure overload hypertrophy[155]. These knockout mice show reduced expression of fatty acid oxidation and oxidative phosphorylation genes similar to wild type mice following pressure overload. This repression was more pronounced in banded PGC-1α knockout mice and coinciding with the onset of heart failure. These banded mice also show increased oxidative stress, which might further contribute towards accelerated heart failure[158]. All these observations suggest that perhaps a component of the mitochondrial dysfunction during the transition from compensated hypertrophy to heart failure might be PGC-1α independent[159]. PGC-1β knockout mice showed reduced oxidative phosphorylation gene expression and palmitoyl-carnitine-supported mitochondrial function but normal fatty acid oxidation. Following pressure overload hypertrophy PGC-1β knockout mice exhibited higher oxidative stress, decreased cardiac efficiency, lower rates of glucose metabolism, and repression of hexokinase II protein thus showing that PGC-1β deficiency, like PGC-1α, accelerated the transition to heart failure in pressure overload hypertrophy[159]. These studies suggest partially overlapping roles of PGC-1α and PGC-1β in maintaining mitochondrial energetics.

5.8.2 The repression of PGC-1 in the failing heart

The shift towards fetal metabolic profile during the development of cardiac hypertrophy is related to the repression of PGC-1 family, ERRα and their downstream target genes. M-CPT I and MCAD, are enzymes catalyzing the rate-limiting steps in the mitochondrial import and oxidation of fatty acids, respectively. Hypertrophy mediated by the α1-adrenergic agonist PE, resulted in a decrease in M-CPT1 levels[160]. The M-CPT1 promoter activity was mapped to a peroxisome proliferator–activated receptor-α (PPARα) response element that was reduced during both PE stimulation as well as during pressure overload in mice. This repression was found to be mediated at the post transcriptional level via the ERK/MAPK pathway. The inhibition of the PE stimulated ERK/MAPK pathway activation using an inhibitor (PD98059) prevented the repression of fatty acid oxidation, while the inhibition of other MAPKs like JNK or p38 had no effect. Also, PPARα was found to be a direct target of ERK/MAPK via phosphorylation sites located in the NH_2 terminal AB domain of PPARα. To summarize, during pathological hypertrophy, fatty acid oxidation is downregulated via the deactivation of PPARα and its coactivator PGC-1α by the action of ERK/MAPK pathway.

The ERK-MAPK pathway has also been shown to phosphorylate and inhibit PPARγ activity in noncardiac cell lines[161]. Adipocyte differentiation is strongly inhibited by many mitogens and oncogenes. Several growth factors that inhibit fat cell differentiation caused ERK/MAPK mediated

phosphorylation of the transcription factor PPARγ and reduction of its transcriptional activity. Expression of PPARγ with a nonphosphorylatable mutation at this site (serine- 112) yielded cells with increased sensitivity to ligand-induced adipogenesis and resistance to inhibition of differentiation by mitogens. Taking this into account, it can be hypothesized that activation of the ERK/MAPK activity during hypertrophy is likely to result in the repression of PPARγ and its coactivator PGC-1β as in the case of PPARα and its coactivator PGC-1α.

Hypertrophy is accompanied by activation of cyclin T/Cdk9, which phosphorylates the C-terminal domain of the large subunit of RNA polymerase II, stimulating transcription elongation and pre-mRNA processing; CDK9 activity was required for hypertrophy in culture, whereas heart-specific activation of CDK9 by cyclin T1 provoked hypertrophy in mice[162]. At pathophysiological levels, Cdk9 activity suppresses many genes for mitochondrial proteins including master regulators of mitochondrial function PGC-1 and nuclear respiratory factor-1[163]. In culture, cyclin T1/CDK9 suppresses PGC-1, decreases mitochondrial membrane potential, and sensitizes cardiomyocytes to apoptosis, effects rescued by exogenous PGC-1. Cyclin T1/Cdk9 inhibits PGC-1 promoter activity and preinitiation complex assembly. Thus, hypertrophy-induced-activation of CDK9 may contribute towards defective mitochondrial function via diminished PGC-1 transcription. Since PGC-1 and miR-378 are cotranscribed, this mechanism could in part also explain the downregulation of miR-378 during hypertrophy.

5.9 Multilevel regulation of signaling pathways

One of the most intriguing aspects of this study is the multilevel regulation of the ERK/MAPK signaling cascade. MiR-378 targets the ERK/MAPK cascade by directly interfering with IGF1R, GRB2, KSR1 and MAPK1. MicroRNAs can be described as fine tuners that aid in the complexity of an organism[164]. Often they have been described to cause changes by effectively rewiring cell specific networks at all levels of organismal hierarchy, from specific pathways to global regulators. Due to speed, reversibility and compartmentalization of microRNA mediated mechanisms, they are ideally suited to affect rapid, adaptive changes in gene expression to maintain homeostasis or to respond to specific signals[165]. To achieve such effects, microRNAs might be required to rapidly repress pathways by targeting them on multiple levels. In this study we have described the targeting of a major signal transduction node on four different levels by miR-378 affecting the cellular response to stress. This is one of the first instances where a much speculated idea has been experimentally validated. The ERK/MAPK signaling node is an important effector of a multitude of cellular processes. The existence of conserved miR-378 targets within this cascade underscores its

evolutionary importance. MicroRNA binding sites are comparatively less prone to evolutionary changes owing to their small sizes compared to other regulatory sites like promoters[165]. Since microRNAs are mostly considered to fine tune cellular processes, for a major phenotypic effect, it can be speculated that several microRNAs would need to act together to exert a combinatorial effect or one microRNA might need to regulate multiple targets within a central pathway. There are few other studies that offer experimental proof for this hypothesis. The miR-17-92 cluster (a cluster of 6 miRs) was found to be a potent inhibitor of TGFβ signaling cascade[166]. They used SILAC and quantitative mass spectrometry techniques to show the cooperation between individual miR-17-92 miRs in different cellular processes involved in cancer like proliferation and cell adhesion. The miR-17-92 cluster was found to be relevant both upstream and downstream of pSMAD2 triggering the inhibition of multiple key effectors in the TGFβ-signaling cascade as well as through direct inhibition of TGFβ-responsive genes. Another study with miR-24 showed the regulation of 7 cell cycle regulatory genes forming a direct interaction network with genes enhancing cell cycle progression[167]. This regulation is rather atypical because miR-24 regulates the 7 targets namely, E2F2, MYC, AURKB, CCNA2, CDC2, CDK4, and FEN1 by recognizing seedless sequences. Our current study describes a direct interaction with the 3' UTR of multiple genes within an important signaling node resulting in a strong phenotype linking a microRNA and a specific signaling cascade to complex phenomena like hypertrophy and heart failure.

5.10 Therapeutic relevance of AAV based gene therapy

Cardiovascular gene therapies have provided newer and better opportunities to overcome the increasing morbidity and mortality rates due to heart failure. *In vivo* gene therapy using AAVs is now a major area of research with successful translation to the clinic. In line with this, our current study shows that targeted delivery of miR-378 to the heart could be an effective therapeutic strategy to combat myocardial disease. One important aspect of AAV therapy is the issue of toxicity due to overexpression of a gene. However, in our current study, we have only attempted to rescue the disease-induced downregulation of miR-378 by bringing it back to physiological levels. It can be speculated that by compensating for the loss of a regulatory molecule in a diseased animal, we merely attempt to right the balance by reexerting the control normally exerted by the microRNA under basal steady state. An issue of concern regarding AAV-based gene therapy is the robust systemic transduction to off target tissues like the liver. Titration of AAV9 levels have shown efficient transduction to heart while minimizing transduction to other tissues like liver and muscle[95]. These strategies that have been proven in mice need to be successfully translated to preclinical large

animal models to better understand the limitations and overcome them. Another limitation of using AAV for gene therapy is their limited packaging capacity. However, since miRs relatively are smaller than other genes, it makes them particularly well suited for AAV-based gene therapy. Limiting the expression of the miR to a specific cell type within the heart is another major challenge. AAV9 has been shown to be myocyte specific in the heart[168]. In our current study we have used AAV9 with a CMV promoter to rescue miR-378 in myocytes. Further studies are required to achieve an even higher specificity perhaps through a myocyte specific promoter.

5.11 Conclusion

MicroRNA-378 is encoded within the intron of the gene *Ppargc1b*. MiR-378 was identified through an automated screening strategy specially designed to identify miRs regulating hypertrophy in myocytes. MiR-378 was found to be enriched within cardiomyocytes and downregulated in the heart. We found that miR-378 negatively regulated cardiac hypertrophy by inhibiting IGF1R, GRB2, KSR1 and MAPK1. Compensation of miR-378 downregulation in a pressure overload mouse model using AAV9-based gene transfer protected the heart against hypertrophy and dysfunction. Together we propose the hypothesis (Fig 21) that miR-378 negatively regulates cardiac hypertrophy by targeting the ERK/MAPK cascade at four different levels leading to significantly improved cardiac function upon pressure overload.

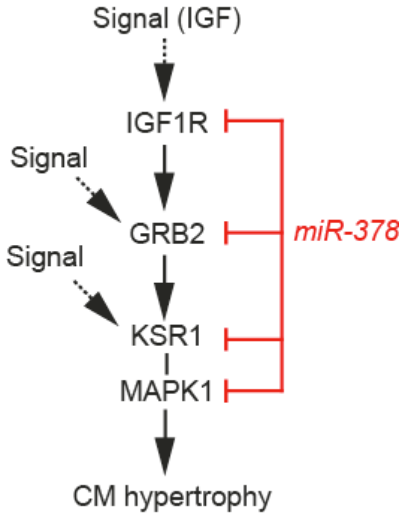

Fig 21. Scheme depicting the control of the MAPK signaling pathway through miR-378.

6 SUMMARY

MicroRNAs are endogenous ≈22 nt long non coding RNA molecules that modulate gene expression at the post transcriptional level by targeting mRNAs for cleavage or translational repression. MicroRNA-mRNA interaction involves a contiguous and perfect pairing within complementary sites usually in the 3' UTR of the target mRNA. Heart failure is associated with myocyte hypertrophy and death, due to compensatory pathological remodeling and minimal functional repair along with microRNA deregulation.

In this study, we identified candidate microRNAs based on their expression strength in cardiomyocytes and by their ability to regulate hypertrophy. Expression profiling from early and late stages of heart failure showed several deregulated microRNAs. Of these microRNAs, miR-378 emerged as a potentially interesting microRNA that was highly expressed in the mouse heart and downregulated in the failing heart. Antihypertrophic activity of miR-378 was first observed by screening a synthetic miR library for morphologic effects on cardiomyocytes, and validated in vitro proving the tight control of hypertrophy by this miR. We combined bioinformatic target prediction analysis and microarray analysis to identify the targets of miR-378. These analyses suggested that factors of the MAP kinase pathway were enriched among miR-378 targets, namely MAPK1 itself (also termed ERK2), the insulin-like growth factor receptor 1 (IGF1R), growth factor receptor-bound protein 2 (GRB2) and kinase suppressor of ras 1 (KSR1). Regulation of these targets by miR-378 was then confirmed by mRNA and protein expression analysis. The use of luciferase reporter constructs with natural or mutated miR-378 binding sites further validated these four proteins as direct targets of miR-378. RNA interference with MAPK1 and the other three targets prevented the prohypertrophic effect of antimiR-378, suggesting that they functional relate to miR-378. In vivo restoration of disease induced loss of miR-378 in a pressure overload mouse model of hypertrophy using adeno associated virus resulted in partial attenuation cardiac hypertrophy and significant improvement in cardiac function along with reduced expression of the four targets in heart.

We conclude from these findings that miR-378 is an antihypertrophic microRNA in cardiomyocytes, and the main mechanism underlying this effect is the suppression of the MAP kinase-signaling pathway on four distinct levels. Restoration of disease-associated loss of miR-378 through cardiomyocyte-targeted AAV-miR-378 may prove as an effective therapeutic strategy in myocardial disease.

Zusammenfassung

MicroRNAs sind ca. 22 Nukleotide lange endogene, nicht-kodierende RNA-Moleküle, die die Expression von Genen posttranskriptionell regulieren, indem sie den Abbau der Ziel-mRNA herbeiführen oder deren Translation hemmen. Die Interaktion von microRNA und mRNA erfolgt durch perfekt komplementäre Bindung in der 3'-untranslatierten Region der Ziel-mRNA. Eine Deregulation der Expression verschiedener microRNAs lässt sich bei Herzinsuffizienz beobachten. Im insuffizienten Herzen laufen kompensatorische pathologische Remodellingprozesse ab und es kommt unter anderem zu Hypertrophie und Apoptose von Kardiomyozyten.

Im Rahmen dieser Arbeit haben wir Kandidaten-microRNAs nach folgenden Kriterien identifiziert: 1) Expressionsstärke in Kardiomyozyten, 2) Fähigkeit zur Regulation von Kardiomyozytenhypertrophie im Screening einer synthetischen microRNA-Bibliothek auf Kardiomyozytengröße und 3) Regulation ihrer Expression in frühem und späten Stadium eines murinen Herzinsuffizienzmodells. Aus den resultierenden Kandidaten-microRNAs wurde im folgenden miR-378 näher untersucht. MiR-378 war im gesunden Mausherz stark exprimiert. Die Expression nahm bei Herzinsuffizienz ab. Weiterhin hatte die Überexpression von miR-378 in neonatalen Kardiomyozyten einen antihypertrophen Effekt. Im Gegenzug führte die Expression von antimiR-378 zu einer verstärkten Hypertrophie. Zur Target-Suche wurden zum einen bioinformatische Vorhersage-Datenbanken verwendet und zum anderen ein Microarray durchgeführt. Diese Analysen zeigten eine Anreicherung von Faktoren des MAP-Kinase-Signalweges: Mitogen-aktivierte Proteinkinase 1 (MAPK1, auch als ERK2 bezeichnet), Insulin-ähnlicher Wachstumsfaktorrezeptor 1 (IGF1R), Wachstumsfaktorbindeprotein 2 (GRB2) und Kinasesuppressor von Ras 1 (KSR1). Die Regulation dieser Targets durch miR-378 wurde durch Bestimmung der mRNA- und Proteinexpression nach Überexpression bzw. Inhibition von miR-378 bestätigt. Durch Luziferaseassays mit Reporterkonstrukten, die jeweils die exakten oder mutierte Bindungsstellen der vier Targets enthielten, konnte gezeigt werden, dass die mRNAs der vier Faktoren direkte Targets von miR-378 darstellen. Durch siRNA-mediierte Herabregulation der Zielproteine konnte der prohypertrophe Effekt von antimiR-378 inhibiert werden. Daraus lässt sich schließen, dass der Hypertrophie-Phänotyp direkt auf miR-378 zurückzuführen ist. Schließlich wurde der Effekt von miR-378 im murinen Herzinsuffizienzmodell (Konstriktion der Aorta, TAC) untersucht. TAC führte zu einer Abnahme der Expression von miR-378 im Herzen. Durch Adeno-assoziierten Virus (AAV) vermittelte exogene Expression von miR-378 wurde das Expressionslevel des gesunden Herzens im TAC-Modell wiederhergestellt und die Expression der vier Targets herabgesetzt. Dies resultierte in weniger ausgeprägten Kardiomyozytenhypertrophie sowie in einer

signifikanten Verbesserung der Herzfunktion.

Aus diesen Daten schließen wir, dass miR-378 einen antihypertrophen Effekt auf Kardiomyozyten hat, der wesentlich durch die Suppression des MAP-Kinase-Signalweges an vier Angriffspunkten vermittelt wird. Die Wiederherstellung des “gesunden” Expressionsniveaus von miR-378 im kranken Herzen durch Kardiomyozyten-spezifische Expression mit AAV-miR-378 könnte eine Therapieoption bei Herzerkrankungen sein.

7 BIBLIOGRAPHY

1. WHO. www.who.int/nmh/publications/ncd_report_full_en.pdf

2. Mathers CD, Loncar D. Projections of global mortality and burden of disease from 2002 to 2030. *PLoS Med.* 2006; 3:e442.

3. Germany W. www.who.int/nmh/countries/deu_en.pdf

4. Heineke J, Molkentin JD. Regulation of cardiac hypertrophy by intracellular signalling pathways. *Nat. Rev. Mol. Cell Biol.* 2006; 7:589–600.

5. Klein L, O'Connor CM, Gattis WA, Zampino M, de Luca L, Vitarelli A, Fedele F, Gheorghiade M. Pharmacologic therapy for patients with chronic heart failure and reduced systolic function: review of trials and practical considerations. *Am. J. Cardiol.* 2003; 91:18F–40F.

6. Lips DJ, deWindt LJ, van Kraaij DJW, Doevendans PA. Molecular determinants of myocardial hypertrophy and failure: alternative pathways for beneficial and maladaptive hypertrophy. *European Heart Journal*. 2003; 24:883–896.

7. Epstein FH, Hunter JJ, Chien KR. Signaling pathways for cardiac hypertrophy and failure. *N. Engl. J. Med.* 1999; 341:1276–1283.

8. Chien KR, Zhu H, Knowlton KU, Miller-Hance W, van-Bilsen M, O'Brien TX, Evans SM. Transcriptional regulation during cardiac growth and development. *Annu. Rev. Physiol.* 1993; 55:77–95.

9. Berenji K, Drazner MH, Rothermel BA, Hill JA. Does load-induced ventricular hypertrophy progress to systolic heart failure? *Am. J. Physiol. Heart Circ. Physiol.* 2005; 289:H8–H16.

10. Sugden PH, Clerk A. “Stress-responsive” mitogen-activated protein kinases (c-Jun N-terminal kinases and p38 mitogen-activated protein kinases) in the myocardium. *Circulation Research*. 1998; 83:345–352.

11. Raman M, Chen W, Cobb MH. Differential regulation and properties of MAPKs. *Oncogene*. 2007; 26:3100–3112.

12. Garrington TP, Johnson GL. Organization and regulation of mitogen-activated protein kinase signaling pathways. *Current Opinion in Cell Biology*. 1999; 11:211–218.

13. Rapp UR, Götz R, Albert S. BuCy RAFs drive cells into MEK addiction. *Cancer Cell*. 2006; 9:9–12.

14. Campbell SL, Khosravi-Far R, Rossman KL, Clark GJ, Der CJ. Increasing complexity of Ras signaling. *Oncogene*. 1998; 17:1395–1413.

15. Bartel DP. MicroRNAs: Genomics, Review Biogenesis, Mechanism, and Function. *Cell*. 2004; 116:281–297.

16. Lee RC, Feinbaum RL, Ambros V. The C. elegans heterochronic gene lin-4 encodes small RNAs with antisense complementarity to lin-14. *Cell*. 1993; 75:843–854.

17. Wightman B, Ha I, Ruvkun G. Posttranscriptional regulation of the heterochronic gene lin-14 by lin-4 mediates temporal pattern formation in C. elegans. *Cell*. 1993; 75:855–862.

18. Lagos-Quintana M, Rauhut R, Lendeckel W, Tuschl T. Identification of Novel Genes Coding for Small Expressed RNAs. *Science*. 2001; 294:853.

19. Lau NC, Lim LP, Weinstein EG, Bartel DP. An Abundant Class of Tiny RNAs with Probable Regulatory Roles in Caenorhabditis elegans. *Science*. 2001; 294:858.

20. Lee RC, Ambros V. An Extensive Class of Small RNAs in Caenorhabditis elegans. *Science*. 2001; 294:862.

21. Lee Y, Kim M, Han J, Yeom K-H, Lee S, Baek SH, Kim VN. MicroRNA genes are transcribed by RNA polymerase II. *EMBO J.* 2004; 23:4051–4060.

22. Borchert GM, Lanier W, Davidson BL. RNA polymerase III transcribes human microRNAs. *Nature Structural & Molecular Biology*. 2006; 13:1097–1101.

23. Winter J, Jung S, Keller S, Gregory RI, Diederichs S. Many roads to maturity: microRNA biogenesis pathways and their regulation. *Nature Cell Biology*. 2009; 11:228–234.

24. Lee Y, Ahn C, Han J, Choi H, Kim J, Yim J, Lee J, Provost P, Rådmark O, Kim S, Kim VN. The nuclear RNase III Drosha initiates microRNA processing. *Nature Cell Biology*. 2003; 425:415–419.

25. Denli AM, Tops BBJ, Plasterk RHA, Ketting RF, Hannon GJ. Processing of primary microRNAs by the Microprocessor complex. *Nature*. 2004; 432:231–235.

26. Gregory RI, Yan K-P, Amuthan G, Chendrimada T, Doratotaj B, Cooch N, Shiekhattar R. The Microprocessor complex mediates the genesis of microRNAs. *Nature*. 2004; 432:235–240.

27. Han J, Lee Y, Yeom K-H, Kim Y-K, Jin H, Kim VN. The Drosha-DGCR8 complex in primary microRNA processing. *Genes & Development*. 2004; 18:3016–3027.

28. Landthaler M, Yalcin A, Tuschl T. The human DiGeorge syndrome critical region gene 8 and Its D. melanogaster homolog are required for miRNA biogenesis. *Curr. Biol.* 2004; 14:2162–2167.

29. Han J, Lee Y, Yeom K-H, Nam J-W, Heo I, Rhee J-K, Sohn SY, Cho Y, Zhang B-T, Kim VN. Molecular Basis for the Recognition of Primary microRNAs by the Drosha-DGCR8 Complex. *Cell*. 2006; 125:887–901.

30. Yi R, Qin Y, Macara IG, Cullen BR. Exportin-5 mediates the nuclear export of pre-microRNAs and short hairpin RNAs. *Genes & Development*. 2003; 17:3011–3016.

31. Lund E. Nuclear Export of MicroRNA Precursors. *Science*. 2004; 303:95–98.

32. Lund E, Dahlberg JE. Substrate selectivity of exportin 5 and Dicer in the biogenesis of microRNAs. *Cold Spring Harb. Symp. Quant. Biol.* 2006; 71:59–66.

33. Zeng Y, Cullen BR. Structural requirements for pre-microRNA binding and nuclear export by Exportin 5. *Nucleic Acids Research*. 2004; 32:4776–4785.

34. Gregory RI, Chendrimada TP, Cooch N, Shiekhattar R. Human RISC couples microRNA biogenesis and posttranscriptional gene silencing. *Cell*. 2005; 123:631–640.

35. Haase AD, Jaskiewicz L, Zhang H, Lainé S, Sack R, Gatignol A, Filipowicz W. TRBP, a regulator of cellular PKR and HIV-1 virus expression, interacts with Dicer and functions in RNA silencing. *EMBO Rep*. 2005; 6:961–967.

36. Lee Y, Hur I, Park S-Y, Kim Y-K, Suh MR, Kim VN. The role of PACT in the RNA silencing pathway. *EMBO J.* 2006; 25:522–532.

37. MacRae IJ, Ma E, Zhou M, Robinson CV, Doudna JA. In vitro reconstitution of the human RISC-loading complex. *Proc. Natl. Acad. Sci. U.S.A.* 2008; 105:512–517.

38. Diederichs S, Haber DA. Dual Role for Argonautes in MicroRNA Processing and Posttranscriptional Regulation of MicroRNA Expression. *Cell*. 2007; 131:1097–1108.

39. Bernstein E, Caudy AA, Hammond SM, Hannon GJ. Role for a bidentate ribonuclease in the initiation step of RNA interference. *Nature*. 2001; 409:363–366.

40. Grishok A, Pasquinelli AE, Conte D, Li N, Parrish S, Ha I, Baillie DL, Fire A, Ruvkun G, Mello CC. Genes and mechanisms related to RNA interference regulate expression of the small temporal RNAs that control C. elegans developmental timing. *Cell*. 2001; 106:23–34.

41. Hutvágner G, McLachlan J, Pasquinelli AE, Bálint E, Tuschl T, Zamore PD. A cellular function for the RNA-interference enzyme Dicer in the maturation of the let-7 small temporal RNA. *Science*. 2001; 293:834–838.

42. Ketting RF. A Dead End for MicroRNAs. *Cell*. 2007; 131:1226–1227.

43. Schwarz DS, Hutvágner G, Du T, Xu Z, Aronin N, Zamore PD. Asymmetry in the assembly of the RNAi enzyme complex. *Cell*. 2003; 115:199–208.

44. Khvorova A, Reynolds A, Jayasena SD. Functional siRNAs and miRNAs exhibit strand bias. *Cell*. 2003; 115:209–216.

45. Filipowicz W, Bhattacharyya SN, Sonenberg N. Mechanisms of post-transcriptional regulation by microRNAs: are the answers in sight? *Nat Rev Genet*. 2008; 9:102–114.

46. Valencia-Sanchez MA, Liu J, Hannon GJ, Parker R. Control of translation and mRNA degradation by miRNAs and siRNAs. *Genes & Development*. 2006; 20:515–524.

47. Tolia NH, Joshua-Tor L. Slicer and the argonautes. *Nat. Chem. Biol.* 2007; 3:36–43.

48. Grimson A, Farh KK-H, Johnston WK, Garrett-Engele P, Lim LP, Bartel DP. MicroRNA Targeting Specificity in Mammals: Determinants beyond Seed Pairing. *Molecular Cell*. 2007; 27:91–105.

49. Wu L, Fan J, Belasco JG. MicroRNAs direct rapid deadenylation of mRNA. *Proceedings of the National Academy of Sciences*. 2006; 103:4034–4039.

50. Behm-Ansmant I, Rehwinkel J, Doerks T, Stark A, Bork P, Izaurralde E. mRNA degradation by miRNAs and GW182 requires both CCR4:NOT deadenylase and DCP1:DCP2 decapping complexes. *Genes & Development*. 2006; 20:1885–1898.

51. Humphreys DT, Westman BJ, Martin DIK, Preiss T. MicroRNAs control translation initiation by inhibiting eukaryotic initiation factor 4E/cap and poly(A) tail function. *Proceedings of the National Academy of Sciences*. 2005; 102:16961–16966.

52. Chendrimada TP, Finn KJ, Ji X, Baillat D, Gregory RI, Liebhaber SA, Pasquinelli AE, Shiekhattar R. MicroRNA silencing through RISC recruitment of eIF6. *Nature*. 2007; 447:823–828.

53. Petersen CP, Bordeleau M-E, Pelletier J, Sharp PA. Short RNAs repress translation after initiation in mammalian cells. *Molecular Cell*. 2006; 21:533–542.

54. Griffiths-Jones S. miRBase: microRNA sequences, targets and gene nomenclature. *Nucleic Acids Research*. 2006; 34:D140–D144.

55. BASKERVILLE S. Microarray profiling of microRNAs reveals frequent coexpression with neighboring miRNAs and host genes. *RNA*. 2005; 11:241–247.

56. Small EM, Olson EN. Pervasive roles of microRNAs in cardiovascular biology. *Nature*. 2011; 469:336–342.

57. Lutter D, Marr C, Krumsiek J, Lang EW, Theis FJ. Intronic microRNAs support their host genes by mediating synergistic and antagonistic regulatory effects. *BMC Genomics*. 2010; 11:224.

58. Callis TE, Pandya K, Seok HY, Tang R-H, Tatsuguchi M, Huang Z-P, Chen J-F, Deng Z, Gunn B, Shumate J, Willis MS, Selzman CH, Wang D-Z. MicroRNA-208a is a regulator of cardiac hypertrophy and conduction in mice. *Journal of Clinical Investigation*. 2009; 119:2772–2786.

59. van Rooij E, Sutherland LB, Qi X, Richardson JA, Hill J, Olson EN. Control of Stress-Dependent Cardiac Growth and Gene Expression by a MicroRNA. *Science*. 2007; 316:575–579.

60. van Rooij E, Quiat D, Johnson BA, Sutherland LB, Qi X, Richardson JA, Kelm RJ Jr, Olson EN. A Family of microRNAs Encoded by Myosin Genes Governs Myosin Expression and Muscle Performance. *Developmental Cell*. 2009; 17:662–673.

61. Choi W-Y, Giraldez AJ, Schier AF. Target protectors reveal dampening and balancing of Nodal agonist and antagonist by miR-430. *Science*. 2007; 318:271–274.

62. Olson EN. Gene regulatory networks in the evolution and development of the heart. *Science*. 2006; 313:1922–1927.

63. Srivastava D, Olson EN. A genetic blueprint for cardiac development. *Nature*. 2000; 407:221–226.

64. Chen J-F, Murchison EP, Tang R, Callis TE, Tatsuguchi M, Deng Z, Rojas M, Hammond SM, Schneider MD, Selzman CH, Meissner G, Patterson C, Hannon GJ, Wang D-Z. Targeted deletion of Dicer in the heart leads to dilated cardiomyopathy and heart failure. *Proc. Natl. Acad. Sci. U.S.A.* 2008; 105:2111–2116.

65. da Costa Martins PA, Bourajjaj M, Gladka M, Kortland M, van Oort RJ, Pinto YM, Molkentin JD, de Windt LJ. Conditional Dicer Gene Deletion in the Postnatal Myocardium Provokes Spontaneous Cardiac Remodeling. *Circulation*. 2008; 118:1567–1576.

66. Chen J-F, Mandel EM, Thomson JM, Wu Q, Callis TE, Hammond SM, Conlon FL, Wang D-Z. The role of microRNA-1 and microRNA-133 in skeletal muscle proliferation and differentiation. *Nature Genetics*. 2005; 38:228–233.

67. Rao PK, Toyama Y, Chiang HR, Gupta S, Bauer M, Medvid R, Reinhardt F, Liao R, Krieger M, Jaenisch R, Lodish HF, Blelloch R. Loss of Cardiac microRNA-Mediated Regulation Leads to Dilated Cardiomyopathy and Heart Failure. *Circulation Research*. 2009; 105:585–594.

68. Zhao Y, Samal E, Srivastava D. Serum response factor regulates a muscle-specific microRNA that targets Hand2 during cardiogenesis. *Nature Cell Biology*. 2005; 436:214–220.

69. Liu N, Williams AH, Kim Y, McAnally J, Bezprozvannaya S, Sutherland LB, Richardson JA, Bassel-Duby R, Olson EN. An intragenic MEF2-dependent enhancer directs muscle-specific expression of microRNAs 1 and 133. *Proc. Natl. Acad. Sci. U.S.A.* 2007; 104:20844–20849.

70. WANG D, Chang PS, Wang Z, Sutherland L, Richardson JA, Small E, Krieg PA, Olson EN. Activation of cardiac gene expression by myocardin, a transcriptional cofactor for serum response factor. *Cell*. 2001; 105:851–862.

71. Zhao Y, Ransom JF, Li A, Vedantham V, Drehle von M, Muth AN, Tsuchihashi T, McManus MT, Schwartz RJ, Srivastava D. Dysregulation of Cardiogenesis, Cardiac Conduction, and Cell Cycle in Mice Lacking miRNA-1-2. *Cell*. 2007; 129:303–317.

72. Liu N, Bezprozvannaya S, Williams AH, Qi X, Richardson JA, Bassel-Duby R, Olson EN. microRNA-133a regulates cardiomyocyte proliferation and suppresses smooth muscle gene expression in the heart. *Genes & Development.* 2008

73. van Rooij E, Sutherland LB, Liu N, Williams AH, McAnally J, Gerard RD, Richardson JA, Olson EN. A signature pattern of stress-responsive microRNAs that can evoke cardiac hypertrophy and heart failure. *Proceedings of the National Academy of Sciences*. 2006; 103:18255–18260.

74. Tatsuguchi M, Seok HY, Callis TE, Thomson JM, Chen J-F, Newman M, Rojas M, Hammond SM, Wang D-Z. Expression of microRNAs is dynamically regulated during cardiomyocyte hypertrophy. *Journal of Molecular and Cellular Cardiology*. 2007; 42:1137–1141.

75. Sayed D, Hong C, Chen IY, Lypowy J, Abdellatif M. MicroRNAs Play an Essential Role in the Development of Cardiac Hypertrophy. *Circulation Research*. 2007; 100:416–424.

76. Carè A, Catalucci D, Felicetti F, Bonci D, Addario A, Gallo P, Bang M-L, Segnalini P, Gu Y, Dalton ND, Elia L, Latronico MVG, Høydal M, Autore C, Russo MA, Dorn GW, Ellingsen Ø, Ruiz-Lozano P, Peterson KL, Croce CM, Peschle C, Condorelli G. MicroRNA-133 controls cardiac hypertrophy. *Nature Medicine*. 2007; 13:613–618.

77. Thum T, Gross C, Fiedler J, Fischer T, Kissler S, Bussen M, Galuppo P, Just S, Rottbauer W, Frantz S, Castoldi M, Soutschek J, Koteliansky V, Rosenwald A, Basson MA, Licht JD, Pena JTR, Rouhanifard SH, Muckenthaler MU, Tuschl T, Martin GR, Bauersachs J,

Engelhardt S. MicroRNA-21 contributes to myocardial disease by stimulating MAP kinase signalling in fibroblasts. *Nature*. 2008; 456:980–984.

78. Thum T, Galuppo P, Wolf C, Fiedler J, Kneitz S, van Laake LW, Doevendans PA, Mummery CL, Borlak J, Haverich A, Gross C, Engelhardt S, Ertl G, Bauersachs J. MicroRNAs in the Human Heart: A Clue to Fetal Gene Reprogramming in Heart Failure. *Circulation*. 2007; 116:258–267.

79. da Costa Martins PA, Salic K, Gladka MM, Armand A-S, Leptidis S, Azzouzi el H, Hansen A, Roo CJC-D, Bierhuizen MF, van der Nagel R, van Kuik J, de Weger R, de Bruin A, Condorelli G, Arbones ML, Eschenhagen T, De Windt LJ. MicroRNA-199b targets the nuclear kinase Dyrk1a in an auto-amplification loop promoting calcineurin/NFAT signalling. *Nature Cell Biology*. 2010; 12:1220–1227.

80. Landgraf P, Rusu M, Sheridan R, Sewer A, Iovino N, Aravin A, Pfeffer S, Rice A, Kamphorst AO, Landthaler M, Lin C, Socci ND, Hermida L, Fulci V, Chiaretti S, Foà R, Schliwka J, Fuchs U, Novosel A, Müller R-U, Schermer B, Bissels U, Inman J, Phan Q, Chien M, Weir DB, Choksi R, De Vita G, Frezzetti D, Trompeter H-I, Hornung V, Teng G, Hartmann G, Palkovits M, Di Lauro R, Wernet P, Macino G, Rogler CE, Nagle JW, Ju J, Papavasiliou FN, Benzing T, Lichter P, Tam W, Brownstein MJ, Bosio A, Borkhardt A, Russo JJ, Sander C, Zavolan M, Tuschl T. A Mammalian microRNA Expression Atlas Based on Small RNA Library Sequencing. *Cell*. 2007; 129:1401–1414.

81. Lee DY, Deng Z, Wang C-H, Yang BB. MicroRNA-378 promotes cell survival, tumor growth, and angiogenesis by targeting SuFu and Fus-1 expression. *Proc. Natl. Acad. Sci. U.S.A.* 2007; 104:20350–20355.

82. Feng M, Li Z, Aau M, Wong CH, Yang X, Yu Q. Myc/miR-378/TOB2/cyclin D1 functional module regulates oncogenic transformation. *Oncogene*. 2011;:1–10.

83. Fang J, Song X-W, Tian J, Chen H-Y, Li D-F, Wang J-F, Ren A-J, Yuan W-J, Lin L. Overexpression of microRNA-378 attenuates ischemia-induced apoptosis by inhibiting caspase-3 expression in cardiac myocytes. *Apoptosis*. 2011;

84. Knezevic I, Patel A, Sundaresan NR, Gupta MP, Solaro RJ, Nagalingam RS, Gupta M. A novel cardiomyocyte-enriched microRNA, miR-378, targets insulin-like growth factor 1 receptor:

implications in postnatal cardiac remodeling and cell survival. *Journal of Biological Chemistry*. 2012; 287:12913–12926.

85. van Rooij E, Olson EN. MicroRNA therapeutics for cardiovascular disease: opportunities and obstacles. *Nat Rev Drug Discov*. 2012; 11:860–872.

86. Zincarelli C, Soltys S, Rengo G, Rabinowitz JE. Analysis of AAV serotypes 1-9 mediated gene expression and tropism in mice after systemic injection. *Mol. Ther.* 2008; 16:1073–1080.

87. Atchison RW, Casto BC, Hammon W. Adenovirus-Associated Defective Virus Particles. *Science*. 1965;

88. Dong JY, Fan PD, Frizzell RA. Quantitative analysis of the packaging capacity of recombinant adeno-associated virus. *Hum. Gene Ther.* 1996; 7:2101–2112.

89. Kotin RM, Siniscalco M, Samulski RJ, Zhu XD, Hunter L, Laughlin CA, McLaughlin S, Muzyczka N, Rocchi M, Berns KI. Site-specific integration by adeno-associated virus. *Proceedings of the National Academy of Sciences*. 1990; 87:2211–2215.

90. Kay MA, Glorioso JC, Naldini L. Viral vectors for gene therapy: the art of turning infectious agents into vehicles of therapeutics. *Nature Medicine*. 2001; 7:33–40.

91. Pacak CA, Byrne BJ. AAV Vectors for Cardiac Gene Transfer: Experimental Tools and Clinical Opportunities. *Nature Cell Biology*. 2011; 19:1582–1590.

92. Schnepp BC, Clark KR, Klemanski DL, Pacak CA, Johnson PR. Genetic fate of recombinant adeno-associated virus vector genomes in muscle. *Journal of Virology*. 2003; 77:3495–3504.

93. Engelhardt S, Hein L, Wiesmann F, Lohse MJ. Progressive hypertrophy and heart failure in beta1-adrenergic receptor transgenic mice. *Proceedings of the National Academy of Sciences*. 1999; 96:7059–7064.

94. Arsic N, Zacchigna S, Zentilin L, Ramirez-Correa G, Pattarini L, Salvi A, Sinagra G, Giacca M. Vascular endothelial growth factor stimulates skeletal muscle regeneration in vivo. *Mol. Ther.* 2004; 10:844–854.

95. Inagaki K, Fuess S, Storm TA, Gibson GA, Mctiernan CF, Kay MA, Nakai H. Robust systemic transduction with AAV9 vectors in mice: efficient global cardiac gene transfer superior to that of AAV8. *Mol. Ther.* 2006; 14:45–53.

96. Zentilin L, Marcello A, Giacca M. Involvement of cellular double-stranded DNA break binding proteins in processing of the recombinant adeno-associated virus genome. *Journal of Virology*. 2001; 75:12279–12287.

97. Jentzsch C, Leierseder S, Loyer X, Flohrschütz I, Sassi Y, Hartmann D, Thum T, Laggerbauer B, Engelhardt S. A phenotypic screen to identify hypertrophy-modulating microRNAs in primary cardiomyocytes. *Journal of Molecular and Cellular Cardiology*. 2012; 52:13–20.

98. Leierseder S. Role of microRNAs in different cell types of the mammalian heart.

99. Razeghi P, Young ME, Alcorn JL, Moravec CS, Frazier OH, Taegtmeyer H. Metabolic gene expression in fetal and failing human heart. *Circulation*. 2001; 104:2923–2931.

100. Lewis BP, Burge CB, Bartel DP. Conserved seed pairing, often flanked by adenosines, indicates that thousands of human genes are microRNA targets. *Cell*. 2005; 120:15–20.

101. Kowarsch A, Preusse M, Marr C, Theis FJ. miTALOS: analyzing the tissue-specific regulation of signaling pathways by human and mouse microRNAs. *RNA*. 2011; 17:809–819.

102. Carrer M, Liu N, Grueter CE, Williams AH, Frisard MI, Hulver MW, Bassel-Duby R, Olson EN. Control of mitochondrial metabolism and systemic energy homeostasis by microRNAs 378 and 378. *Proc. Natl. Acad. Sci. U.S.A.* 2012;

103. Nagalingam RS, Sundaresan NR, Gupta MP, Geenen DL, Solaro RJ, Gupta M. A Cardiac-enriched MicroRNA, miR-378, Blocks Cardiac Hypertrophy by Targeting Ras Signaling. *Journal of Biological Chemistry*. 2013; 288:11216–11232.

104. Burger D, Lei M, Geoghegan-Morphet N, Lu X, Xenocostas A, Feng Q. Erythropoietin protects cardiomyocytes from apoptosis via up-regulation of endothelial nitric oxide synthase. *Cardiovascular Research*. 2006; 72:51–59.

105. Bueno OF. Involvement of Extracellular Signal-Regulated Kinases 1/2 in Cardiac Hypertrophy and Cell Death. *Circulation Research*. 2002; 91:776–781.

106. Clerk A, Bogoyevitch MA, Anderson MB, Sugden PH. Differential activation of protein kinase C isoforms by endothelin-1 and phenylephrine and subsequent stimulation of p42 and p44 mitogen-activated protein kinases in ventricular myocytes cultured from neonatal rat hearts. *Journal of Biological Sciences.*1994

107. Bogoyevitch MA, Glennon PE, Andersson MB, Clerk A, Lazou A, Marshall CJ, Parker PJ, Sugden PH. Endothelin-1 and fibroblast growth factors stimulate the mitogen-activated protein kinase signaling cascade in cardiac myocytes. The potential role of the cascade in the integration of two signaling pathways leading to myocyte hypertrophy. *Journal of Biological Sciences.*1994

108. Glennon PE, Kaddoura S, Sale EM, Sale GJ, Fuller SJ, Sugden PH. Depletion of Mitogen-Activated Protein Kinase Using an Antisense Oligodeoxynucleotide Approach Downregulates the Phenylephrine-Induced Hypertrophic Response in Rat Cardiac Myocytes. *Circulation Research*. 1996; 78:954–961.

109. Yue T-L, Gu J-L, Wang C, Reith AD, Lee JC, Mirabile RC, Kreutz R, Wang Y, Maleeff B, Parsons AA, Ohlstein EH. Extracellular Signal-regulated Kinase Plays an Essential Role in Hypertrophic Agonists, Endothelin-1 and Phenylephrine-induced Cardiomyocyte Hypertrophy. *Journal of Biological* Sciences.2000

110. Ueyama T, Kawashima S, Sakoda T, Rikitake Y. Requirement of Activation of the Extracellular Signal-regulated Kinase Cascade in Myocardial Cell Hypertrophy. *Journal of Molecular and Cellular Cardiology.* 2000;

111. Rapacciuolo A, Esposito G, Caron K, Mao L, Thomas SA, Rockman HA. Important role of endogenous norepinephrine and epinephrine in the development of in vivo pressure-overload cardiac hypertrophy. *J. Am. Coll. Cardiol.* 2001; 38:876–882.

112. Purcell NH, Wilkins BJ, York A, Saba-El-Leil MK, Meloche S, Robbins J, Molkentin JD. Genetic inhibition of cardiac ERK1/2 promotes stress-induced apoptosis and heart failure but has no effect on hypertrophy in vivo. *Proceedings of the National Academy of Sciences*. 2007; 104:14074–14079.

113. Kehat I, Davis J, Tiburcy M, Accornero F, Saba-El-Leil MK, Maillet M, York AJ, Lorenz JN, Zimmermann WH, Meloche S, Molkentin JD. Extracellular Signal-Regulated Kinases 1 and

2 Regulate the Balance Between Eccentric and Concentric Cardiac Growth. *Circulation Research*. 2011; 108:176–183.

114. Pearson G, Robinson F, Gibson TB, Xu B-E, Karandikar M, Berman K, Cobb MH. Mitogen-Activated Protein (MAP) Kinase Pathways: Regulation and Physiological Functions. *Endocrine Reviews*. 2001

115. Kolch W. Coordinating ERK/MAPK signalling through scaffolds and inhibitors. *Nature Publishing Group*. 2005; 6:827–837.

116. Therrien M, Michaud NR, Rubin GM, Morrison DK. KSR modulates signal propagation within the MAPK cascade. *Genes & Development*. 1996; 10:2684–2695.

117. Kortum RL, Lewis RE. The molecular scaffold KSR1 regulates the proliferative and oncogenic potential of cells. *Molecular and Cellular Biology*. 2004; 24:4407–4416.

118. Nguyen A, Burack WR, Stock JL, Kortum R, Chaika OV, Afkarian M, Muller WJ, Murphy KM, Morrison DK, Lewis RE, McNeish J, Shaw AS. Kinase Suppressor of Ras (KSR) Is a Scaffold Which Facilitates Mitogen-Activated Protein Kinase Activation In Vivo. *... and cellular biology*. 2002;

119. Müller J, Ory S, Copeland T, Piwnica-Worms H, Morrison DK. C-TAK1 regulates Ras signaling by phosphorylating the MAPK scaffold, KSR1. *Molecular Cell*. 2001; 8:983–993.

120. Matheny SA, Chen C, Kortum RL, Razidlo GL, Lewis RE, White MA. Ras regulates assembly of mitogenic signalling complexes through the effector protein IMP. *Nature*. 2004; 427:256–260.

121. Hartsough MT, Morrison DK, Salerno M, Palmieri D, Ouatas T, Mair M, Patrick J, Steeg PS. Nm23-H1 metastasis suppressor phosphorylation of kinase suppressor of Ras via a histidine protein kinase pathway. *J. Biol. Chem.* 2002; 277:32389–32399.

122. Clapéron A, Therrien M. KSR and CNK: two scaffolds regulating RAS-mediated RAF activation. *Oncogene*. 2007; 26:3143–3158.

123. Rabizadeh S, Xavier RJ, Ishiguro K, Bernabeortiz J, Lopez-Ilasaca M, Khokhlatchev A, Mollahan P, Pfeifer GP, Avruch J, Seed B. The scaffold protein CNK1 interacts with the

tumor suppressor RASSF1A and augments RASSF1A-induced cell death. *J. Biol. Chem.* 2004; 279:29247–29254.

124. Chiloeches A, Paterson HF, Marais R, Clerk A, Marshall CJ, Sugden PH. Regulation of Ras·GTP Loading and Ras-Raf Association in Neonatal Rat Ventricular Myocytes by G Protein-coupled Receptor Agonists and Phorbol Ester. *jbc.org*.

125. Avruch J, Xavier R, Bardeesy N, Zhang X-F, Praskova M, Zhou D, Xia F. Rassf family of tumor suppressor polypeptides. *J. Biol. Chem.* 2009; 284:11001–11005.

126. White MF, Kahn CR. The insulin signaling system. *J. Biol. Chem.* 1994; 269.

127. Froesch ER, Schmid C, Schwander J, Zapf J. Actions of insulin-like growth factors. *Annu. Rev. Physiol.* 1985; 47:443–467.

128. DeBosch BJ, Muslin AJ. Insulin signaling pathways and cardiac growth. *Journal of Molecular and Cellular Cardiology*. 2008; 44:855–864.

129. Duret L, Guex N, Peitsch MC, Bairoch A. New insulin-like proteins with atypical disulfide bond pattern characterized in Caenorhabditis elegans by comparative sequence analysis and homology modeling. *Genome Research*. 1998; 8:348–353.

130. Kim JJ, Accili D. Signalling through IGF-I and insulin receptors: where is the specificity? *Growth Hormone & IGF Research*. 2002; 12:84–90.

131. Anversa P, Kajstura J, Cheng W, Reiss K, Cigola E, Olivetti G. Insulin-like growth factor-1 and myocyte growth: the danger of a dogma part II. Induced myocardial growth: pathologic hypertrophy. *Cardiovascular Research*. 1996; 32:484–495.

132. Donohue TJ, Dworkin LD, Lango MN, Fliegner K, Lango RP, Benstein JA, Slater WR, Catanese VM. Induction of myocardial insulin-like growth factor-I gene expression in left ventricular hypertrophy. *Circulation*. 1994; 89:799–809.

133. Butt RP, Bishop JE. Mechanical load enhances the stimulatory effect of serum growth factors on cardiac fibroblast procollagen synthesis. *Journal of Molecular and Cellular Cardiology*. 1997; 29:1141–1151.

134. Delaughter MC, Taffet GE, Fiorotto ML, Entman ML, Schwartz RJ. Local insulin-like growth factor I expression induces physiologic, then pathologic, cardiac hypertrophy in transgenic mice. *FASEB J.* 1999; 13:1923–1929.

135. Elia L, Contu R, Quintavalle M, Varrone F, Chimenti C, Russo MA, Cimino V, De Marinis L, Frustaci A, Catalucci D, Condorelli G. Reciprocal regulation of microRNA-1 and insulin-like growth factor-1 signal transduction cascade in cardiac and skeletal muscle in physiological and pathological conditions. *Circulation*. 2009; 120:2377–2385.

136. McMullen JR. The Insulin-like Growth Factor 1 Receptor Induces Physiological Heart Growth via the Phosphoinositide 3-Kinase(p110) Pathway. *Journal of Biological Chemistry*. 2003; 279:4782–4793.

137. McMullen JR, Jennings GL. Differences between pathological and physiological cardiac hypertrophy: novel therapeutic strategies to treat heart failure. *Clinical and Experimental Pharmacology and Physiology*. 2007; 34:255–262.

138. DeBosch B, Treskov I, Lupu TS, Weinheimer C, Kovacs A, Courtois M, Muslin AJ. Akt1 is required for physiological cardiac growth. *Circulation*. 2006; 113:2097–2104.

139. Condorelli G, Drusco A, Stassi G, Bellacosa A, Roncarati R, Iaccarino G, Russo MA, Gu Y, Dalton N, Chung C, Latronico MVG, Napoli C, Sadoshima J, Croce CM, Ross J. Akt induces enhanced myocardial contractility and cell size in vivo in transgenic mice. *Proceedings of the National Academy of Sciences*. 2002; 99:12333–12338.

140. Matsui T, Li L, Wu JC, Cook SA, Nagoshi T, Picard MH, Liao R, Rosenzweig A. Phenotypic spectrum caused by transgenic overexpression of activated Akt in the heart. *J. Biol. Chem.* 2002; 277:22896–22901.

141. Lowenstein EJ, Daly RJ, Batzer AG, Li W, Margolis B, Lammers R, Ullrich A, Skolnik EY, Bar-Sagi D, Schlessinger J. The SH2 and SH3 domain-containing protein GRB2 links receptor tyrosine kinases to ras signaling. *Cell*. 1992; 70:431–442.

142. Downward J. The GRB2/Sem-5 adaptor protein. *FEBS Letters*. 1994; 338:113–117.

143. Gong Q, Cheng AM, Akk AM, Alberola-Ila J, Gong G, Pawson T, Chan AC. Disruption of T cell signaling networks and development by Grb2 haploid insufficiency. *Nat. Immunol.* 2001; 2:29–36.

144. Ross RSR, Borg TKT. Integrins and the myocardium. *Audio, Transactions of the IRE Professional Group on*. 2001; 88:1112–1119.

145. Zhang S, Weinheimer C, Courtois M, Kovacs A, Zhang CE, Cheng AM, Wang Y, Muslin AJ. The role of the Grb2–p38 MAPK signaling pathway in cardiac hypertrophy and fibrosis. *Journal of Clinical Investigation*. 2003; 111:833–841.

146. Finck BN, Kelly DP. Peroxisome Proliferator–Activated Receptor γ Coactivator-1 (PGC-1) Regulatory Cascade in Cardiac Physiology and Disease. *circ.ahajournals.org*.

147. Schilling J, Kelly DP. The PGC-1 cascade as a therapeutic target for heart failure. *Journal of Molecular and Cellular Cardiology*. 2011; 51:578–583.

148. Puigserver P, Wu Z, Park CW, Graves R, Wright M, Spiegelman BM. A cold-inducible coactivator of nuclear receptors linked to adaptive thermogenesis. *Cell*. 1998; 92:829–839.

149. Eichner LJ, Perry M-C, Dufour CR, Bertos N, Park M, St-Pierre J, Giguère V. miR-378* Mediates Metabolic Shift in Breast Cancer Cells via the PGC-1 beta/ERR gamma Transcriptional Pathway. *Cell Metabolism*. 2010; 12:352–361.

150. Taegtmeyer H, Golfman L, Sharma S, Razeghi P, van Arsdall M. Linking gene expression to function: metabolic flexibility in the normal and diseased heart. *Annals of the New York Academy of Sciences*. 2004; 1015:202–213.

151. Stanley WC, Recchia FA, Lopaschuk GD. Myocardial substrate metabolism in the normal and failing heart. *Physiol. Rev.* 2005; 85:1093–1129.

152. Young ME, Laws FA, Goodwin GW, Taegtmeyer H. Reactivation of peroxisome proliferator-activated receptor alpha is associated with contractile dysfunction in hypertrophied rat heart. *J. Biol. Chem.* 2001; 276:44390–44395.

153. Lai L, Leone TC, Zechner C, Schaeffer PJ, Kelly SM, Flanagan DP, Medeiros DM, Kovacs A, Kelly DP. Transcriptional coactivators PGC-1 and PGC-l control overlapping programs required for perinatal maturation of the heart. *Genes & Development*. 2008; 22:1948–1961.

154. Huss JM, Imahashi K-I, Dufour CR, Weinheimer CJ, Courtois M, Kovacs A, Giguère V, Murphy E, Kelly DP. The nuclear receptor ERRalpha is required for the bioenergetic and functional adaptation to cardiac pressure overload. *Cell Metabolism*. 2007; 6:25–37.

155. Arany Z, Novikov M, Chin S, Ma Y, Rosenzweig A, Spiegelman BM. Transverse aortic constriction leads to accelerated heart failure in mice lacking PPAR-gamma coactivator 1alpha. *Proceedings of the National Academy of Sciences*. 2006; 103:10086–10091.

156. Lehman JJ, Barger PM, Kovacs A, Saffitz JE, Medeiros DM, Kelly DP. Peroxisome proliferator-activated receptor gamma coactivator-1 promotes cardiac mitochondrial biogenesis. *Journal of Clinical Investigation*. 2000; 106:847–856.

157. Lehman JJ, Kelly DP. Transcriptional activation of energy metabolic switches in the developing and hypertrophied heart. *Clinical and Experimental Pharmacology and Physiology*. 2002; 29:339–345.

158. Lu Z, Xu X, Hu X, Fassett J, Zhu G, Tao Y, Li J, Huang Y, Zhang P, Zhao B, Chen Y. PGC-1α Regulates Expression of Myocardial Mitochondrial Antioxidants and Myocardial Oxidative Stress After Chronic Systolic Overload. *Antioxidants & Redox Signaling*. 2010; 13:1011–1022.

159. Riehle C, Wende AR, Zaha VG, Pires KM, Wayment B, Olsen C, Bugger H, Buchanan J, Wang X, Moreira AB, Doenst T, Medina-Gomez G, Litwin SE, Lelliott CJ, Vidal-Puig A, Abel ED. PGC-1β deficiency accelerates the transition to heart failure in pressure overload hypertrophy. *Circulation Research*. 2011; 109:783–793.

160. Barger PM, Brandt JM, Leone TC, Weinheimer CJ, Kelly DP. Deactivation of peroxisome proliferator-activated receptor-alpha during cardiac hypertrophic growth. *Journal of Clinical Investigation*. 2000; 105:1723–1730.

161. Hu E, Kim JB, Sarraf P, Spiegelman BM. Inhibition of adipogenesis through MAP kinase-mediated phosphorylation of PPARgamma. *Science*. 1996; 274:2100–2103.

162. Sano M, Abdellatif M, Oh H, Xie M, Bagella L, Giordano A, Michael LH, DeMayo FJ, Schneider MD. Activation and function of cyclin T–Cdk9 (positive transcription elongation factor-b) in cardiac muscle-cell hypertrophy. *Nature Medicine*. 2002; 8:1310–1317.

163. Sano M, Wang SC, Shirai M, Scaglia F, Xie M, Sakai S, Tanaka T, Kulkarni PA, Barger PM, Youker KA, Taffet GE, Hamamori Y, Michael LH, Craigen WJ, Schneider MD. Activation of cardiac Cdk9 represses PGC-1 and confers a predisposition to heart failure. *Nature Cell Biology*. 2004; 23:3559–3569.

164. Makeyev EV, Maniatis T. Multilevel Regulation of Gene Expression by MicroRNAs. *Science*. 2008; 319:1789–1790.

165. Hobert O. Gene Regulation by Transcription Factors and MicroRNAs. *Science*. 2008; 319:1785–1786.

166. Mestdagh P, Boström A-K, Impens F, Fredlund E, Van Peer G, De Antonellis P, Stedingk von K, Ghesquière B, Schulte S, Dews M, Thomas-Tikhonenko A, Schulte JH, Zollo M, Schramm A, Gevaert K, Axelson H, Speleman F, Vandesompele J. The miR-17-92 microRNA cluster regulates multiple components of the TGF-β pathway in neuroblastoma. *Molecular Cell*. 2010; 40:762–773.

167. Lal A, Navarro F, Maher CA, Maliszewski LE, Yan N, Day EO, Chowdhury D, Dykxhoorn DM, Tsai P, Hofmann O, Becker KG, Gorospe M, Hide W, Lieberman J. miR-24 Inhibits Cell Proliferation by Targeting E2F2, MYC, and Other Cell-Cycle Genes via Binding to Seedless 3′UTR MicroRNA Recognition Elements. *Molecular Cell*. 2009; 35:610–625.

168. Hulot J-S, Fauconnier J, Ramanujam D, Chaanine A, Aubart F, Sassi Y, Merkle S, Cazorla O, Ouillé A, Dupuis M, Hadri L, Jeong D, Mühlstedt S, Schmitt J, Braun A, Bénard L, Saliba Y, Laggerbauer B, Nieswandt B, Lacampagne A, Hajjar RJ, Lompré A-M, Engelhardt S. Critical role for stromal interaction molecule 1 in cardiac hypertrophy. *Circulation*. 2011; 124:796–805.

169. Ganesan J, Ramanujam D, Sassi Y, Ahles A, Jentzsch C, Werfel S, Leierseder S, Loyer X, Giacca M, Zentilin L, Thum T, Laggerbauer B, Engelhardt S. MiR-378 controls cardiac hypertrophy by combined repression of mitogen-activated protein kinase pathway factors. Circulation. 2013; 127:2097–2106.

8 ADDENDUM

8.1 Abbreviations

AAV	Adeno-associated virus
AGO	Argonaute
ANP	Atrial natriuretic peptide
BCA	Bicinchoninic acid
BSA	Bovine serum albumin
CDC42	Cell division control protein 42 homolog
CDK	Cyclin-dependent kinase
DCM	Dilated cardiomyopathy
DGCR8	DiGeorge critical region 8
DYRK1A	Dual-specificity tyrosine-(Y)-phosphorylation regulated kinase 1a
EF	Ejection fraction
ERK	Extracellular signal-regulated kinases
ERR	Estrogen-related receptors
FCS	Fetal calf serum
FS	Fractional shortening
FUS1	Fused in sarcoma 1
GDP	Guanosine diphosphate,
GPCR	G protein coupled receptor
GRB2	Growth factor receptor-bound protein 2
GTP	Guanosine-5'-triphosphate
IGF1	Insulin-like growth factor 1
IGF1R	Insulin-like growth factor 1 receptor
ITR	Inverted terminal repeats
IVS	Intraventricular septal thickness
JNK	c-Jun N-terminal kinase
KSR1	Kinase suppressor Ras 1
LVID	Left ventricular internal diameter
LVPW	Left ventricular posterior wall thickness
MAPK	Mitogen-activated protein kinase
MCS	Multiple cloning site
MEF2	Myocyte enhancer factor-2
MiRNA/miR	MicroRNA
MIRNP	Micro-ribonucleoprotein
NELFA	Negative elongation factor A
NFAT	Nuclear factor of activated T-cells
NRCM	Neo natal rat cardiomyocyte
PACT	Protein activator of PKR
PBS	Phosphate buffered saline
PE	Phenylephrine

PGC1	Peroxisome proliferator-activated receptor gamma coactivator 1
PI3K	Phosphatidylinositol-4,5-bisphosphate 3-kinase
PIWI	P-element induced wimpy testis
QPCR	Quantitative real time PCR
RAS	Rat sarcoma
RASA1	Ras GTPase activating protein
RASSF1	Ras-association domain family-1
RHEB	Ras homolog enriched in brain
RHOA	Ras Homolog Family Member A
RISC	RNA-induced silencing complex
SDS	Sodium dodecyl sulfate
SHRNA	short hairpin RNA
SIRNA	small interfering RNA
SRF	Serum response factor
SUFU	Suppressor of fused homolog
TAC	Transverse aortic constriction
TAE	Tris-acetate-EDTA
TGFβ	Transforming growth factor beta
TRBP	Tar RNA binding protein)
TUNEL	Terminal deoxynucleotidyl transferase dUTP nick end labeling
UTR	Untranslated region
WGA	Wheat germ agglutinin
XPO5	Exportin-5
βMHC	Myosin heavy chain beta

8.2 Acknowledgments

First and foremost I would like to thank Prof. Stefan Engelhardt for giving me an opportunity to do my PhD under him and for his valuable guidance and supervision. I am immensely grateful to him for his support and for the innumerable things I learnt from him. I would also like to thank my other supervisors Prof. Utz Fischer and Prof. Hermann Schindelin for their timely guidance and help. I would like to thank GSLS, Wuerzburg for their valuable support

I have to specially mention the people whose experimental support was immensely helpful in finishing this work. A big thank you to Deepak Ramanujam, Yassine Sassi, Andrea Ahles, Claudia Jentzsch, Simon Leierseder, Xavier Loyer and Stanislas Werfel for all the hours you spent to make this work possible. I would also like to thank all my other colleagues for countless suggestions and discussions. Thank you Petra Goebel, Fabrice Jaffre, Andrea Rinck and Megha Saraiya for your support. I am especially grateful to the TA's Isabel Flohrschütz, Ursula Kremser, Sabine Brummer and Astrid Vens for all their support. I would like to thank Bernhard Laggerbauer for his help with writing the manuscript and for his suggestions. I would also like to thank my colleagues from Würzburg namely Sabine, Lydia and Morgan for all the good times as well as valuable advice.

Special thanks to my friends from Germany (Shambhavi, Partho, Preeti and Kathleen) for all the fun times and for being with me through all the ups and downs. A big thank you to Revu, Srividya and Adithya for always being there for me.

Finally, I would like to dedicate this work to my parents and thank them for their unconditional love and support.

8.3 Publications

1. Ganesan J, Ramanujam D, Sassi Y, Ahles A, Jentzsch C, Werfel S, Leierseder S, Loyer X, Giacca M, Zentilin L, Thum T, Laggerbauer B, Engelhardt S. MiR-378 controls cardiac hypertrophy by combined repression of mitogen-activated protein kinase pathway factors. Circulation. 2013; 127:2097–2106.

8.4 Scientific presentations

1. Presentation: Leduq foundation – 4th Meeting of the transatlantic network of excellence on micoRNAs. 19th – 20th Sep 2012, Amsterdam, Netherland
2. Presentation: German center for cardiovascular research (DZHK)/ MHA winter meeting, 21st Jan 2013, Munich, Germany
3. Presentation: 79th Meeting of DGPT (German society for experimental and clinical pharmacology and toxicology), 05th – 07th Mar 2013, Halle (Saale), Germany
4. Presentation: Bavarian research network for molecular biosystems meeting, 07th Mar 2013, Munich, Germany
5. Presentation: 79th Meeting of DGK (German society of cardiology), 03rd – 06th Apr 2013, Mannheim, Germany
6. Presentation: German center for cardiovascular research (DZHK) meeting, Epigenetics and system biology in cardiovascular disease, 22nd Apr 2013, Berlin, Germany